Methods and Devices for Corrosion Fatigue Testing without Acceleration

by
Douglas E. Jonart

Naval Engineer
Massachusetts Institute of Technology, 2014

S.M. Materials Science and Engineering
Massachusetts Institute of Technology, 2014

M.S. Systems Technology (C3)
Naval Postgraduate School, 2008

B.S. Mathematics
University of Wyoming, 1995

Submitted to the Department of Mechanical Engineering
in Partial Fulfillment of the Requirements for the Degree of

Doctor of Philosophy in Ocean Engineering

June 2016

Signature of Author: Signature redacted
Department of Naval Construction and Architecture
May 20, 2016

Certified by: Signature redacted
Alexander H. Slocum
Pappalardo Professor of Mechanical Engineering
Thesis Advisor and Committee Chairman

Certified by: Signature redacted
Ronald G. Ballinger
Professor of Nuclear Science and Engineering, and Materials Science and Engineering
Thesis Advisor

Accepted by: Signature redacted
Rohan Abeyaratne
Chairman, Department Committee on Graduate Studies
Department of Mechanical Engineering

THIS PAGE INTENTIONALLY LEFT BLANK

Methods and Devices for Corrosion Fatigue Testing without Acceleration

By

Douglas E. Jonart

Submitted to the Department of Mechanical Engineering on May 20, 2016 in Partial Fulfillment of the Requirements for the Degree of Doctor of Philosophy in Ocean Engineering

ABSTRACT

Substantial submarine procurement and maintenance costs could be saved by extending the submarine propulsion shaft inspection interval from 6 to 12 years as part of the design of the next class of vessels. On existing classes, corrosion fatigue limits this interval, but data on corrosion fatigue life is sparse and incomplete. An existing model from previous research has been updated and stands ready to provide predictions, given more relevant data. Techniques and devices are developed to obtain this data.

First, traditional fatigue machines and samples are adapted to provide information on corrosion fatigue on pre-pitted and unpitted samples. Artificial seawater is used for comparative consistency; tests with enzymatic or actual seawater are recommended. Next, direct-current potential drop is proven as a means to detect transitions in the corrosion fatigue failure chain on a bending fatigue specimen exposed to artificial seawater. This method can be used to detect transition of pits to cracks in situ, and it is believed that it can be used to detect ingress of water through protective coatings, which has not previously been measured or credited in a review of predictive models and design life analyses. This technique should be verified and expanded to detect additional transitions and to apply to the devices developed as part of this research.

Second, test devices are developed to more accurately reflect the operational submarine propulsion shaft, in terms of loading, environment, and number of test cycles. The benchtop prototype intended to prove the concept jas been identified by the Navy as an improvement over existing machines, and is subsequently redesigned as an inexpensive and rapidly deployable test stand for uncoated shaft specimens. The originally envisioned device is also designed and assembled. It leverages non-contact air bearings and motors, as well as flexural pivots, to enable very high cycle fatigue testing while minimizing the parasitic loads imparted on the sample by the test machine. The next recommended step is deployment of this device as a tool for verification testing of fully coated samples, necessary based on the large scope of the desired increase in shaft life.

Thesis Supervisor:	Alex Slocum
Title:	Pappalardo Professor of Mechanical Engineering
Thesis Supervisor:	Ronald Ballinger
Title:	Professor of Nuclear Science and Engineering, and Materials Science and Engineering

Acknowledgments

This thesis is no exception to the rule that such a large endeavor requires a team of people standing behind the person whose name gets attached to the final document. The list of people who have helped me, supported me, and shared with me their skills and talents is longer than this page could ever contain, and insofar as there are omissions and oversights, I apologize.

Key contributors who could never be forgotten, nor ignored, start with my committee. Dr. Slocum is a force of nature, a tireless genius who seeds my own creative fields with equal parts fun and challenge. His balance in life helped me to use outlets, exercise, literature, and those around me to keep the fires better fueled for productivity than will or desire alone could muster. Dr. Ballinger, in addition to the obvious contributions and assistance evident throughout this thesis, filled a similar lead role in the first thesis and project, and did much to get me and these documents into the research shape that he knew was required. Dr. Johnson and CAPT Harbour were both true to their word: neither was ever anything but helpful and giving to solve whatever problems led me to their offices. The many distractions and difficulties that arose in my life outside of research were often tackled with my captain, and the modeling effort (and my own understanding of it) didn't get off the ground without Dr. Johnson's discussions. Those discussions led to a very rewarding interaction with one of his expert colleagues. Dr. Ali Mosleh, who sits as a Distinguished Professor and as the Evelyn Knight Chair in Engineering at UCLA, provided me time and wisdom that are greatly appreciated; the simple solution for modeling presented in this thesis is indicative neither of the length of time nor of the depth of knowledge that these two men generously shared with me.

The Production Engineering Research Group, my fellow Pergies, rose to the occasion every time I needed a laugh, a helping hand, or a few minutes' distraction. Looking back, there may have been times when they were overly exuberant with the distractions, but that too helps us learn the lessons of restraint and of moderation! I won't expose specific names to searches, but I will say the distinguished have earned their rewards and my gratitude as they have been given in person. And in the Uhlig Corrosion Laboratory, several scientists worked with and under me in this effort, completing their own work that I hope they publish and from which I hope they benefitted as much as the project benefitted from their contributions.

My support network includes friends and very much the friends that are family. This is not the venue from which to thank them, but their love and confidence certainly warrant much thanks and praise. I have drawn energy and strength from, and tried to work and achieve to the best of my ability for, a wonderful host of beautiful souls. Some are in my life; some lie outside, on the periphery and with a vantage only our own memories can respect and explain, and at least one has moved beyond these shores. All are felt, and for them I feel great gratitude.

1 Table of Contents

List of figures

List of symbols and abbreviations

BLP	Bench Level Prototype
COV	Coefficient of Variance
FEA	Finite Element Analysis
GRP	Glass reinforced plastic
Hp	Horse power
Hz	Hertz, measure of frequency in cycles/second
J	Polar moment of inertia
K_b	Stress concentration factor for bending stress, Mil-H-2189
lbf	pounds of force
M_t	Total bending moment applied, including stress concentrations factors
OD	Outside diameter of shaft
OR	OHIO Replacement, usually referring to the submarine itself
ORP	OHIO Replacement Program, referring to the program office or the program itself
PD	Potential Drop; Direct Current PD (DCPD) or Alternating Current PD (ACPD)
Q	Torsional load on the shaft based on propulsive power
Q_t	Total torsional load used for design purposes; including 20% turning resistance
RC2	A specific clearance fit used in manufacturing, based on OD/ID interface of a shaft/sleeve
RPM	Revolutions per minute, another measure of cyclic frequency
S_b	Bending stress, Mil-H-2189
STD	Specialized Test Device

1 Introduction

The Navy's submarine design community faces a complex problem, and this thesis represents one thrust in a multi-faceted solution to the problem of corrosion fatigue of submarine shafts. This work grows out of and builds upon another thesis performed primarily by the same project team. In broad terms, the first thesis took one attempt at a partial solution as far as it could go, and this thesis begins another solution, in two separate thrusts. This first chapter will provide context by presenting the problem at hand, including a working model of the failure chain under study. The second chapter gives a summary of the solution from the first thesis; the full thesis is included in the appendices for reference. The following two chapters will address development of each of the two thrusts of the current work. The fifth chapter presents the results and lessons learned in this thesis, which can be summarized in terms of major contributions as follows:

- Defined a new process by which laboratory testing can better approximate and predict the steps of corrosion fatigue to provide a better path to modeling
- Developed an initial test device, adopted by the Navy, that can be built cheaply and rapidly to provide S-n curves with in-situ torsion for uncoated shafts
- Designed and built a test device that can recreate propulsion shaft life conditions for shaft life durations and cycles
- Both devices reduce parasitic loads on the load in significant ways

The sixth and final chapter will provide a summary of the current position and the path forward, for future work on this problem.

1.1 Problem: corrosion fatigue failure of submarine propulsion shafting

For the next class of submarines, the OHIO Replacement (OR), the US Navy seeks to design a propulsion shafting system with a 12-year operational interval between scheduled major maintenance. At the end of each operational period, the shaft is taken out of service for refurbishment and then returned to a rotating stock of propulsion shafts. Refurbishment includes removal of all protective coatings and wear sleeves, inspection through non-destructive testing, and repair of all unacceptable conditions (defects and "indications") identified. Coatings and finishes are then replaced, and the shaft is ready for service again. Current shaft designs use a carbon steel shaft with a multi-layered protective coating system and operate for 6 years between inspections. Those inspections (just over 60 to date) reveal signs of environmental attack on the shaft steel, including precursors to cracks and even a few cases with discernible cracks. Having crack precursors and cracks at 6 years suggests that a 12-year inspection system will require improvement of the coating system and/or changes in design and material. The design changes, testing and analysis required to justify doubling of the shaft inspection interval will be neither easy nor inexpensive, but the motivation is great: a 12-year inspection interval would allow the Navy to buy 2 fewer of these vessels, without compromising their ability to meet mission requirements. Designers recently committed to reducing the cost of each of these vessels to

$4.9B, so the motivation to solve the shaft life challenge stands at more than ten billion dollars of savings incentives (much more, as the cost of manning, operating, and maintaining these two vessels would far exceed their purchase cost).

The submarine navy's shaft history is one of suffering from, identifying, and overcoming methods of failure. In essence, a number of failure modes are operating in parallel, but only the mode with the earliest limit on shaft life exhibits itself and becomes a problem. Solving, or extending the life due to this mode tends to reveal the next-most limiting mode, buying some additional life but often not the anticipated or desired amount. This experience with overlapping physics and failure modes is not uncommon in the study and design of components with safe design lives [1]. The iterative method in use has led to a shaft system that has satisfactorily completed more than 60 of the current 6-year shaft life cycles with no failures. Corrosion fatigue is the current limiting mode, and is therefore the failure mode that must be addressed to achieve a longer shaft life.

1.2 Approaches and challenges

Corrosion fatigue is a complex phenomenon[1], enough so that several theories compete to explain the specific physics and reactions involved. Each theory can match and predict some cases and

---

[1] Early work on this project was documented in another thesis, in which corrosion fatigue and the specific issues of the submarine navy are developed more fully. The full document is included in Appendix B, as it is referenced a number of times throughout this thesis.

experiences of corrosion fatigue, but not all. This makes it notoriously hard to model. Predicting failure and adequate performance of component life, when subject to and limited by corrosion fatigue, is most often based on direct testing coupled with empirical modeling. For very large components being designed to last 12 years, full scale and full duration testing will likely only be "accomplished" by placing the actual submarine into service. Information is required much sooner than this to make decisions and to inform the design.

The first choice in strategy is a physics-based model that directly links parameters to a general model, numerically calculates or approximates the physical interactions, and produces predictions or results that can be interpreted in terms of predictions for failure. The academic and research communities have not yet achieved a consensus on the specific physics involved, still being at the stage where several theories compete to explain some data sets. This means there is no direct path yet available to encode or model the atomic and lattice level interactions that a powerful computer code might integrate to predict life experiences at the level of engineering components.

Direct physics modeling being therefore unavailable, the next logical attempt might be to break the corrosion fatigue process down into several steps that can each be modeled at a more macroscopic scale. Indeed, a working model of the corrosion fatigue failure chain can be, and has been, studied in previous work. Component pieces have been associated to literature models at of each stage of the failure chain, through which modeling and predictions might be made possible. This was the first goal of this project, and is documented in Appendix B: Thesis for Engineer's Degree. A brief discussion of the working model of the thesis conclusions follows in

the course of these first two chapters. In short, though, this method was investigated to its limits. Literature simply does not have the correct combination of materials, environments, and analysis to create a reliable model for the kind of life extension that the Navy desires, and the existing data is inadequate to draw conclusions regarding a 12-year shaft system.

With the limited success of these approaches, the next logical step is to turn to experimentation and empirical methods. The best tests would of course match all parameters: size, speed, loading, environment, material, etc. Scaled tests are often an acceptable compromise, although for a 12-year component life, scaling in time would be the first choice. Unfortunately, the complex interactions of physical, environmental, and material properties involved in corrosion fatigue interfere with traditional methods of accelerating tests, a solution that might normally provide adequate data and verification testing in these earlier stages of design. For example, traditional fatigue testing can be performed at higher frequencies to reduce test times and facilitate large data sets. Corrosion fatigue, however, is frequency dependent. At high frequencies, the crack tip of a corrosion fatigue crack may open and close rapidly, acting as a pump for the environment in which the testing is being done. This may remove material and allow fresh exposures, or it may limit the chemical reactions at the tip and the crack surfaces. In either case, these phenomena can invalidate the extrapolation from test conditions to operating conditions. It has also been shown that the transition from pits to cracks is frequency dependent, with a change in transition conditions at about 5 Hz [2]. Since the submarine shaft would typically operate below 5 Hz (300 RPM), this puts an upper limit on the allowable frequency without invalidating the extrapolation, and thereby severely limits the ability to accelerate such tests. One of the key challenges faced by the design team, then, is the difficulty of performing

adequate corrosion fatigue testing, both early on to gather data for analysis and design, and later for verification of the performance of proposed designs or design improvements.

Existing testing machines are not designed to provide the conditions and environment experienced by submarine shafts. The purpose of the propulsion shafting is to transmit torque from the main engines to a propulsor[2] (traditionally a propeller[3] but many types exist), which converts torque to thrust, propelling the submarine. Propulsion shafts are thus loaded in torsion. Propulsors are very large and heavy, and they are located at the end of the shaft. From the last support of the shaft, then, this large weight is cantilevered, creating a bending load on the shaft. As the shaft rotates, the weight of the shaft pulls constantly downward. This means the shaft loading includes fully-reversed, cyclic bending in addition to the torque. A more in-depth description of the loading conditions is provided in section 4.1.2 Loading and stress.

Existing test devices are most common that provide a single loading system, either torsion or bending. Devices that offer combined loading do exist, but they accomplish this by holding one of the loads static or by cycling the loads in conjunction. For the submarine, the fully-reversed bending loading is constant for a given geometry (and therefore class of submarine), while torsion is contingent on the ordered speed and recent speed history. This is the first of several mismatches between desired testing conditions and existing test devices.

---

[2] A propulsor is any device that converts torque into thrust. Propellers are the most common form of propulsor. Recently, the term propulsor has been applied to specific sub-classes of propulsors, deliberately distinguishing new, advanced types from the traditional-though highly developed and efficient-propellers.

[3] Although efficient, it is noted that God himself chose not to install propellers on fish, because (S)He knew there would be problems with the seals!

A large length of the shaft passes through the ballast tanks; these are full of seawater during submerged operations. Though the shaft is coated with various paints and glass-reinforced plastic (GRP), some portions are necessarily exposed to seawater, and others may suffer from coating failure during their lifetime. Clearly, then, the shaft must be considered to have some probability of getting wet, a condition that should then be matched in proper testing. For most existing test machines, test specimen geometries are prescribed, and the application of an environment is not considered. While it is often possible for a clever researcher to design methods to locally apply an environment to at least part of the sample, this is usually a constrained area. It may only allow for a stagnant, small pool of water or other fluid, which does not exhibit many of the properties of a submerged specimen and a larger volume of water. Some machines can take advantage of specially-adapted environmental cells, with slightly larger volumes and an ability to monitor the fluid inside, but even the best combination of machine and cell currently available does not provide the combination of bending, torsion, and exposure needed to replicate the submarine propulsion shaft operating conditions[4].

---

[4] This conclusion comes after a significant number of discussions with testing professionals, Navy subject matter experts, and representatives from companies who specialize in test equipment, including Instron and Systems Integrators. It is a consensus opinion and does not have a specific reference.

1.3 Working model of the corrosion fatigue process

Corrosion fatigue limits the shaft's safe inspection interval, and the submarine community must implement and demonstrate improvements against corrosion fatigue in order to design and to justify a 12-year shaft system. The process under evaluation begins when a shaft/submarine is put into service, with coatings and protective features initially keeping the shaft steel "dry." Corrosion fatigue begins when seawater comes into contact with the carbon steel of the shaft to cause corrosion[5]. The failure chain has a number of other distinct steps, which will be modeled in this thesis according to Figure 1.

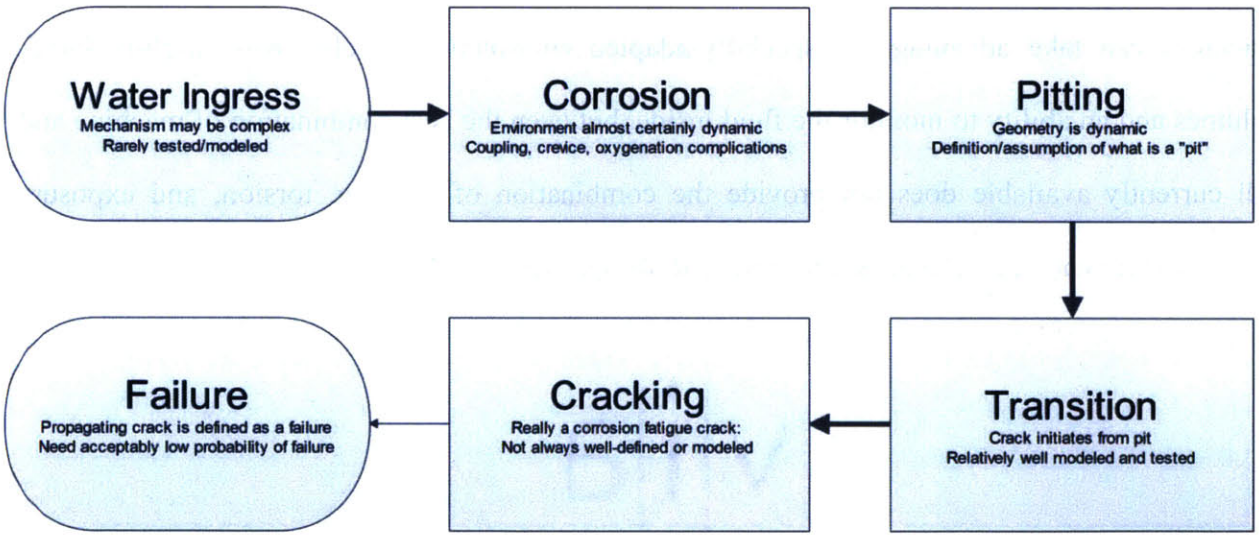

Figure 1: Working Model of Corrosion Fatigue Process

5 A full development, including schematics that detail the regions of concern, is available in Appendix B.

In this figure, "Water Ingress" lasts from the time a shaft is put into service until seawater first accesses the base steel through coating failure or another mechanism. Corrosion is assumed to begin instantly, beginning the second step in this failure chain. As the current shaft is a carbon steel shaft, it is expected to undergo general corrosion when in a seawater environment. This corrosion may appear uniform, but in actuality for mild steels in a corrosive environment, anodic and cathodic areas tend to move around on the surface to create the impression of uniform corrosion often referred to as "general corrosion [3]." Although it is possible for this corrosion to create areas of locally high stress concentrations, more likely is that depressions develop over time where the corrosion has been slightly faster and therefore gone deeper in one region than in the surrounding region, creating a low aspect ratio pit. This pit marks the beginning of the next phase. The pit also creates a stress concentration factor, and the cyclic bending stress now repeatedly acts on this region, as well as the rest of the shaft. Over time, as the corrosion deepens the pit and worsens the surface conditions of all wetted areas of the shaft, small cracks begin to form at areas of high local stress. Figure 2 shows cracks forming from pits in the work of Fang, et al. [4]. Figure 2 (a) shows one typical pit and general surface conditions, and 2 (b) provides a larger scale and more detail, in which a crack can clearly be seen at the bottom of the picture. These images demonstrate the overall roughness and complexity of the corroding surface; clearly the stress concentration factor and local stresses vary greatly across the captured area. Roughness, sharp transitions, and even undercuts are evident. In 2 (c) (which is the same crack as 2 (b) with higher magnification) and 2 (d) the large spacing and shapes of the forming cracks indicate that they are not simply sharp cracks, but rather a combination including corroded and wider surfaces and gaps exacerbated by cracking [4].

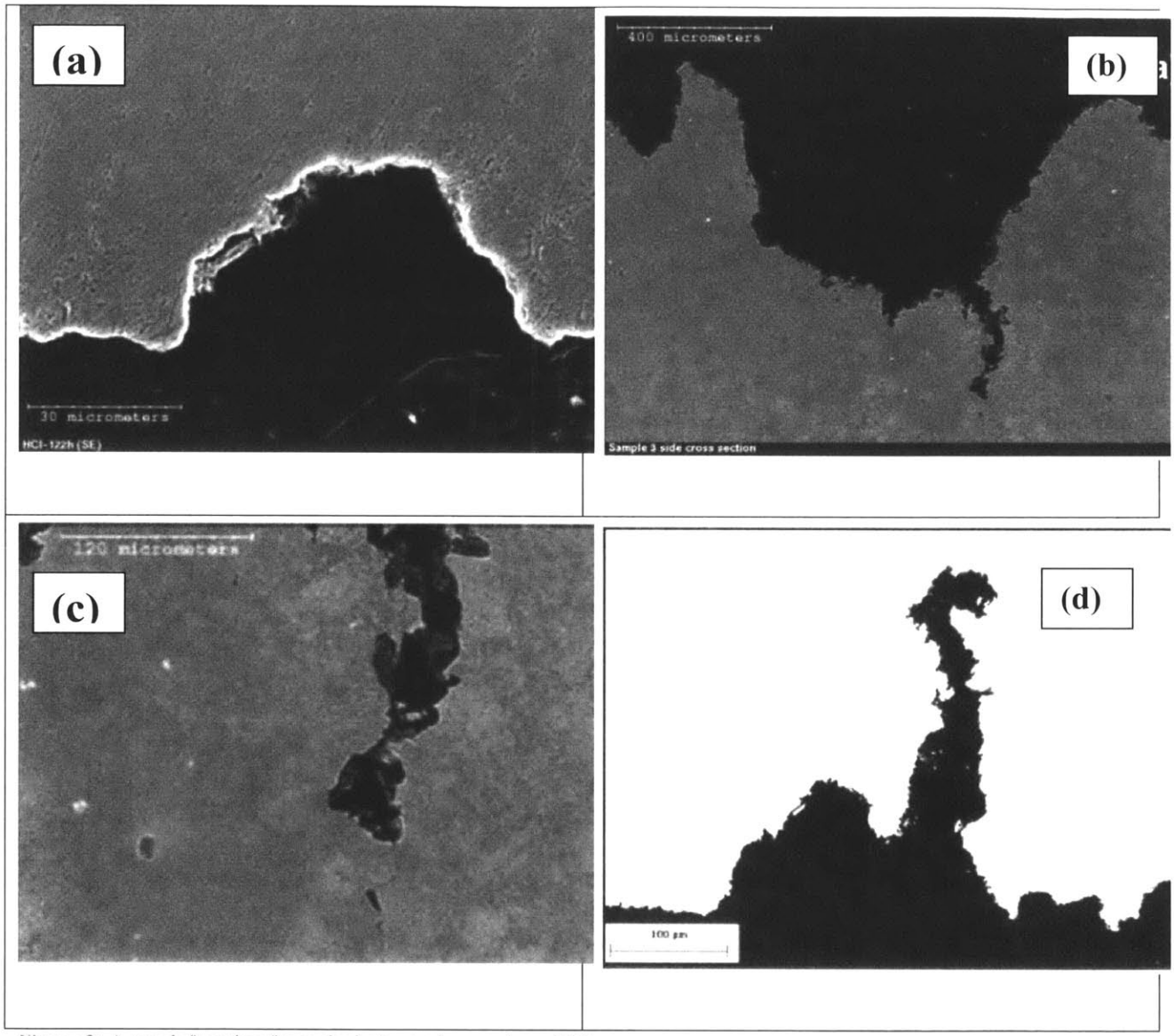

Figure 2: A crack forming from the bottom of corrosion pit [4]

Not every crack that forms grows rapidly; some may be absorbed or blunted by continuing corrosion, and others may act to relieve the local stress that caused them. When one of these small cracks begins to grow in size with each bending cycle, then Transition is said to have occurred, and Pitting has proceeded to Cracking. Figure 3 shows a view of one of the broken

bending samples tested in this project[6]. The corrosion pit has clearly initiated a number of small cracks; but one primary crack has grown and propagated to cause failure of the piece. Note that for other areas of the shaft, many stages of this failure chain are happening simultaneously, though it is only the worst crack that defines the life of the shaft, like the primary crack indicated in this figure. For most crack growth models, the Cracking stage for a submarine shaft is relatively short due to the speed at which a rotating propulsion shaft accumulates cycles. Failure can be defined as a crack beyond a specific size, or as a crack that exhibits itself visually or through vibration that requires premature replacement of the shaft, or even as a catastrophic failure of the shaft. The working definition being used by the designers in this case is "any propagating crack."

---

[6] This picture is from the Master's work done by Stefano Danzi as part of this larger project. Reprinted with permission.

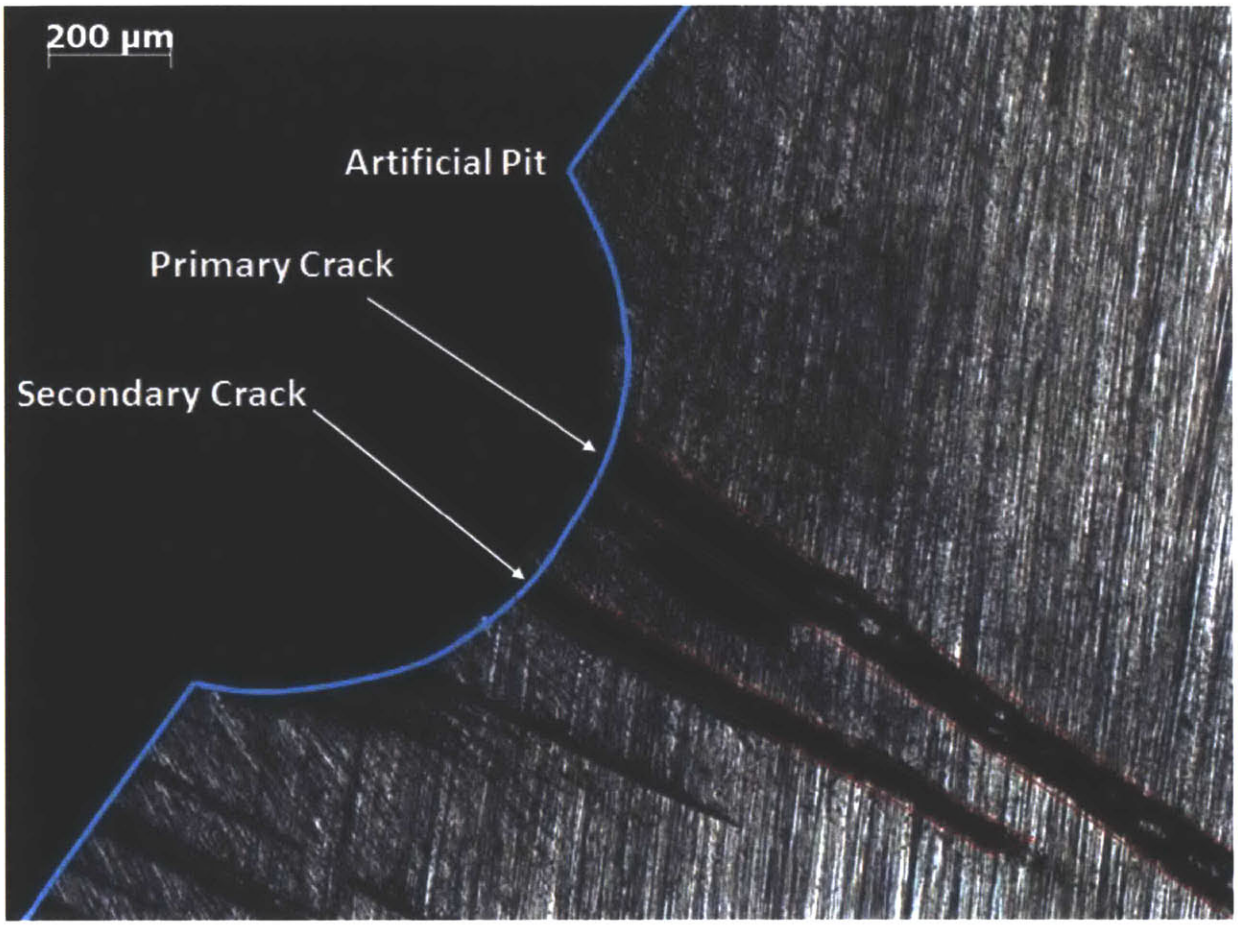

Figure 3: Cracks initiated from an artificially grown corrosion pit

While the conceptual, 6-stage model applies to any material that suffers from corrosion fatigue in a hostile environment, the model presented here is calibrated to match existing inspection data, and therefore the specific distributions are most appropriate for the current shaft system design. That design uses steel that is not commonly used outside of Navy shafting. In fact, the Navy designed and tested a number of steels for shafting, and they have some similarities to commercial grades of steel and some differences. Navy steels are poured to the chemistry specifications in Figure 4:

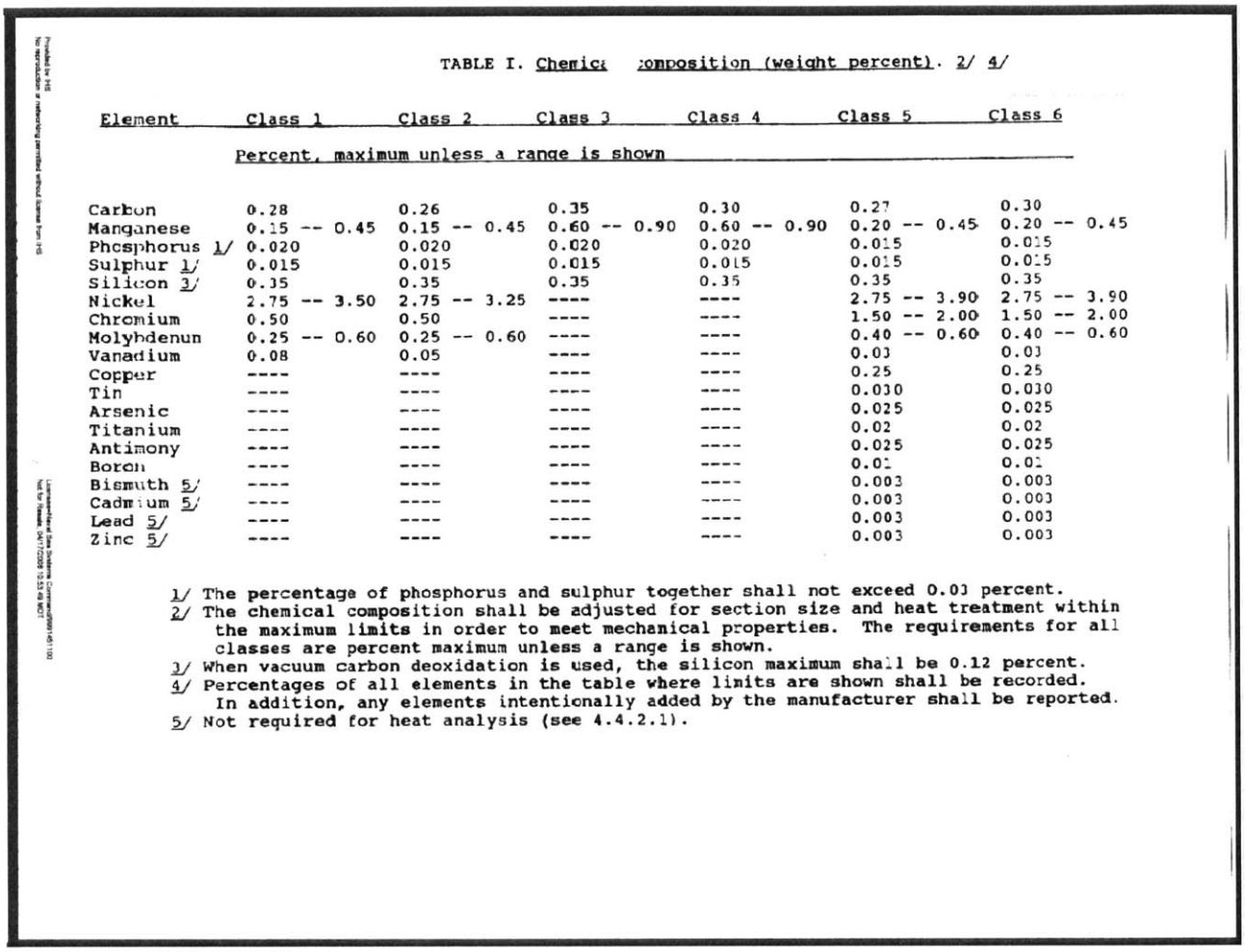

TABLE I. Chemical composition (weight percent). 2/ 4/

Element	Class 1	Class 2	Class 3	Class 4	Class 5	Class 6
	Percent, maximum unless a range is shown					
Carbon	0.28	0.26	0.35	0.30	0.27	0.30
Manganese	0.15 -- 0.45	0.15 -- 0.45	0.60 -- 0.90	0.60 -- 0.90	0.20 -- 0.45	0.20 -- 0.45
Phosphorus 1/	0.020	0.020	0.020	0.020	0.015	0.015
Sulphur 1/	0.015	0.015	0.015	0.015	0.015	0.015
Silicon 3/	0.35	0.35	0.35	0.35	0.35	0.35
Nickel	2.75 -- 3.50	2.75 -- 3.25	----	----	2.75 -- 3.90	2.75 -- 3.90
Chromium	0.50	0.50	----	----	1.50 -- 2.00	1.50 -- 2.00
Molybdenum	0.25 -- 0.60	0.25 -- 0.60	----	----	0.40 -- 0.60	0.40 -- 0.60
Vanadium	0.08	0.05	----	----	0.03	0.03
Copper	----	----	----	----	0.25	0.25
Tin	----	----	----	----	0.030	0.030
Arsenic	----	----	----	----	0.025	0.025
Titanium	----	----	----	----	0.02	0.02
Antimony	----	----	----	----	0.025	0.025
Boron	----	----	----	----	0.01	0.01
Bismuth 5/	----	----	----	----	0.003	0.003
Cadmium 5/	----	----	----	----	0.003	0.003
Lead 5/	----	----	----	----	0.003	0.003
Zinc 5/	----	----	----	----	0.003	0.003

1/ The percentage of phosphorus and sulphur together shall not exceed 0.03 percent.
2/ The chemical composition shall be adjusted for section size and heat treatment within the maximum limits in order to meet mechanical properties. The requirements for all classes are percent maximum unless a range is shown.
3/ When vacuum carbon deoxidation is used, the silicon maximum shall be 0.12 percent.
4/ Percentages of all elements in the table where limits are shown shall be recorded. In addition, any elements intentionally added by the manufacturer shall be reported.
5/ Not required for heat analysis (see 4.4.2.1).

Figure 4: Chemistry data on Navy shaft steels from the Mil Spec [5][7]

By specification, these steels provide the mechanical properties listed in Figure 5. This table also lists the properties of other shaft materials, including Alloy 625, which is used on the bearing sleeves and is addressed in this thesis.

[7] This table is reprinted from Mil-S-23284A(SH), reference [5], with NAVSEA permission

Table I. Mechanical properties of shafting and sleeve materials.

Material Specification	Density lb/in³	*E* x 10⁶ Elastic Modulus lb/in²	*G* x 10⁶ Shear Modulus lb/in²	*UT* Ultimate Tensile Strength lb/in²	*YP* Yield1/ Strength lb/in²	*FL* FATIGUE2/ LIMIT (in air) lb/in²
Steel, forged						
class 1 MIL-S-23284	0.284	29.5	11.75	95,000	75,000	47,500
class 2 MIL-S-23284	0.284	29.5	11.75	80,000	55,000	40,000
class 3 MIL-S-23284	0.284	29.5	11.75	75,000	45,000	34,000
class 4 MIL-S-23284	0.284	29.5	11.75	60,000	35,000	27,000
class 5 MIL-S-23284	0.284	29.5	11.75	105,000	75,000	47,500
K Monel, forged						
QQ-N-286 (UNS N05500)	0.305	26.0	9.50	140,000	100,000 3/	50,000
Nickel aluminum bronze, forged						
ASTM B150 alloy C63000	0.274	17.0	6.40	80,000	40,000 4/	26,000
Ni-Cr-Mo-Cb, alloy 625						
cast (centrifugally): MIL-C-24615	0.305	26.9	10.50	70,000	40,000 1/	20,000 5/
forged:	0.305	30.0	11.50	120,000	60,000 1/	51,000 5/
welded inlay MIL-E-22200 and MIL-E-22200/3 type MIL-IN12 MIL-E-21562 type MIL-EN625	0.305	25.0	9.60	110,000	60,000	25,000 6/
Copper-Nickel (70-30), cast ASTM B 369 alloy C96400	0.323	22.0	8.50	60,000	32,000 4/	13,000
CPP oil, 2190	0.031	0	0	0	0	0
Sand	0.064	0	0	0	0	0

1/ 0.10 percent offset
2/ At 10^8 cycles
3/ 0.20 percent offset
4/ 0.50 percent extension under load
5/ In seawater and air
6/ In seawater (also used for in-air)

MIL-STD-2189(SH)
SECTION 243-1

Figure 5: Mechanical properties of shaft materials [6][8]

---

[8] This table is an excerpt from Mil-HDBK-2189 (SH). Reprinted with permission from NSWC Carderock

2 Existing model from previous work

This thesis continues the work of a previous effort that created a probabilistic model for predicting corrosion fatigue life of submarine propulsion shafts; that effort is included in Appendix B. While the intent was to create a model that would aid in setting safe operating life of a new shaft design with some modest improvements, it became clear that the existing data set was inadequate; specifically the uncertainty was too large for the desired level of confidence in a 12-year shaft life. In fact, the data available gives some high-level indication that the steel in use for shafting lacks adequate resistance to corrosion fatigue in general, and that the only path to a 12-year shaft of similar design and material is to protect the steel with improved coatings and sealing systems. As the Navy is willing neither to guarantee a specific duration of "dry time" nor to gamble on a shaft that fails prematurely if it gets wet prematurely, a need has arisen for improved data with less uncertainty, which will require improved methods of gathering data.

The previous work modeled the corrosion fatigue failure chain of Figure 1 to provide a first order predictive tool. Component models were taken from literature and combined to produce a Monte Carlo simulator. Key details of the distributions are given below. Searches of the literature yielded no cases of life prediction studies that measure and incorporate the time a component is kept dry by coatings or other methods. This is surprising, given the very large industry of coatings alone, but coating studies tend to not account for flexure and fatigue loading, and corrosion fatigue failure studies begin with components exposed to the environment. Therefore, distributions were identified from the literature for the other steps in the failure chain depicted in

Figure 1, and a large number of proposed water ingress distributions were tested. Monte Carlo simulations were used to predict the 6-year inspection results and the proposed water ingress distributions were graded based on the agreement between predicted results and the summary results of actual OHIO class inspections to date. The distribution identified by the metrics in use as providing the best match between inspection predictions and inspection data is detailed in this thesis. The full development, including information regarding other distributions, is in Appendix B.

2.1 Water ingress

In the work of Appendix B, the water ingress distribution is identified though Monte Carlo analysis as the most likely description of the time between when a new or refurbished shaft is placed into service and when seawater penetrates coatings or seals to access the shaft steel itself. Time to water ingress is modeled as a highly skewed Weibull distribution based on the limited data from to-date shaft inspections. The large skew of this distribution indicates that some shafts are experiencing failures very early in service life. This suggests that some shafts may suffer from failure in sealing and coating immediately upon entry into service. This could possibly be captured with a compound distribution, wherein a given percentage of shafts have 0 dry life, and the remaining shafts would experience a more typical Weibull failure distribution, one that is much less highly skewed. Testing on such a compound distribution in the previous work did not significantly improve the metrics in use. With no clear improvement to justify the added

complexity, the compound distribution was discarded. It should, however, be noted that the compound distribution was able to nearly match the selected Weibull distribution, while many other proposed distributions could not. As more data becomes available, and the model is improved, the idea of a compound solution should be revisited.

2.2 Pitting: corrosion, pit nucleation, pit growth and transition to cracking

During the previous work, electrochemical testing was done to obtain data on corrosion rates, and a very strong galvanic couple was identified between the shaft material (carbon steel) and the bearing sleeve (Alloy 625). The Navy's design strategy, to overcome the many challenges of corrosion fatigue, involves defining a safe operating time for a wetted component, given the best information they can obtain easily, multiplying that time by a safety factor to account for uncertainties, and then making attempts to keep the shaft "dry." The bending loading used by the Navy is well below the endurance limit of dry Class I steel, and a dry shaft should have an operational life exceeding the life of the ship itself. This design strategy has a fallacy, though; the assumption that the shaft will be kept dry "as much as possible" tends to allow choices that are detrimental to a wetted shaft. Specifically, where the shaft passes through bearings, a shrink-fit sleeve is added to the shaft to provide a wear surface. The materials used as sleeves are electrochemically more noble than the shaft steel, so if the shaft gets wetted near the sleeve-shaft interface, a galvanic couple is established which accelerates corrosion of the shaft. Inconel 625 is one of the sleeve materials in use, and it was found during previous research that this galvanic

corrosion can result in a doubling of shaft corrosion current (and some outside research indicates that localized corrosion could increase by as much as tenfold [7]). As the submarine designers develop their shaft sytem, the results from this thesis as well as the preceding work recommend a further investigation of specific corrosion rates and an evaluation of the effects of galvanically coupling exposed components.

The operational shaft system is exposed to a very complex environment that may, or may not, be affected by dynamic conditions of flow, chemistry, wetted area, the presence of anaerobic organisms, and many more. Thus, it was not attempted to directly link the corrosion rates measured in the laboratory to the model. Instead, the time from when wetting occurs to when a pit has formed was modeled as a log normal distribution with a mean of 1500 and a coefficient of variance (COV) of 0.05. At the end of this time, a hemispherical pit is assumed to have formed with depth determined from a normal distribution having mean 1.98 x 10^{-3} mm and a COV of 0.50. The growth of this pit is calculated using the equation:

$$\frac{2}{3}\pi\emptyset_k^2(a^3 - a_0^3) = \frac{MI_{p_0}(k)}{nF\rho}exp\left[-\frac{\Delta H}{RT}\right]t \qquad 1$$

In this equation, the initial pitting current, I_{p0} (k), is a function of k, the number of constituent particles initiating a given pit. This value is taken from a Pareto distribution with shape parameter 1 and scale parameter 4. $\emptyset_k$ is the aspect ratio (1 for this thesis), a is pit depth, a_0 is initial pit depth, M is molecular weight, n is the valence, F is Faraday's constant, ρ is the density,

ΔH is the activation enthalpy, R is the universal gas constant, T is temperature in kelvin, and t is time [8].

The depth of the critical pit that transitions into a crack is modeled as a normal distribution with mean of 0.5 mm. Rearranging equation 1 to solve for time, the time to grow this critical pit can be calculated as:

$$t_{pg} = \frac{2\pi nF\rho}{3MI_{P_0}(k)}(a_{ci}^3 - a_0^3)e^{\Delta H/RT} \quad (2)$$

This set of calculation yields a time in days that encompasses the phases of "corrosion," "pitting," and "transition."

2.3 Cracks: crack growth and failure

Adding the dry time to this time gives the time from a shaft being placed in service until the time that this shaft has a defect that an inspector would categorize as a visible crack. Crack growth follows a Paris Law:

$$\frac{da}{dN} = C(\Delta K)^m = C\left(\Delta\sigma Y\sqrt{\pi a}\right)^m \quad 3$$

Here, a is the crack size, N is the number of cycles, and ΔK is a range of the stress intensity factor, or in the alternate form $\Delta\sigma$ is the range of stress amplitude, and Y is a geometry-dependent constant (dimensionless). C and m are crack growth parameters, in this analysis established by estimating the average time between transition and inspection, and setting these parameters to grow visible cracks approximately the size of those reported (anecdotally) in inspections, about 1 inch.

2.4 Summary of initial model

The full model is compiled in Appendix B, section 3.0 on Research Methods. Justification for each of the component parts is in section 2.0 on existing models. These selections and the above required calculations are summarized by the model depicted in Figure 6:

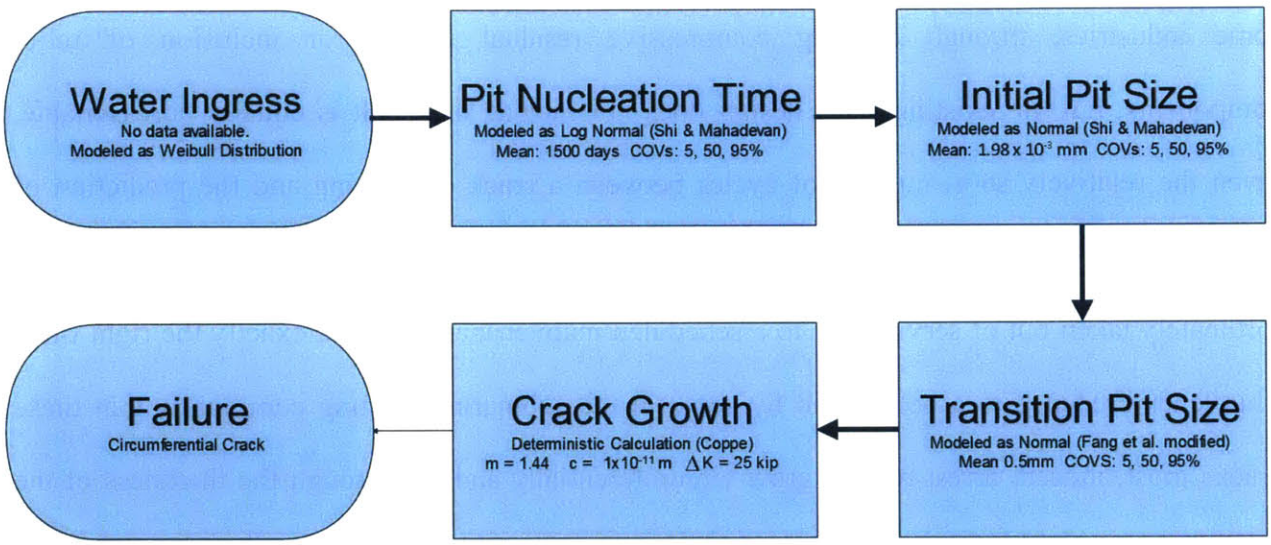

Figure 6: Corrosion fatigue as modeled in initial work

This model is then used to analyze the required water ingress distribution in order to get similar inspection results on a shaft with a 12-year inspection cycle to the existing inspections on the OHIO shaft with the 6-year inspection cycle.

2.5 Major conclusions of previous work

The analysis done with the previously developed model strongly suggests that a 12-year shaft life with the existing design is unlikely. Based on having some cracks at 6 years, and most shafts progressing through the failure chain beyond their initial dry time, it is unreasonable to believe that these cracks will not grow to failure in another 6 years, short of an imposed or as yet unknown crack growth arrest condition or mechanism. Such a condition has been enforced in some industries, through creating compressive residual stresses or inclusion of relief components, but the existing shaft design does not include these. It is equally unreasonable, given the relatively short number of cycles between a crack developing and the prediction of failure, that each crack discovered was growing at the predicted rate but that the shaft was fortunately taken out of service due to a scheduled maintenance period at exactly the right time. This lends credence to a belief held by some in the submarine shafting community that these cracks must, indeed, arrest or else grow circumferentially and not through the thickness of the shaft. However, as cracks in general are not desirable, and as the Navy does not desire to gamble on an unknown arresting mechanism for crack growth, further study of cracking in Navy shafts has been left for future work, with the focus on eliminating or greatly delaying their initiation.

One complicating factor for modeling and predicting shaft life is a general lack of prototypic data. The majority of the data available and in use by navy designers comes from S-n curve development under several conditions, and that information is very old. In this type of testing, samples are attached to a fatigue machine and run until they fracture, often exposed to some

seawater environment through a variety of mechanisms. These data points span the time from wetting to failure (initiation plus propagation), and they do not well inform the component parts of a predictive tool based on the failure chain depicted in Figure 1; nor do they provide any information on the dry time provided by coatings. A purely empirical strategy, which such S-n data would inform perfectly, would need to model failure as a function of control traits such as material, stress, environment, frequency, coatings, and other test parameters. While useful, this strategy is not desirable due to the predictions being limited to very specific geometries and parameters, which may not be indicative of operational situations, nor of future designs.

In short, more and better data is required, specifically information on the effectiveness of the coatings and the average time to water ingress as well as more detailed information on the conditions and times for transitions from phase to phase. The current model relies on literature distributions that are the best selections from available sources, but the materials and processes are not always a perfect fit for the propulsion shaft. It is desirable to develop a more complete submarine shafting database and to update the model.

As a first step, this thesis updates the model with the capability to accept and incorporate new data as it becomes available. In order to address concerns with the accuracy of the data, as well as the previously mentioned concerns with how the available data coincides with that needed for the model, this thesis investigates the application of more sophisticated detection techniques to existing test devices, and it develops new test devices better suited for the submarine shaft application.

3 Data available using or adapting existing test devices

Much of the information desired to make design decisions for the ORP shaft can be obtained from existing test devices and techniques, with slight modifications. This section details the techniques pursued, accomplished, and still desired.

3.1 Bending fatigue

One common design for bending specimens provides a uniform bending load throughout a portion of the specimen. A picture of a typical specimen is shown in Figure 7. In these specimens, the large base is clamped into a vice affixed to a test machine. The head at the other end of the specimen is also clamped into an arm that reciprocates, often through use of a rotary device and an eccentric cam. This design matches its geometry to the point of load application on a test machine; the sides of the neck region visible in the part drawing meet at a point (often just off of the physical specimen) that must align with the point of application of load.

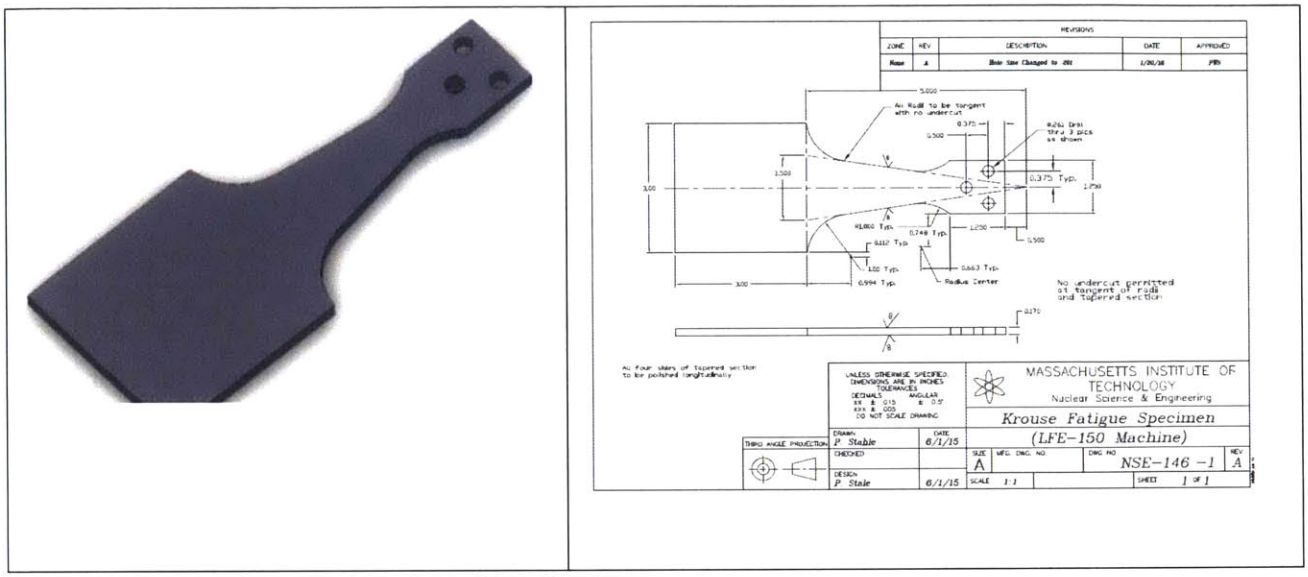

Figure 7: Bending specimen solid model and part drawing

Treating the test machine load as a point load, the moment created at any point, x, measured from the loading point, is

$$M = Px \tag{4}$$

At that point along the length of the neck, the width of the piece can be expressed as

$$W(x) = x\left(\frac{L_{overall}}{W_{overall}}\right) \tag{5}$$

and the stress can be calculated

$$\sigma_{bending} = \frac{My}{I} = \frac{Px\left(\frac{t}{2}\right)}{\frac{1}{12}x\left(\frac{L_{overall}}{W_{overall}}\right)t^3} = \frac{6PL_{overall}}{W_{overall}t^2} \quad (6)$$

This final expression is independent of the distance down the neck, x, which means that for this design, the bending stress is constant throughout the neck region, and can be readily calculated based on applied load. Outside of this neck region, cross-sectional areas are larger, and stress is therefore theorized to be lower, ensuring that the break will happen in the neck, at a known stress. Many factors complicate this, including clamping forces, fretting damage, misalignment of parts or of the specimen, and others. However, proper procedures can control many of these variables to provide reliable test settings and results.

In many cases, including the machines used in this thesis, a specific deflection is set vice a required load. The deflection is calculated based on the desired stress or load, and can be directly set and measured as part of specimen installation. These are referred to as constant deflection machines and/or tests.

Such machines are routinely used to develop S-n curves for materials, and the widely accepted minimum acceptable method for generating an S-n curve for design purposes is to obtain three data points at a single high stress, three at a single medium stress, and three at a single low stress. The low stress may be defined by a "runout" or "fatigue limit," meaning no fracture is observed

after an acceptably large number of cycles. This value defines, for the testing being done, the fatigue limit or the endurance limit, depending on the material[9].

Using these machines to create an S-n curve for Navy Class I steel is the first goal of the testing program. A dry S-n curve provides valuable information to designers, although it does not specifically inform the model that this thesis seeks to create, of a shaft undergoing corrosion fatigue. Therefore the second goal is to perform testing and to create similar curves that more closely mimic the shaft conditions. Ideally, a set of (at least) nine data points can be obtained for samples that have pits, and another for samples that are exposed to a seawater environment, and finally a set that are both pitted and wetted.

From the standpoint of modeling corrosion fatigue failure using purely empirical techniques, this constitutes a full factorial design of experiments for the three variables: pitting (2 levels pit/no pit), wetting (2 levels wet/dry), and stress (3 levels hi/med/low), with the single output of time to failure. Note that the working model considers the time to failure of a shaft to be the sum of times for several intermediate steps, and this empirical treatment provides very little information to inform the working model's components. Nevertheless, an empirical model may prove useful in determining the magnitude and interactions of the listed factors, and although it is not pursued directly in this thesis, it could be immediately undertaken.[10]

---

[9] Steels and some other materials have a stress below which no failure is ever observed, defined as the endurance limit. Aluminums and many other materials have no such threshold behavior, so designers define a fatigue limit as above, an effective limit of design life cycles that needn't be surpassed, commonly 5×10^8 cycles [9].

[10] Throughout this thesis, "working model" refers to Figure 1and the 6-stage model it portrays. "Empirical model" refers to a model that is based solely on the outcomes of experiments, usually using a single output linked to a set of input variables, losing intermediate data like time to wetting or probability of transition.

This thesis uses two different machines. The first is a constant speed machine with a load capacity of 40 pounds (CS-40). This machine runs at 1800 RPM and is not suitable for wetted samples or the application of environmental cells, so it provides the bulk of the data for dry samples, both pitted and unpitted. For lower stresses, the large number of cycles to failure creates some challenges for this old design. Fretting at the clamps causes some samples to break at the root of the sample, vice in the uniform bending section. Generally accepted practice is to discard this data, as the stress is not known in the way that it is for the constant-stress region in the neck, due to the complexities of the discrete geometry and uncalculated stress concentration factors where the crack initially starts. It is also common that surface condition of the samples become an issue at lower stresses, wherein cracks can initiate at a multitude of flaws smaller than the specified surface roughness, creating results that are more dependent on sample surface condition than on material characteristics. S-n data exhibits significant scatter in general, with especially large variation at low stresses [9]. The presence of the artificially grown pit on pitted samples works to manage these issues somewhat.

The larger machine, a lifecycle tester with a capacity of 150 pounds (LFE-150) can be reasonably run at speeds down to about 90 RPM (there is some dependence on the load in use) and allows for larger samples, both in terms of length and thickness. These samples are much better suited to the application of an environment, and several techniques were attempted before a simple glue barrier proved to be the most advantageous.

In the LFE-150 sample configuration, a sample is prepared per the drawing in Figure 7 and then a pit is grown if required for that test. A "moat" of RTV glue is then created. If the sample is a

pitted and wetted sample, then the moat is established to put the pit roughly in the center, and a pool of artificial seawater fills the bounded region. For an unpitted sample, the same size and location moat, along with seawater, provides for some control in terms of exposed area and corrosion rate. Both conditions are depicted in Figure 8.

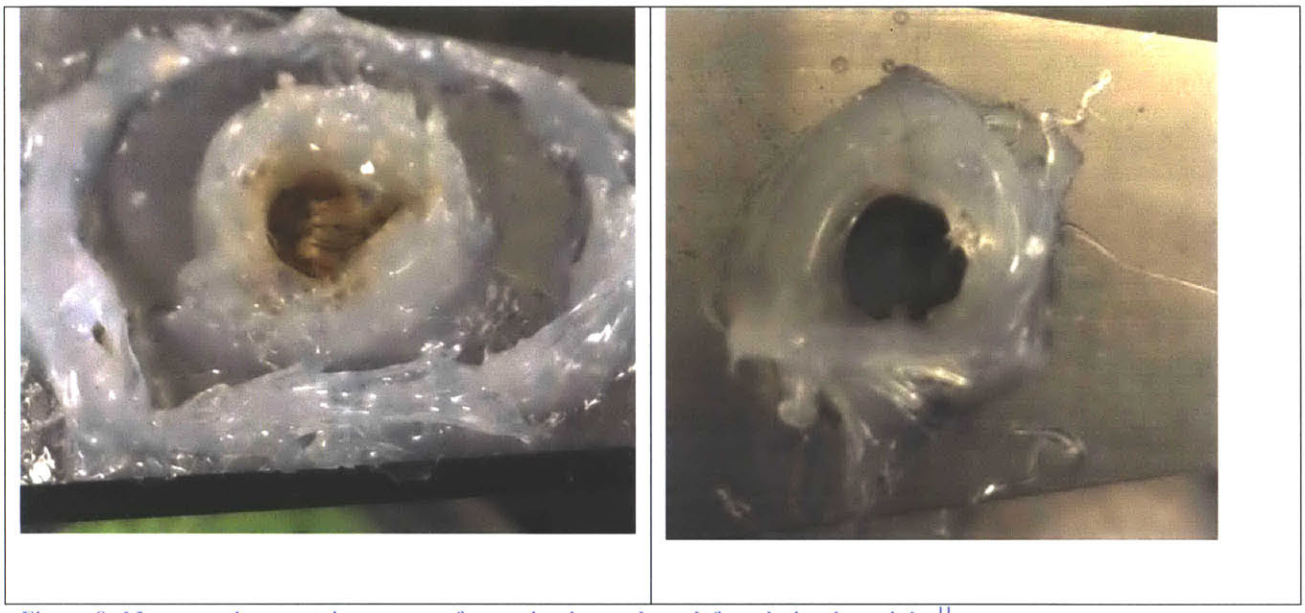

Figure 8: Moats used to contain seawater for unpitted sample on left and pitted on right.[11]

These fatigue tests suffer from a set of common problems. First, for even very well-controlled test specimens, variability can be quite high, as was detailed in the earlier work from this project in Appendix B, section 4.3. Second, as the systems are not designed to accept environments, a number of compromises are made in order to obtain at least preliminary data. The small amount

---

Note the backup moat was left off in later tests when it proved to be unnecessary. Water was only loaded into the inner regions of roughly similar size[11]

of seawater does not provide a robust environment with circulation and mixing as may be available for larger cells similar to the one found in Figure 9, below. The cell depicted is a commercially available cell for an alternate type of fatigue tester that uses a round and usually tapered specimen.

Figure 9: Commercially available corrosion cell for rotating beam fatigue tester

Second, the consistency of stresses depends on a number of factors that can be difficult to control, such as precise thickness of a sample, alignment of the sample in the test device, temperature changes, and others. Although precise measurements of thickness could be made, the challenge of adjusting the deflection of the device to precisely match each thickness

overcomes the benefit, especially in light of the expected high variability under even perfect conditions. In this case, each stress is calculated based on the measured thickness, without corrections for the other listed conditions.

The Navy has some historical data on fatigue/corrosion-fatigue life of shaft steels. There are at least two reports that detail some version of testing similar to that done in the current thesis. There is a debate in the Navy community about the relevance of the existing data, in that some of the methods have now been called into question. The Navy is beginning a course of testing for comparison and validation, and that work will not be addressed here. In short, though, in some cases water from a local river was dripped onto samples while being tested on a fatigue device; in some cases samples were soaked in seawater (source unknown to this thesis team) and then tested on a fatigue tester (anecdotally these all broke "immediately"), and in most cases the frequency was appropriate for fatigue testing but not for corrosion fatigue testing, around 30 Hz.

In all cases, the Navy fits the final data to the best fit equation:

$$\log(S_a - S_e) = m \log N + b \quad [10]$$

7

Where S_a is the maximum nominal stress amplitude in psi, S_e is the endurance stress (asymptote of best-fit curve at N=∞), m is the slope, b is the intercept, and N represents the cycles to failure. The Navy reports for Class 5 shaft material are the most comprehensive and contain the most

reliable data, and they list the regression information for Class 1 steels, though the data is not supplied [11].

For Class 1 data, the Navy best fit curve parameters are listed in Figure 10. This data also confirms one of the troublesome traits of designing steels against corrosion fatigue: an endurance limit no longer exists when steel is operated in a saltwater environment.

TABLE 3 - RESULTS OF FATIGUE AND CORROSION FATIGUE TESTS OF NICKEL-MOLYBDENUM STEEL (MIL-S-23284, Class 1)

RPM	Environment	Best-Fit Curve Parameters				Sa, Fatigue Strength at N cycles,(ksi)*		
		Slope (m)	Intercept (b)	Endurance Stress S_e(ksi)	Correlation Coefficient (r)	10^6	10^7	10^8
1725	Air	-0.1391	5.0793	40.0	0.91	57.6	52.8	49
960	Saltwater	-0.4193	7.0414	0	0.99	33.5	12.8	4.9
645	Saltwater	-0.3994	6.8896	0	0.99	31.1	12.4	4.9
Combined 960 and 645 rpm		-0.4077	6.9532	0	0.99	32.1	12.6	4.9

*Calculated from best-fit equation.

Figure 10: Navy data excerpted from Navy Report[12]

[12] This data is an excerpt from a report detailing the performance of new and refurbished Navy shafts, reference [10], though it references and takes this data from the study documented in the "Link Report," which does not provide this specific table. The Link Report is reference [11]

The ultimate goal of the test program will be to inform designers, initially in order to make a selection among Navy shaft materials. For reference, the following graph is a good representation of the utility of the available S-n curve data, although it would ideally include information on pre-pitted samples and multiple metals. This thesis is providing information on Class 1 steel, and the Navy is testing several classes of steels in addition, intent on using the techniques and machines developed in this thesis.

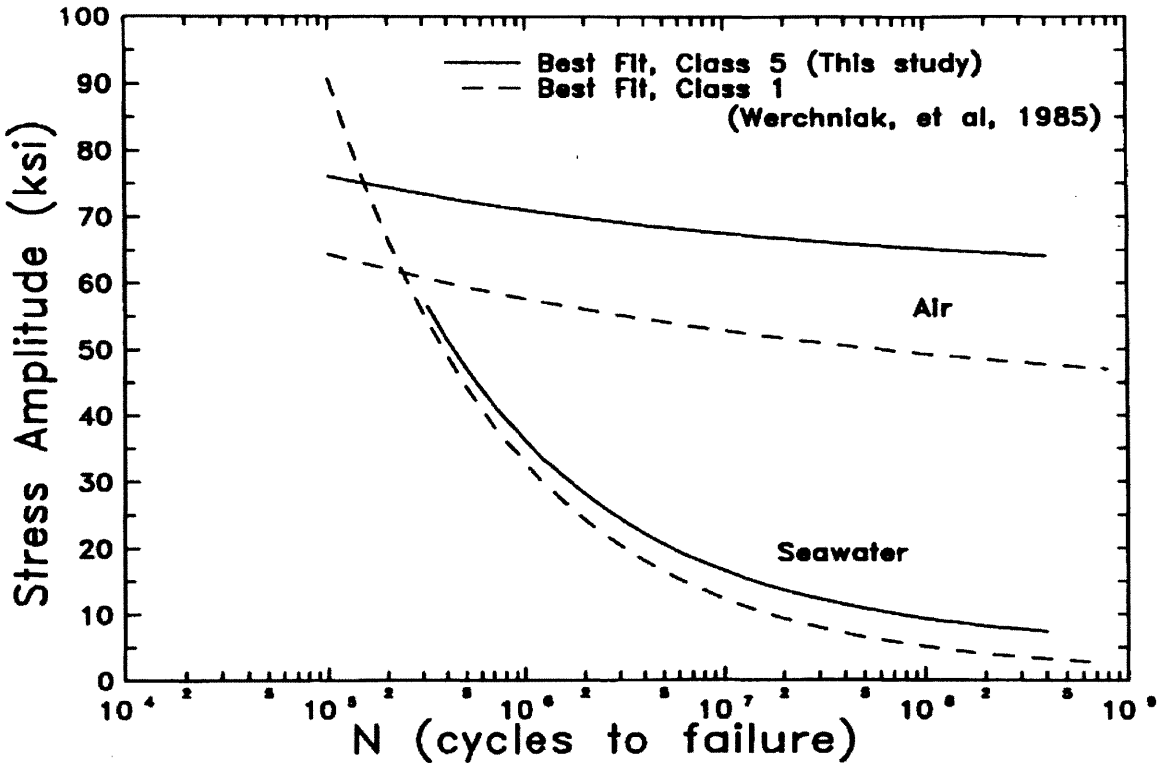

Figure 11: Navy comparison curve between materials in air and seawater [11][13]

[13] This graph appears in the Link Report, though the data can only be found partially in the "Gross Report", which is reference [34]. Reprinted with NAVSEA permission.

3.2 Torsion fatigue

The LFE-150 test bed can also be adapted to perform tests in cyclic torsion. Different components are required, though these are available, and a set has been obtained for this project. The torsion device comes with an integrated load cell, and it is outfitted with an interface for data collection. A set of clamps must be manufactured to interface between the purchased torsion attachments and the samples themselves, and this has been accomplished. Once reconfigured for torsion, the test bed clamps a cylindrical sample at one end and uses the reciprocating plate that provided bending loading for the work detailed in Section 2.1 above to manipulate a loading arm. This arm is attached to the other end of the cylindrical sample, and provides a torque based on the length of the arm (fixed) and the deflection setting of the machine. Cyclic torsion is less applicable to the submarine shafting system. Additionally, the historical Navy design data has never taken torsion into account, so no comparison can be made. For these reasons, S-n curves are not obtained for torsion in this thesis.

3.3 Potential drop techniques

Potential Drop (PD) techniques have been in use in non-destructive testing for several decades [12]. Both alternating current (ACPD) and direct current (DCPD) techniques exist and have been approved for use in many industries [13]. Each has benefits and challenges. Their operations are similar; essentially a current is forced through the test sample, and very precise

measurements are taken to measure the potential drop across the damaged region-typically a growing crack. Properly calibrated, these techniques can give accurate non-destructive measurements of crack size, and therefore can be used to gather information on crack growth per unit time, per cycle, or other metrics. They are primarily used for detecting and measuring cracks [13].

In order to get accurate enough data to distinguish between noise and signal on a large sample actively being stressed in a fatigue device such as the LFE-150, much more information is required, as well as possibly requiring several methods to condition and filter the signal. As one example, the standard test procedure states that it may prove necessary to pause the test to take data (specifically ACPD may require data points taken only at the maximum amplitude of the stress cycle) [13]. For this thesis, the goal is to establish proof of principle for the use of DCPD on the LFE-150 by insulating the vices and grips, and to investigate the quality of signal from a pit, a growing pit, and a growing crack. Ideally, the system can be calibrated to detect the step change in potential drop when a crack first forms from a pit, but this thesis intends to demonstrate that there are readable changes, leaving refinements to exploit this information for later work.

Once proven, these techniques would be employed in a two-step process. First, coated samples would be tested, either bending samples on a traditional fatigue device or shaft samples on one of the machines developed in this thesis. In either case, the sample would be isolated electrically, with the first lead of the current supply attached to the sample, and the other attached to, it is envisioned, the tank or environmental cell. Similarly, the first lead in the measurement of the

potential drop would be on the sample, and the other on the tank, or possibly in the electrolyte. Here the goal is for the coatings to insulate against any current path, with the first detection of current marking the failure of the coatings; this would mark a first-of-its-kind capability and would provide the previously unavailable data of water ingress times and eventually distribution.

The second step of the process would be for a sample (possibly the same sample) to be monitored by PD while corrosion and then transition occur. Similar to the current set of traditional tests, the environment may remain, or it may be removed during the measurement of cracking, based on the needs for fractography, time to failure, or other data.

4 Test device design

Given the limitations of existing test devices already detailed in this thesis, and given the critical need for information specific to Navy shafting materials and usage, this thesis provides the designs and prototypes for a new test device that better replicates the submarine propulsion shaft environment and operations.

4.1 Requirements and design space

These devices are intended, initially, for immediate use by the Navy in obtaining needed data on submarine propulsion shaft corrosion fatigue behavior. As such, speed, loading, and environment are all chosen to match as closely as possible the operating conditions of the submarine. Due to the current interest in long-lived shafts, these machines need to test shafts to a high number of cycles. Whenever possible, design decisions also provide for flexibility and for expanded future use both within the navy and also by other industries. These designs use (but don't specifically require) a steel test shaft, and it is desired to allow for a collar or sleeve of another material to match the wear sleeve of the shaft if possible.

4.1.1 Number of cycles

Corrosion fatigue requires a cyclic stress. The gravitational load applied by the heavy, cantilevered propulsor imposes a bending stress on the shaft. As the shaft rotates, the fibers of the steel experience tension when they are at the top of their rotation, and compression when they are at the bottom of the rotation. Therefore, the bending stress alternates, progressing through a full cycle from maximum tensile stress to maximum compressive stress for each location on the perimeter of the shaft during each rotational cycle, regardless of the rotational speed of the shaft (within the limits of whirling at very high rotational speeds, which these shafts do not reach). This provides the cyclic stress that drives the corrosion fatigue problem, and one of the most important variables in determining the potential level of damage that a shaft must survive is the number of fatigue/corrosion fatigue cycles that it must undergo.

To estimate the number of bending cycles in the desired shaft inspection interval, it is reasonable to assume an average frequency of rotation. At low speeds, the propulsion shaft may only be rotating at a few revolutions per minute (RPM). At maximum (flank) speed, the propulsion shaft is typically operating at up to a few hundred RPM. The mission profile for this type of submarine tends towards slower speeds, so selecting 120 RPM (2 Hz) as the average speed to estimate total number of cycles is conservative but representative[14]. In terms of time, a ten-year span of operations can be converted as follows:

---

[14] Note also that 2 Hz provides margin to the previously-argued upper limit of 5 Hz.

$$10 \text{ years} = 3650 \text{ days} = 87{,}600 \text{ hours} = 5{,}256{,}000 \text{ minutes} \quad (8)$$

And at 120 RPM, a total number of cycles for one shaft inspection interval would be:

$$5{,}256{,}000\ minutes\ x\ \frac{120\ rotations\ (cycles)}{minute} \approx 6.3\ x\ 10^8 cycles \quad (9)$$

This number assumes the shaft is in continuous operation for the entire 10-year period, which is of course not true. Nominally, these submarines are at sea for about 75 days, and then in port for about 30 days of maintenance and crew turnover[15]. Making assumptions on the amount of downtime, and allowing for up to 12 years of life, this estimate varies between 10^8 and 10^9 cycles. For this research, $5x10^8$ cycles was chosen as the goal.

From a testing perspective, then, duplicating the 120 RPM speed, a non-accelerated test duration of:

$$5x10^8 cycles\ @\ 120\ rpm = \frac{5x10^8 cycles}{2\ cycles/second} = 2.5x10^8 seconds = 7.9\ years \quad (10)$$

Therefore, the desire is to design a test device that could be put into operation and reliably run for a period of 8 years. Additionally, the test device should be capable of running at higher RPM

---

[15] Other classes of submarines have more varied schedules, based on mission profile, and typically less regularity in their deployments, as well as much longer deployments, but the overall average number of operational days per year is slightly lower.

in order to accelerate testing within the constraints dictated by environmental variables. As pointed out above, as the frequency increases there is a danger of underestimating the environmental effect due to inadequate time for the environment to act on the material during a cycle, and this interaction must be managed, but the capability to run faster should be part of the design.

Air bearings, though not explicitly required, are believed to be the most reliable method of applying support and loads to achieve both the bending stress and high number of bending cycles required. Sizing the bearings is a function of the required lift/loading and the supply pressure of the air. Using porous graphite bushings, the entire cylindrical area of the bushing can pass air flow. Looking at the projection of this air that actually provides lift to the shaft, it is sufficient to calculate the lift using an efficiency factor [14]:

$$F_{lift} = P_{supply} Area_{projected} \eta \quad (11)$$

Or, in terms of the diameters for the bushing and shaft,

$$F_{lift} = P_{supply} D_{shaft} L_{bushing} \eta \quad (12)$$

For example, with a ½-inch shaft, a 2-inch bearing, a supply pressure of 90 psi, and an efficiency of 0.4, an available lift of 36 pounds is available.

4.1.2 Loading and stress

4.1.2.1 Bending

The document Mil-Handbook-2189 governs much of the design of Navy shafting [6]. Many of the requirements for the scaled tests specimens are derived from this source. Appendix A: Mil-Handbook-2189 Requirements contains a list of the applicable equations and measurements provided in Mil-H-2189. In this document, the Navy specifies a maximum bending stress, after application of appropriate stress concentration factors, of 6,000 lb/in^2. These devices are therefore designed to operate a shaft at this stress level for the cycles described above, although they are also designed to operate at higher stresses for shorter durations to generate S-n data.

4.1.2.2 Torsion

The purpose of the shaft is to transmit torque from the engines to the propulsor, which converts the transmitted torque into thrust. At steady speed, thrust overcomes the resistance of the ship as it moves through the water, while accelerating requires additional thrust. Resistance of a body to motion through a fluid can be expressed by [15]:

$$R = C_D \rho_f A U^2$$

Where C_D is a coefficient that defines the drag on the body, ρ_f is the density of the fluid, A is the surface area of the body (sometimes wetted surface), and U is the speed of the body. During design, volume ($\forall$) is often defined much earlier than the final shape, so representations of the area are related to volume through a coefficient. For a given vessel in a given fluid, the drag coefficient and fluid density are both constants, which can be combined with the volume-to-area coefficient to create a single constant, K. Now the force that overcomes the drag resistance can be viewed (at steady speed) as:

$$F = R = K\forall^{2/3}U^2 \tag{14}$$

But power is force times distance over time, meaning power required to propel a vessel requires an additional speed (U) term, and can be written:

$$P = K\forall^{2/3}U^3 \tag{15}$$

Thrust therefore varies with speed. This relationship, called the powering curve of a submarine, is cubic in nature [15], and means that thrust, and thereby torque, vary significantly over the range of velocities. Since a submarine is a warship at heart, it is usually designed to have its full power and torque available whenever called upon by the situation, so a conservative design might assume high torque at all times, although this is not representative of operations. After discussions with the sponsor, it was decided that the test device should be designed to have full torque capability, and the torque (or variable torque profile) applied for specific tests could be dictated at a later date.

To establish that torque loading, openly available information declares that the OHIO engines are rated for 60,000 shaft horse power [16]. Using this torque, the assumed speed of 120 RPM, and the equation:

$$Power = \frac{Force\ x\ Distance}{Time} = \frac{\left(\frac{Torque}{Radius}\right) * \left(\frac{Radius\ x\ 2\ x\ \pi}{Revolution}\right) * Revolutions}{Minute}$$
$$= 2\pi * Torque * Speed$$

16

Solving for torque and converting from Horse power (defined as 550 ft-lb/s), torque on the shaft under these conditions is 3.15 x 10^7 in-lbf, which the Navy guidance in Mil-H-2189 directs be increased by 20% for the added torque from the resistance of the water on the shaft while turning, for a torque value of 3.78 x 10^7 in-lbf. That shaft is large, at about 21 inches in OD and 11 inches in ID. Maximum shear stress in a circular shaft is dictated by

$$Tmax = \tau max\, J / R$$

17

Where T_{max} is the maximum torque, τ_{max} is the maximum shear stress, J is the polar moment of inertia of the shaft, and R is the radius of the shaft. Polar moment of inertia for a solid shaft of diameter D is given by:

$$J = \frac{\pi D^4}{32}$$

18

And for a hollow shaft of outer diameter OD and inner diameter ID by:

$$J = \frac{\pi(OD^4 - ID^4)}{32} \text{ [17]}$$

19

These equations calculate the OHIO maximum shear stress to be 2.19 x 10^4 psi, which is the scaled value to be matched during testing of a test shaft. For a test shaft of ¼" OD (and solid), this requires a torque of 67 in-lb at 120 RPM, achievable if one uses about a 1/8 Hp motor. Based on the continuous loading in this application, a motor rating that provides a torque factor of safety of 2 is appropriate. With this in mind, a list of possible test shaft diameters, necessary torques and approximate recommended motor sizes are listed in Table 1.

Table 1: Trend of motor sizes for various test shaft diameters

Test Shaft OD (in)	Torque Required (in-lb)	Recommended motor size (Hp)
0.25	67.3	1/4
0.375	227	1
0.5	538	2
1.0	4300	15
2	34400	100

A cubic relationship between shaft size and required torque is immediately evident and has dramatic effects on sizing components for the test device. For reference, during the evaluation of

the upper end of possible shaft sizes, a 15 Hp motor was quoted for potential use. It weighed 297 lbs and was rated to draw 44 Amps of 440 Volt, 3-phase power. Next, a 100 Hp motor was evaluated for this work, rated for ultra-high efficiency at 1800 RPM. It weighed 1400 lbs and was over 3 feet long with a nearly 2 foot diameter. Powering it from a 220 Vdc source, it would have drawn more than 200 Amps. At 1.5 tons for just the motors, it is evident that creating and demonstrating a test device at this scale is impractical, and even the 15 Hp motor is very suspect. Based on this effect, and the relatively low design stress for bending, the required motor torque is the driving factor in sizing and designing the test device. Larger test shaft diameters provide for easier manufacture of sleeves (shrink-or press-fit), in that manufacturing tolerances are less of a factor compared to the required interference fit for a larger shaft compared to a smaller shaft. The torque requirement to balance these competing demands is a machine capable of putting a ½" test shaft under the same torsional loading, in terms of shear stress, as an OHIO class shaft as derived above.

4.1.3 Braking alternatives

While the use of one motor can theoretically provide the torque values listed in Table 1 above to move the shaft, the torque required to turn the shaft against the natural resistance in a test device is much lower than the torque required to turn the propulsion shaft and provide thrust to the submarine. For this reason, some resistance system must be in place to keep the torque applied at the given speed; otherwise the shaft would simply undergo a rotational acceleration. Any

form of rotational brake should be able to provide such resistance. The high number of cycles, however, necessarily rules out several possibilities. Friction brakes, similar to those on standard automobiles, bicycles, and many rotary systems, would be required to operate under constant application and would show problems of wear through such heavy, constant usage. Magnetic brakes, seen on devices that turn bicycles into stationary trainers and on some large rail systems, would not exhibit wear, due to a lack of physical contact. However, they may produce substantial heat and/or require some combination of independent power, monitoring instrumentation, and cooling systems. Several options exist that create friction through the use of small particles. Wear and usage over time might, in these systems, imply that the particles were ground or damaged and therefore became increasingly fine. In this case, they would still provide friction (sometimes more effectively) and thus would not be seen to "wear out." The decision for the first prototype is based on convenience, speed of acquisition, and efficiency in shared parts. The second prototype uses a similar but more efficient system. Braking in each case is provided by a second motor that is driven as a generator.

4.1.4 Environment

Wetting of the shaft can be accomplished a number of ways. Historically, systems that either spray or flow the fluid onto the shaft are common [6]. Some machines primarily intended for dry fatigue testing allow for a static cell to be attached that encases the specimen, or more commonly part of the specimen, in a fluid, though these systems are often relatively crude like the one in

Figure 9. For a variety of reasons, full immersion is preferred and therefore required for these test devices. Several benchtop tests verify that a tall tank with holes that allowed a shaft to pass through could be designed, along with a properly sized pump, to elevate water above the level of the shaft, and this is the system chosen for both designs.

4.1.5 Scaling requirements

One of the goals of this research is to create scaled test articles upon which to perform both accelerated and non-accelerated testing. In every case, care must be given to which scaling laws are most appropriate. As an example, the following scaling laws and effects had to be considered in the design of the shrink-fit specimens for immersion corrosion testing:

Table 2: Example of scaling laws and considerations

Law	Rule	Effects
Exposed areas of two metals	Same ratio as real shaft	• Affects (galvanic) corrosion rate
Stress distribution in shrink fit components	Same stresses as real shaft and sleeve	• Dictates thickness and interference fit • Dictates manufacturing tolerances • May affect corrosion rate

Currently, only cylindrical samples have been tested whenever torsion is applied, with no changes in diameter. For sleeved samples, one of the next appropriate steps, both of these conditions can only be met if the exposed length of shaft is controlled with coatings to match the required area ratio. For coated samples, with and without sleeves, this requirement will not apply (though stress distribution will still be controlling for sleeved samples). In general, the scaling laws in effect must be made appropriate for each specific test and its goals.

4.1.6 Alternative models considered

Three-point and cantilevered bending were each considered, such as the concept illustrated in Figure 12. In this figure, the shaft is supported at each end by an air bearing, while load is applied to a third air bearing at the mid-span point. In this arrangement, the internal bending

moment experienced by the test shaft changes as a function of position along its length [17]. For convenience, such a loading arrangement usually uses a tapered specimen that changes in size proportional to the change in load along its length, such that the bending stress is held constant. Unfortunately, such a tapered specimen vastly complicates the design and application of a sleeve. Three-point bending was eventually rejected, primarily based on this complication.

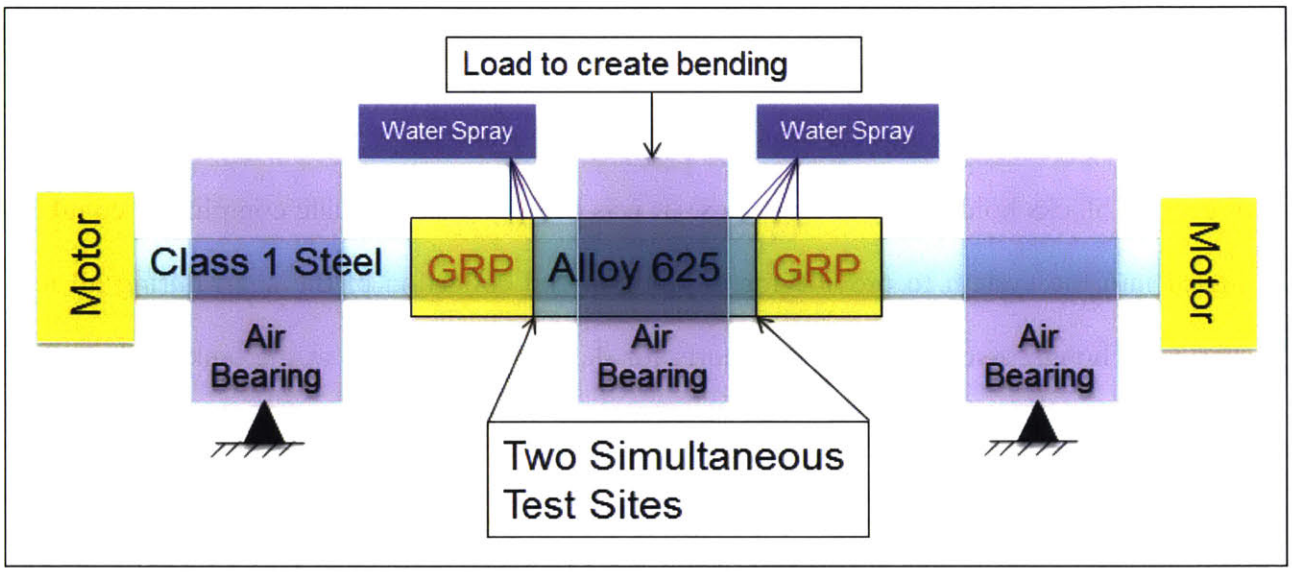

Figure 12: An early concept design, allowing sleeved shafts and side-by-side testing

The use of four point bending subjects the test shaft to a loading that has a length of the shaft where bending load is effectively constant, and therefore highly predictable. This facilitates testing samples of different constructions and geometries, to provide large flexibility. Sleeves, joints, and coatings would be easiest to construct and to apply if a larger section of the test specimen were at a constant loading, allowing for the design of tests with a specific loading and combination of joints and materials. When 4-point bending was initially considered, the desire

was to mount one pair of bearings in the sides of the test tank, seen in Figure 13, in a manner providing adequate compliance to accommodate shaft motions. The inner pair of bearings were planned to be loaded by a hanging weight system that would attach to the bearings using a rocker mechanism which would ensure equal loading on the pair. This arrangement would give 4-pt bending, a fully submerged test shaft, and deflections of the shaft in the downward direction inside the tank. Adequate air supply would ensure that the bearing air would press into the tank from the outside bearings, removing the requirement for additional sealing systems at these joints. The only water-to-air seal required would have been O-ring systems between the tank wall and the blocks holding the air bushings. It was believed that adequate compliance could be designed into the system to provide for the motion and deflection of the shaft during all test scenarios. Though essentially static supports for deflection, the joints at the tank walls would allow the shaft to flex and bend, meaning that under test loads the test shaft would exit the tank, and associate bearings, at an angle. This would, in turn, require that the motors (supplying torsional loading and rotational motion) would have to accommodate an angled shaft, either through adequate tolerances or through a mounting system which could both elevate them and rotate them. With no additional, significant loads on the shaft external to the air bushings at the tank wall, the shaft would be seen to rise in elevation at a constant angle. Under no bending loads, the shaft should be horizontal, and the pivot of the rotor would be on the horizontal axis of the air bushing. Under maximum bending loads, however, the pivot of the rotor would need to be at an elevation to match the shaft rise, as well as at an angle to match the shaft angle, or able to accommodate these through a combination of deflections and tolerances. This was seen to

greatly complicate the mountings external to the test tank, and it was determined that a rigid system that combined both the bending and torsional loading systems was preferred.

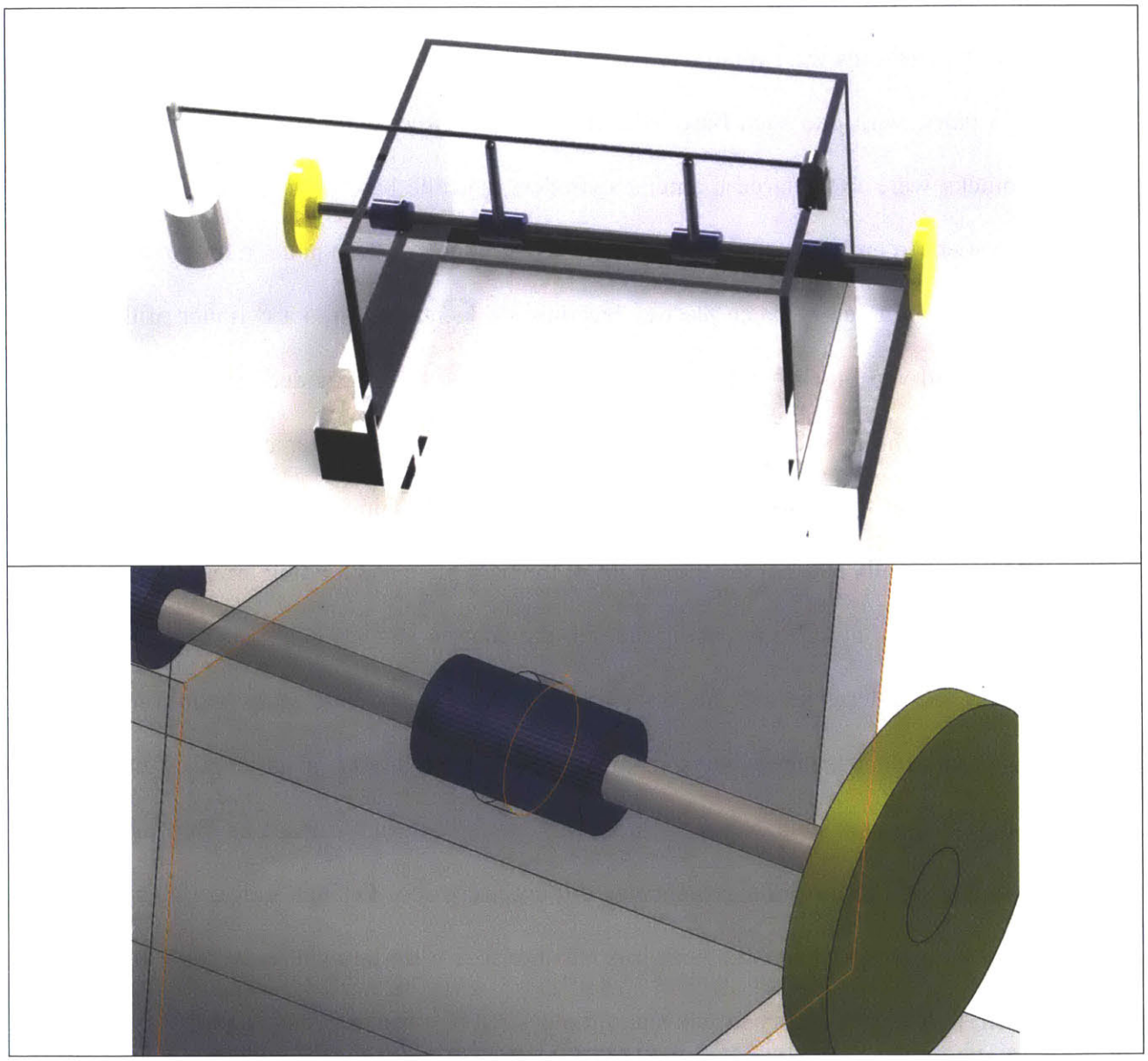

Figure 13: Early concept design with 4-pt bending

In this figure, the top drawing depicts a sketch of the design, with a large tank, four bearings to provide bending on a long test shaft, a hinged weight system to apply bending loads, and pancake motors. The bottom drawing shows a detail of the air bearings penetrating the tank walls.

Another design concept, illustrated in Figure 14, was explored that also had four air bushings, each loaded with equal magnitude, in pairs with opposite direction, to create a four-point bending scheme with constant bending loading conditions for a length of the test shaft. In this arrangement, the bushings were relatively close to one another, and rigidly mounted to a loading base plate in pairs, with one such base plate arranged on either end of the test shaft. The air bushings' blocks were to be large diameter cylinders, and the base plate would include a vee block arrangement to enforce concentricity of the axes. On each base plate, a motor would also have been rigidly mounted between the two bushing blocks, and set into a cylinder of the same, large diameter and vee block. A hinge system would have been provided on each base plate, below the inner bushing, and a weight suspended from below the outer bushing, creating the loading conditions on the shaft, effectively applied at each bushing. This arrangement would keep the shaft essentially straight for the length of the base plate and loading arrangement, which would provide proper alignment conditions for the motors (they simply need to be axially aligned within the tolerances of the rotor-to-stator gap). The test shaft would have had effectively no additional loads, bending or torsional, for the majority of its length, between the inner bushings. The tank boundaries did not reach as far out on the shaft as the bushing and loading arrangements, so this arrangement also did not necessitate O-rings and sealing systems at the bearings. However, seals at the tank-to-shaft interface were thought to increase the design risk too much, in terms of ability to withstand the desired number of cycles, and it was revealed that Class 1 material was not readily available in longer stock, necessitating a change to a system with drive shafts coupling to a shorter test shaft.

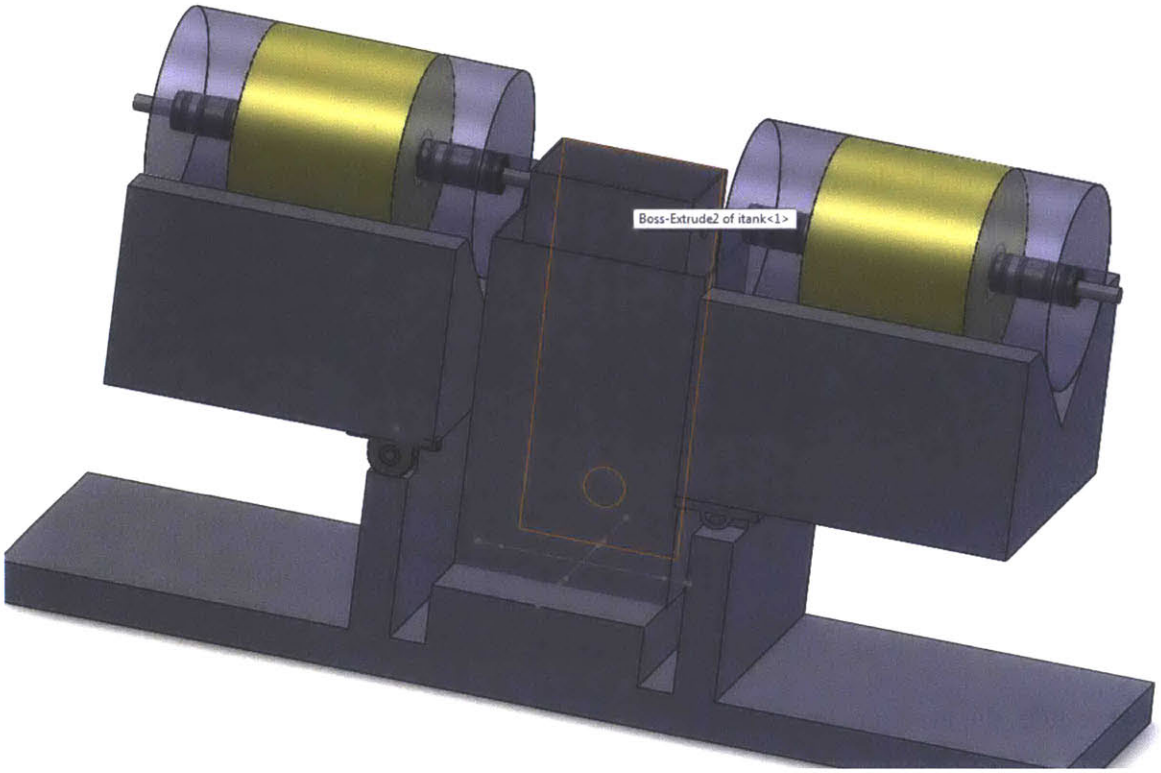

Figure 14: Concept design sketch using vee mounting blocks and cylindrical housings

In this schematic, the purple and transparent blocks each hold an air bushing. The gold cylinders represent frameless motors mounted in cylinders of the same diameter as the bushing blocks. Each vee block maintains coaxiality of the held components, and each pivots about a bushing (two styles shown). The tank in the middle allows flow past the shaft penetrations and spillover into the outer tank, or reservoir. The orange highlighting shows the pump discharge from into the inner tank from the outer tank.

4.1.7 Selected arrangement

The concept illustrated above in Figure 14 is recognizable in a functional manner: on each side of the tank lies an arrangement of paired bearings and a rotary drive mechanism. This functionally is not all that different from the spindle of a lathe or other tool, and once this is

recognized, the shape of the design, paired with the need for shorter test shafts, follows a natural step.

Considering each side of the design to be a spindle-like module that provides torsional loading and motion, and taking the pair to create the necessary alignment and connections to a test shaft, the other modules can be separated, and several modules can be purchased commercially based on required function and specifications.

In terms of modules, then, the machine requires two matched spindle-like systems, including the test shaft connections, one seawater immersion system including tanks and pumps, a support frame and connections, and a system to apply a bending load. When decoupled and assigned functions by module, the machine takes shape.

4.2 Phase 1: Bench Level Prototype

In order to prove several of the concepts, a Bench Level Prototype (BLP) is developed. The design is originally meant to prove the ability to subject a shaft to bending, torsion, and submersion in seawater. The plan for the BLP is to operate it for several months, in parallel with other efforts and with early design work on the full test device. During these months of operation, the BLP is also meant to provide lessons learned that will inform the more complete version of the design, and it is recognized that new requirements might be discovered. This

design is eventually adopted and used by the Navy, which will be discussed in the following chapters.

4.2.1 Spindle modules

In order to facilitate a rapid proof-of-concept device, commercial-off-the-shelf motors are selected for the spindle drive systems and put in contention: they are attached to the same shaft with power applied to only one, so that the second motor acts as a backdrive, generating power. Even without electrical loads, it is understood that the losses and required toque to back-drive the gearbox provides some loading on the driven motor, thereby ensuring a torque is maintained on the shaft. Simple loads are added to provide additional braking/torsional loading; two light bulbs are connected. The spindle connections are made up with readily available rigid couplings to complete the spindle modules.

4.2.2 Bending load and compliance

For bending, the included faceplates are replaced with machined aluminum housings, from which a threaded rod is extended, upon which matching weights are suspended. The system is built schematically in Figure 15. The housings are mounted using shoulder bolts through self-lubricating brass bushings; the bushings provide compliance as the test shaft is put into bending

and therefore deflects. Balancing the motor mounts is accomplished by adding weight to the threaded rods until a level confirms that the motors and housings are flat and level. This load is left on as a balance load, and the shaft is attached to both sides. Additional weights are now added to create the desired bending load in the test shaft.

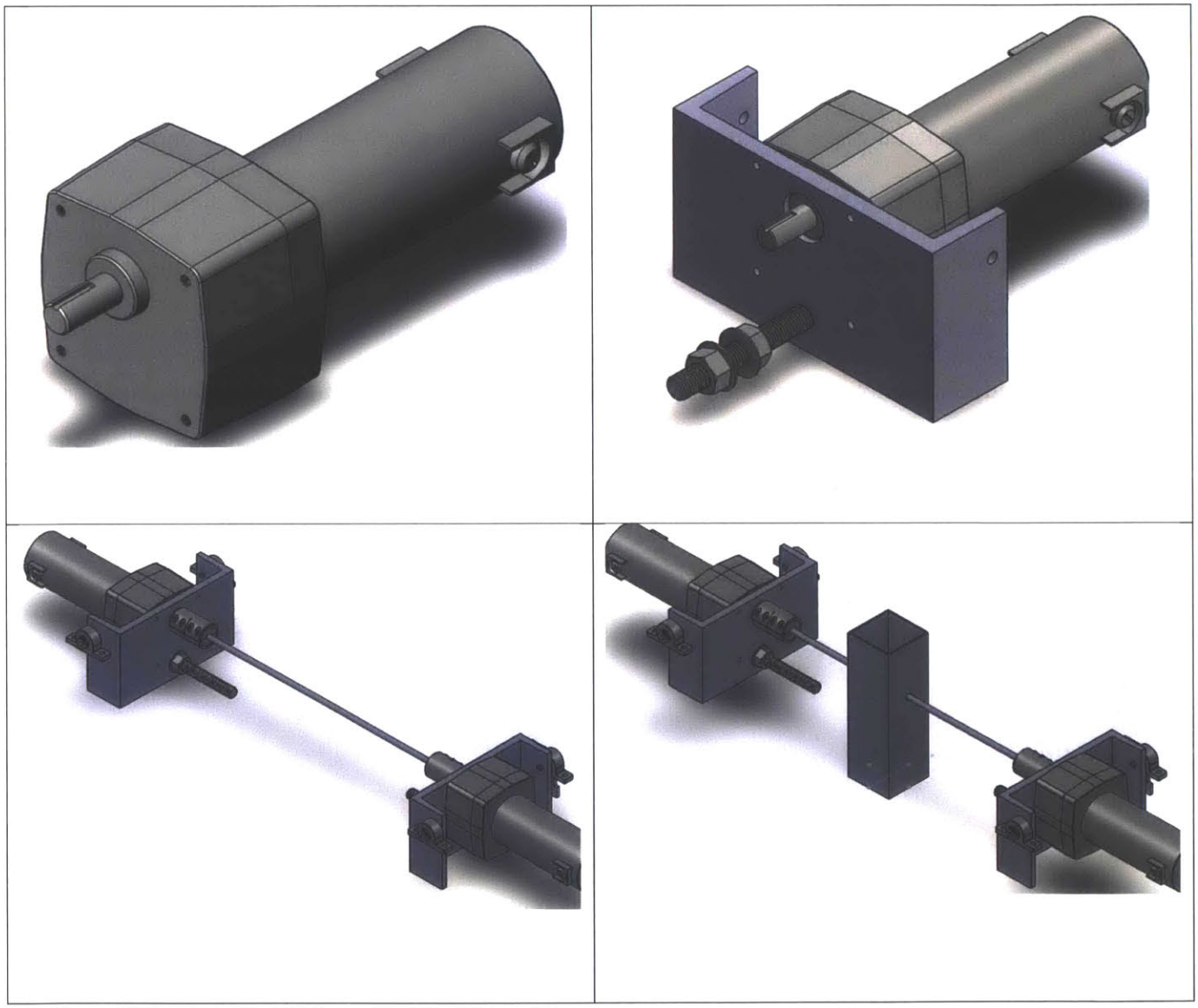

Figure 15: Renderings of BLP components and assembly:
a) DC gear motor; b) with mounting bracket and threaded rod from which weights can be suspended; c) opposed motors and test shaft with original pivots; d) with tank

4.2.3 Environment

Seawater immersion[16] is provided by having the test shaft pass through a tank made of tall aluminum channel, closed at the bottom with marine grade polyethylene. A pump draws from a reservoir and discharges into the bottom of this tank. The pump is sized to provide static head as well as to provide makeup flow for the annular region between the shaft and the tank holes through which the shaft passes, which are not sealed. Using a common aquarium pump sized for one gallon per minute at 2.5 feet of head, the pump is able to achieve and to maintain a water level several inches above the test shaft, and the small adjustment available on the pump is effective in changing the height of water above the shaft access holes.

4.3 Phase 2: Specialized Test Device

With the successful demonstration of the BLP, focus shifts to the full device. Functionally very similar to the BLP, the longevity of this primary rig needs to be vastly greater. As a design strategy, non-contact components receive a focus to avoid issues with wear and friction for the very high cycle testing that will be required for coated specimens.

---

[16] In this thesis, the two terms, immersion and submersion, both imply that the shaft is fully underwater, though not necessarily a specific depth of water.

4.3.1 Spindle modules

Due to the lack of availability of long test shafts, wherein the test shaft might run through the bearings and motors and be directly driven such as the concepts in Figure 12, Figure 13, and Figure 14 , a paired spindle approach with individual drive shafts is selected for the module-level design of this device. The first part of the non-contact strategy includes that air bearings become a fundamental component of the final design. In each spindle, then, two air bearings are placed; one is to be a standard air bushing, and the other a customized bearing with both a journal element and a thrust element. Both configurations are depicted in Figure 16.

Standard Air Bushing, 2" ID

Thrust bushing: image shows 5/8" journal ID

Figure 16: Air bearings similar to those incorporated into the final design

Similar to the bearings, a non-contact motor is chosen, using a permanent magnet DC motor with a rotor that can be bolted directly to the drive shaft of the spindle. The stator must be integrated into the housing for the spindle, but so-called frameless motors, where only the electromotive

force components are supplied (leaving the customer to provide structure and bearings) are commonly available.

The air bearings, then, must support the weight of the drive shaft as well as the rotor, and they must also supply the force that will become the bending load for the test shaft. Based on preliminary calculations of required force, weight, and the lift/load characteristics of different available bearings, a 2-inch drive system is selected, with a 2" nominal OD for the drive shaft and journal bearing components. These bushings make available 150 lbf of lift each, and the assembled shaft and rotor weigh 60 lbs. The thrust bearings must be custom designed, insofar as existing designs needed to be scaled up to this diameter. When complete, the thrust components of these bearings are each able to provide 220 lbf, although for the design only 10-20 lbf are required to meet the desired preload.

The selected motor is rated to provide 9.36 Hp at rated speed, but working with the manufacturer, it can provide the required 800 in-lb of torque at 120 RPM continuously. This is consistent with the rough calculations detailed in Table 1. A motor drive controller with power supply and resolver complete the list of components required to create motive force for the spindles. The chosen components provide a capability to power one motor in speed mode, wherein the drive unit will interface with the motor and resolver (which acts as an encoder) to maintain rotation at the desired speed, while the second motor can be provided power and operated in torque mode, where power will be cycled to provide a specified value of torque (and if desired to provide a torque profile).

Figure 17: Selection of frameless motors (rotors and stators separated)

With the externally sourced components selected, the shaft and housings are designed. The shaft is selected to be 17-4 PH steel, with a 2.0" diameter on the bearing surfaces, and other dimensions as required for the selected components. There is a step down in diameter at one end for the resolver's rotor, as well as a large diameter middle section onto which the motor's rotor fits with an RC2 sliding fit. The rotor then bolts into an integrated flange of slightly larger

diameter that is fitted with the appropriate countersunk bolt holes. At the drive end of the shaft, a large radius transition reduces the stress concentration of the final step down to the diameter for the chosen rigid collars. The shaft is illustrated in Figure 18.

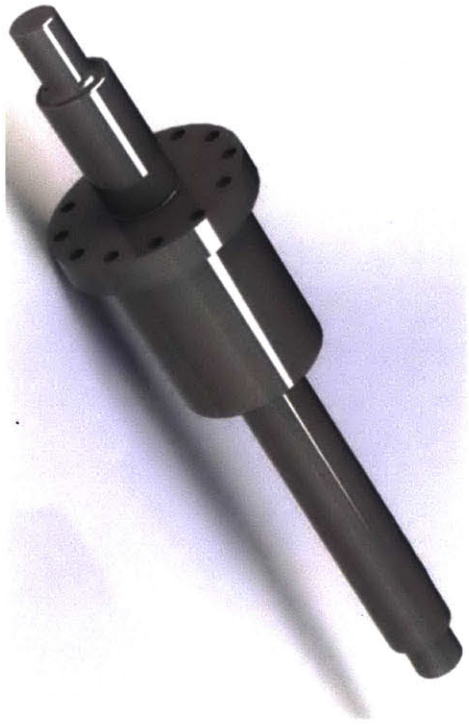

Solidworks rendering of drive shaft

Drive shafts during manufacture

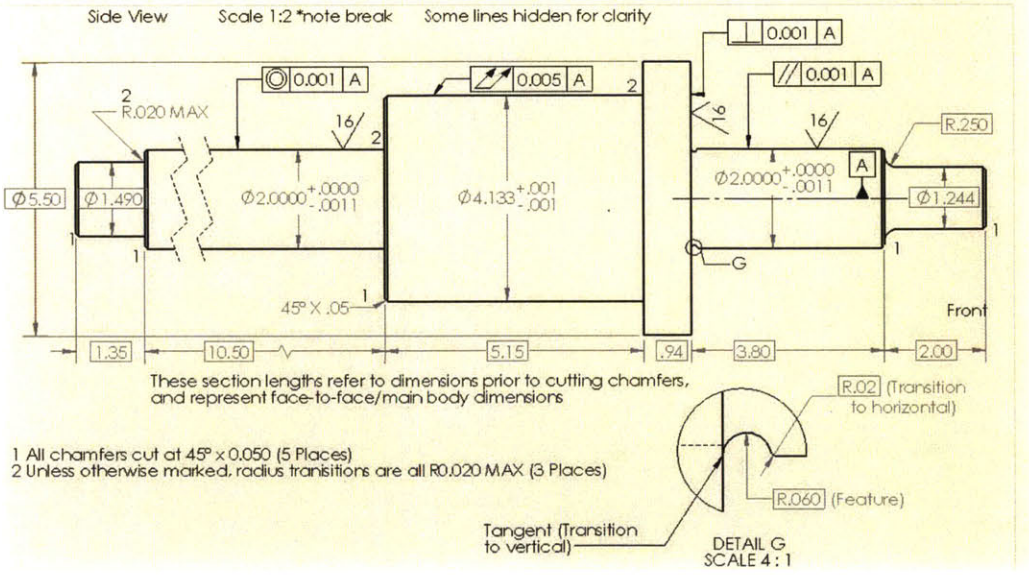

Excerpt from part drawing, illustrating the steps in diameter for various components. Full drawings are available in appendices

Figure 18: The drive shaft at various points in development

The length of the shaft appears long at first glance; in fact it will extend beyond the designed housings by several inches. The reason for this is assembly: when inserting the powerful permanent magnet rotor into the stator, a system must be in place to keep it restrained in all directions such that it can neither pull itself into contact with the stator ("Poling") nor use its magnetic forces to slide uncontrollably quickly into the stator when it is close to alignment, possibly overshooting and/or damaging components. The design of the housing, due to the need to use some of the bearing lift capability to provide bending moment on the test shaft, already requires precise alignment of the axes of the two bearings (which will be in separate pieces of the housing, as will be shown), and it is decided that the assembly order shall be:

1. Bolt rotor onto drive shaft
2. Glue stator into Master Housing (one side of the housing, which will be clamped)
3. Set air bearings in place
4. Clamp master housing to table
5. Insert drive shaft into thrust bearing and clamp to Pinch Housing (the other side of the housing) using a collar on the back side to force preload onto the thrust face
6. Align pinch housing and shaft assembly into rails and insert shaft into air bushing in Master housing
7. Slowly slide housing together, using shaft for alignment of rotor and rails for alignment of housings, until housings connect
8. Bolt housings together

From this procedure, it can be seen that the shaft, in addition to the required length for all components, must have an additional length to span the distance between the two housings when this process is begin. Tolerances are set to maintain alignment, and all diameters are determined from external component interfaces and the appropriate fits (RC2 or 0.010" engineered gap for glued components). The housing components and the rails are illustrated in Figure 19. The first image in this figure represents a section view of the beginning of the assembly process. Note

that the rotor and stator are not included in the first two images for clarity. On the left of the image lies the pinch housing and thrust bearing (clamp not shown), and the required length of shaft is evident from the right side of the image, depicting the shaft just set in the air bushing, prior to any magnetic force being felt. The next image (top right) shows the housing after sliding together and the fit of components, as well as the artifact length of shaft protruding from the rear of the housing. The third image shows the master housing bolted into the rails, with the stator visible from this end view. A first attempt to use the shaft alone to align the components revealed that, though the shaft and air bearings maintained proper alignment, the tolerance of the O-rings that set the air bearings into the housings provide enough play to allow for the rotor and stator to pole. Just before the pinch housing guide slides into the master housing, enforcing a strict alignment, the master housing had enough play moving around the relatively static shaft and bearing for the magnetic forces to close the gap and pole. The components were separated, and the rotor required minor repairs. With the rails in place, the master housing alignment was maintained as well as the bearing alignment, and the insertion went smoothly. The final image in Figure 19 shows the Solidworks rendering again. This section view has the rotor and stator slightly rotated out of the cut plane to provide a better visual of how the components fit inside the closed housing. Figure 20 shows one assembled module.

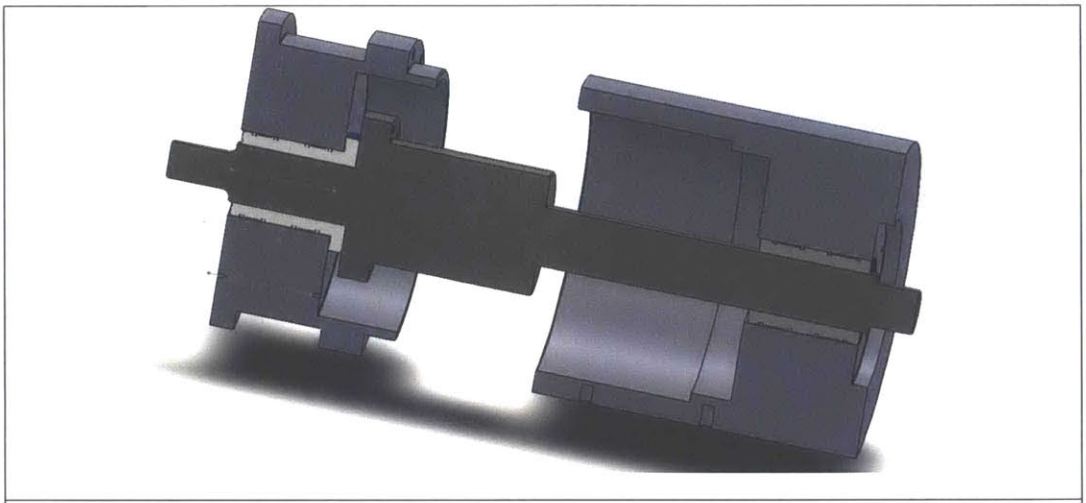

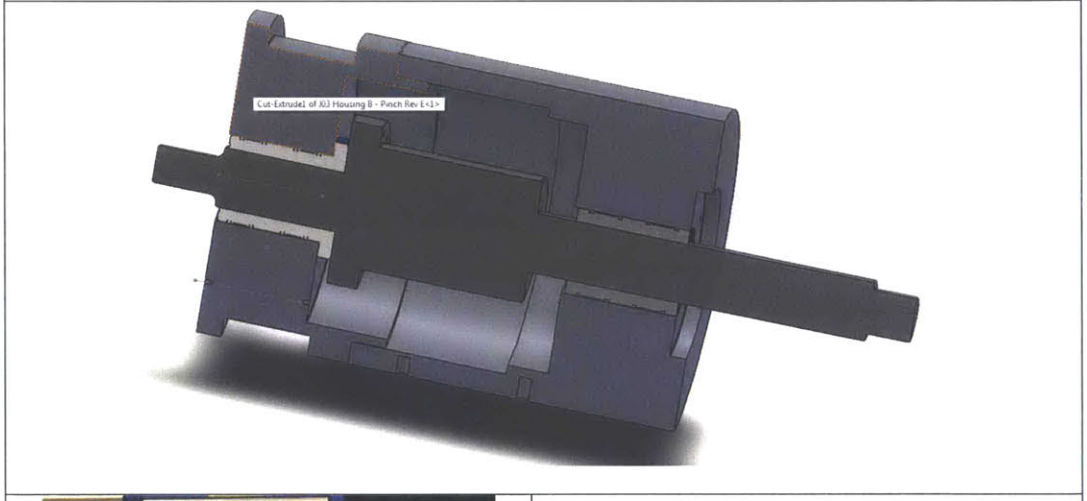

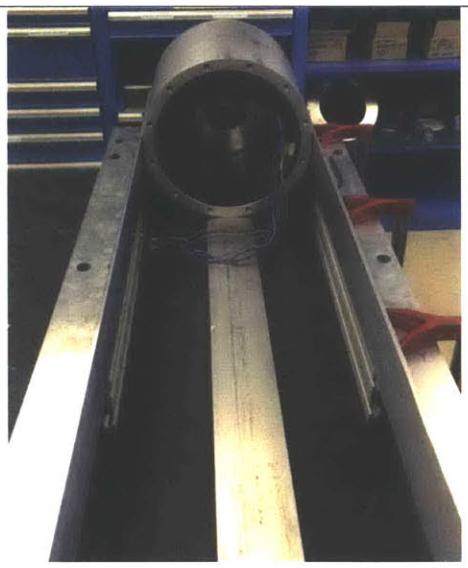

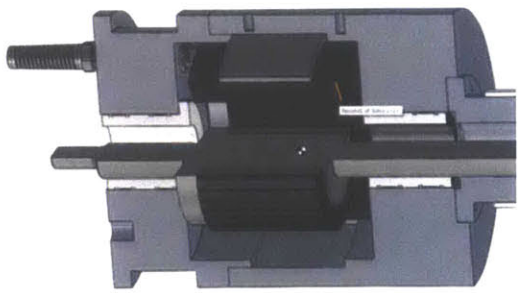

Note that in this view the stator and shaft/rotor have been rotated slightly to make them and their fit more apparent

Figure 19: Views of housing assembly

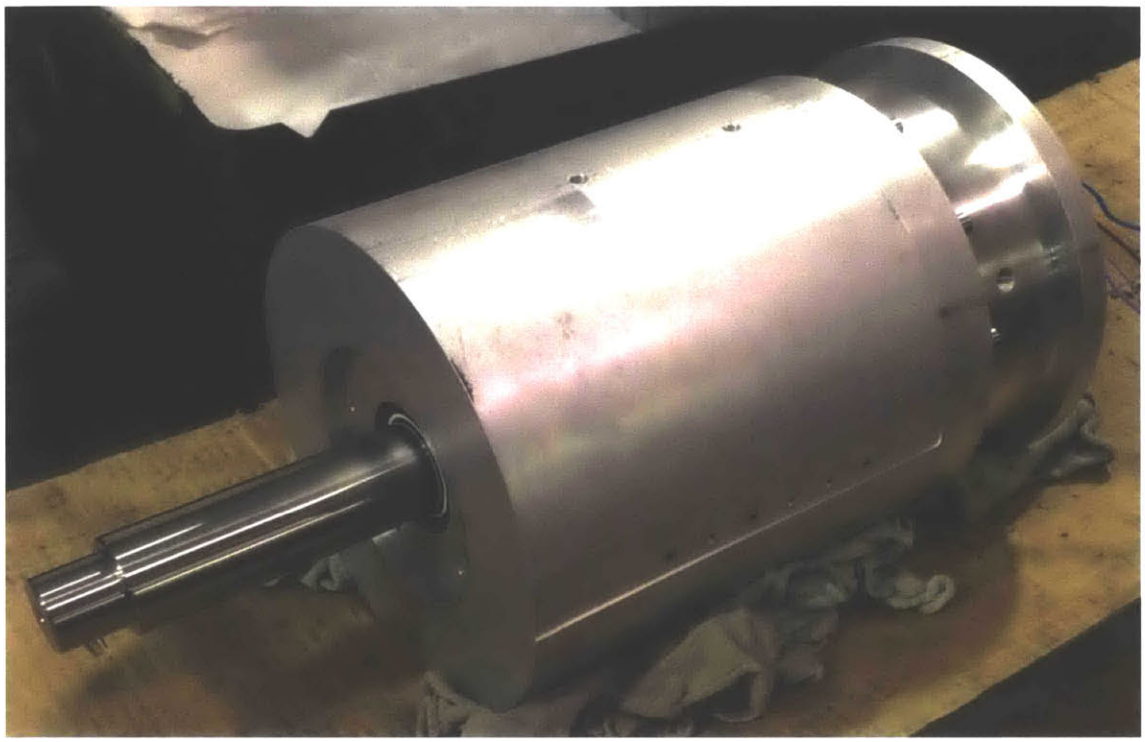

Figure 20: Picture of one assembled housing, prior to support system attachment

With the housings assembled, a magnetic preload system and the resolver are attached to the shaft, and the spindles are ready for electrical and air support systems.

4.3.2 Bending load and compliance

Flexures are used to attach the spindles to the frame, providing for the motions of an imperfect test shaft with very low parasitic loads from the frame and spindles. This is a lesson learned from the BLP, and will be discussed in results under Section 5.4. A hanging design is

incorporated to alleviate any concerns with buckling, as the spindle assemblies with all support systems are approximately 180 lbs each. Hanging of the flexures is also consistent with the lessons learned from the BLP. Figure 21 shows the assembled spindles, frame, and flexures.

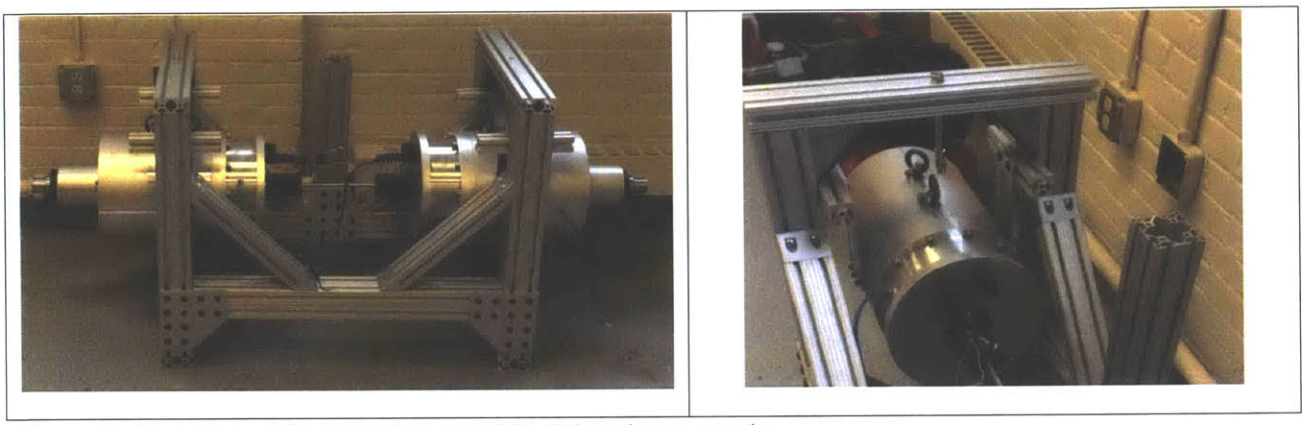

Figure 21: Two views of the mechanical assembly of the primary test rig

4.3.3 Environment

The frame is assembled using extruded aluminum framing, similar to the BLP, and the tank is constructed based on lessons learned from the BLP, suspended to help manage water loss but made of aluminum and marine grade HDPE. The frame and tank design allow for a more open user interface with the machine, with no components or framing members unnecessarily interfering with test shaft installation or other operations. With hookup of support and electrical systems, the machine is ready for testing, detailed in Machine design phase 2 results: Specialized Test Device.

5 Results

5.1 Modeling results

One of the conclusions of both the previous thesis and this thesis is that the existing model takes the concept of a literature-based model as far as it can go. To move forward, more data is needed, and there are two options on how to integrate that data.

The first option recognizes that the component models being used are all the best existing matches in literature, but they are not excellent matches in all cases, due to differences in material or environmental conditions, for example. It would be possible to replicate the types of studies done, and begin with a new "baseline model" wherein a study is done to create a distribution for each phase of the working model from Figure 1. Once this "clean-sheet" model and the appropriate associated studies are completed, new data would be integrated using Bayesian updating.

The second option recognizes that, over time and with sufficient data, the Bayesian updating will tend to "average out" the errors from an imperfect baseline. The cost and effort associated with commissioning new studies may be prohibitive, so the best path forward may be to simply begin updating the existing model with data in whatever form it becomes available.

This thesis has updated the previous model to adapt it to language whose source code is publically licensed, R. Bayesian updating capability is now provided, and a test model

demonstrating that capability has been documented. The full code, due to its simplicity, is available in Appendix E: Full code for updated model.

On the next page is a demonstration of the model after being updated with some hypothetical data. For demonstrative purposes, the data is a set of pitting time data that demonstrates several years, on average, for corrosion to transition into pits that form growing cracks. As can be seen in Figure 22, the prior and posterior wetting distributions are the same, as no additional data was provided on wetting. The pitting for the posterior shows a shift to the right to match the data's longer pitting time, and this change can be seen propagating through the follow-in times to cracking and failure events. Note that the distributions for cracking and failure are unchanged, but those times begin based on the new pitting times. Updating a distribution modeled as a normal distribution with data that is normally distributed allows for a closed-form distribution to be produced as the posterior, which is convenient for demonstration. In most cases for the distributions actually used in the model, however, posterior distributions will be obtainable only through numerical integration.

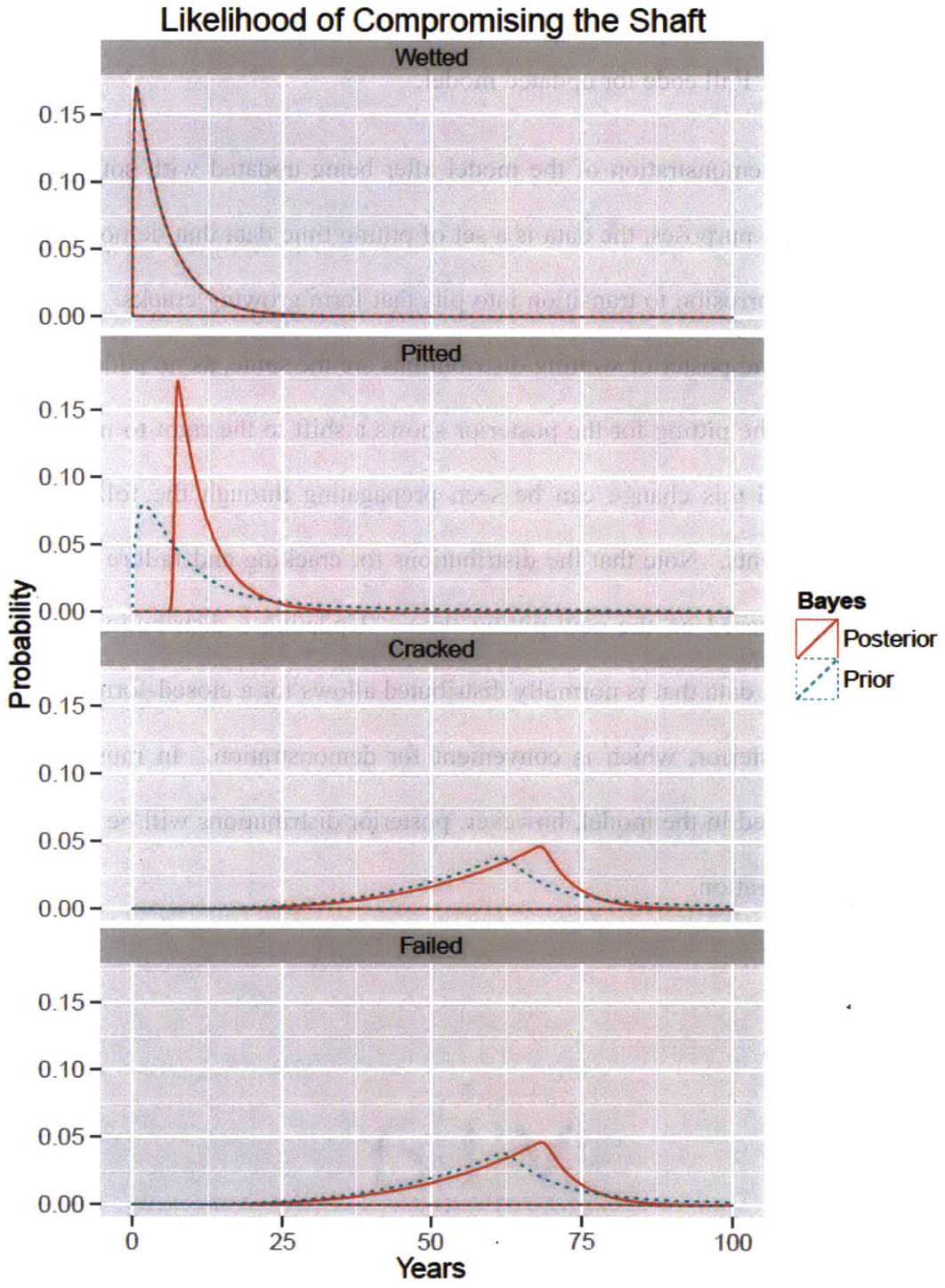

Figure 22: Demonstration of new model with Bayesian updating capability

5.2 Bending fatigue results: S-n curves

The data derived in this thesis can be graphed along with the Navy's historical fit curves, for comparison. This is presented in Figure 23. In this figure, the Navy's curve for dry fatigue specimens is graphed in orange, and the Navy's combined wetted curve is graphed in light blue. The data from this thesis shows, visually at least, good agreement with the historical curves. More data is required for a robust analysis, and as mentioned the Navy has already embarked on a program to obtain the quantity of data desired.

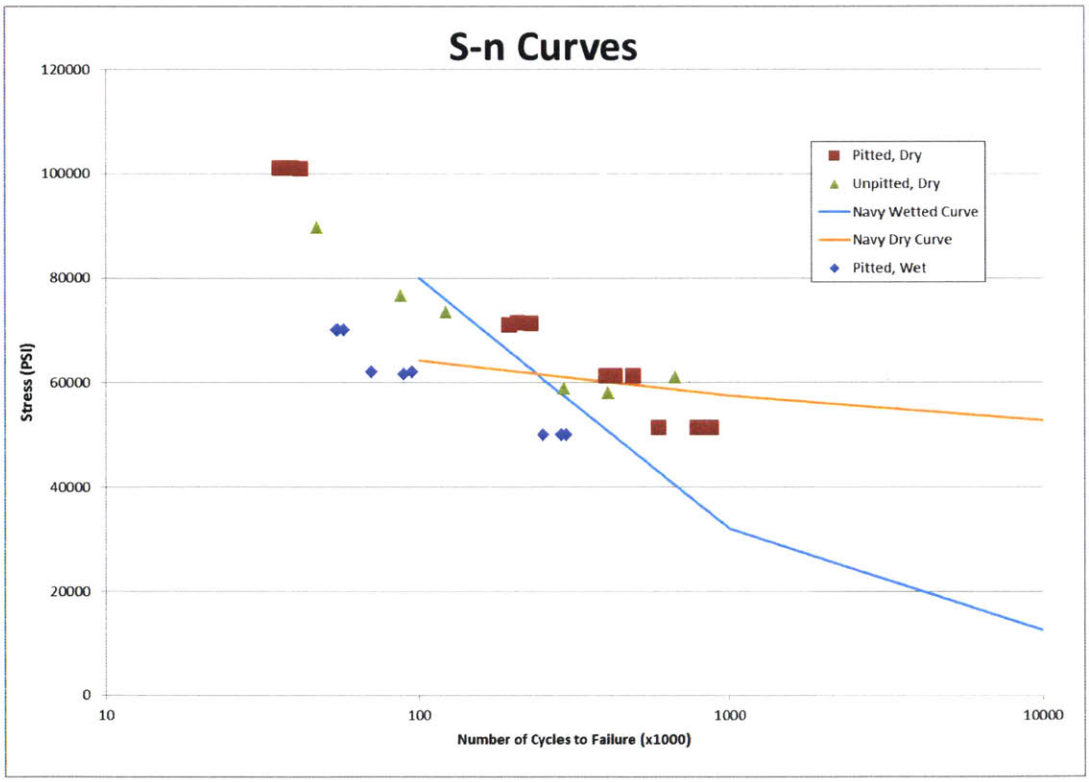

Figure 23: S-n curve data and Navy historical curves

5.3 Potential drop results

Potential drop techniques are used routinely to monitor crack growth, so the first goal was to verify its use and application to the cracks in fatigue samples. In tandem, the techniques to connect an active fatigue sample to the PD system require verification. Four leads are spot-welded directly to Class 1 bending fatigue sample. Two of these leads, the outside pair typically located near the ends of the sample or to the ends of the tapered, constant-stress section, are connected to a power supply. The power supply is set to provide a DC voltage at a given number of amps, though once fully connected the characteristics of the circuit dictate that only some of this voltage drop is seen across the leads. The second pair of leads connects to a meter capable of detecting very small differences in potential. For the first test, the sample is one of the broken halves of a completed fatigue specimen, with no obvious damage or other feature between the measurement leads. After collecting data on the "clean" sample, a file is used to create a gouge, between the measurement leads, roughly simulating a surface crack across the face. Before and after images appear in Figure 24.

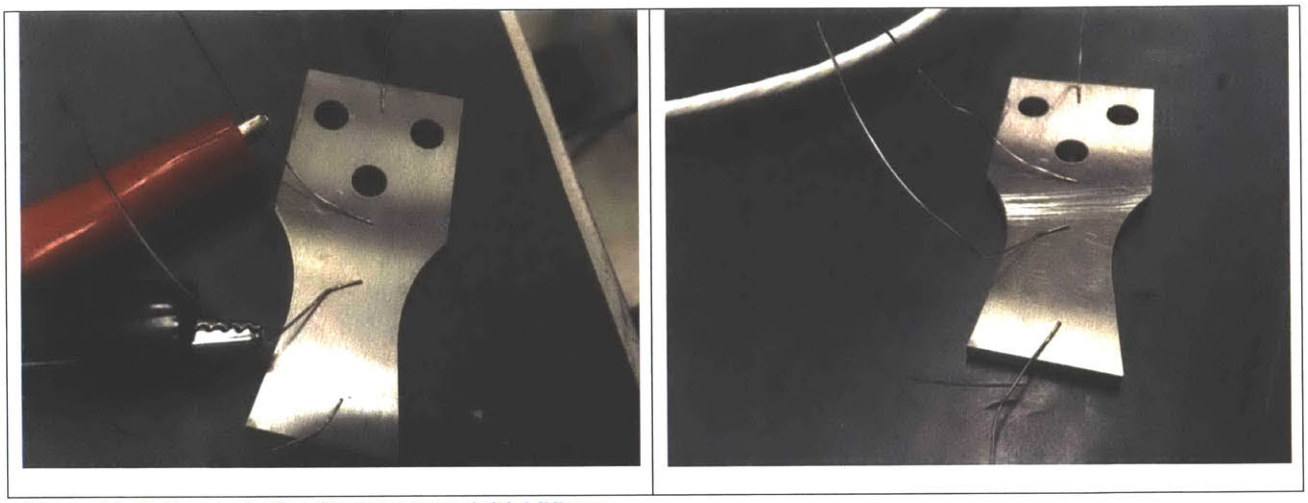

Figure 24: Before and after file damage on initial PD test

Ten data points of the potential drop between the inner pair of leads were taken before the pictured damage and ten after. A t-test was performed to evaluate for a change in the mean value of the potential drop due to the damage. With a confidence level of 99%, the change from a mean of 5.96 $x10^{-5}$ V to 7.4 $x10^{-5}$ V was due to the damage, verifying that PD detects this damage, as expected.

Next, a similar test is performed in three stages on an unbroken fatigue sample. After the leads are attached, data is taken. An artificial pit is then grown, and another set of data is taken. Then the sample is tested on the LFE-150 until a crack becomes visible, after which the final set of data is taken.

Photos of the sample at all stages appear in Figure 25.

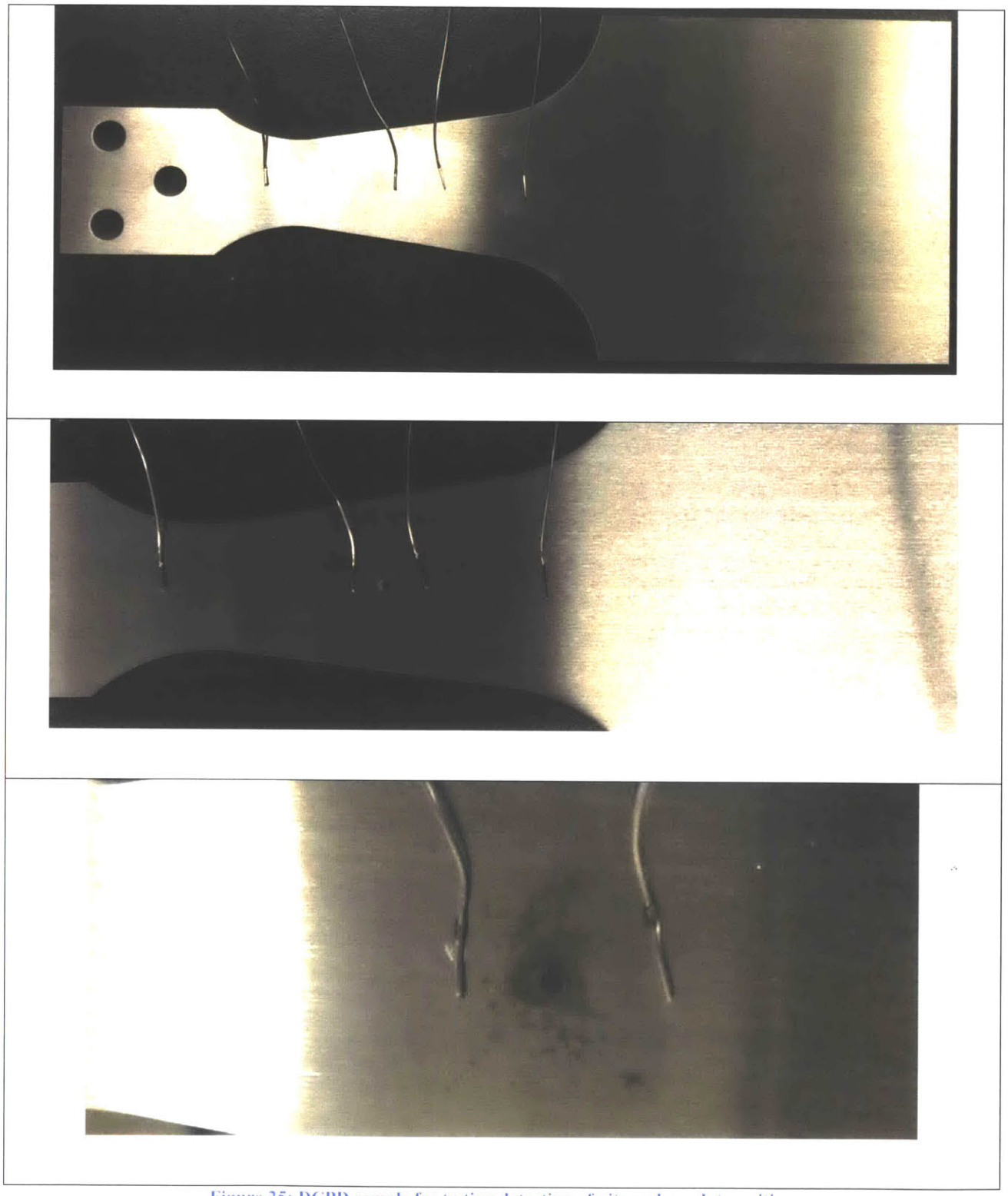

Figure 25: DCPD sample for testing detection of pits and crack transition

Again t-tests are used to verify a change in mean for pitting and then for a (fatigue) crack. Measured data is presented in Figure 26. The differences in these series are due to the pitting and to the cracking, and not to random errors, with a greater than 99% confidence level. DCPD clearly can be used to identify pitting and cracking and next should be tested in situ to determine if it can detect transition and measure pitting rate similar to its use to measure cracking rates in industry.

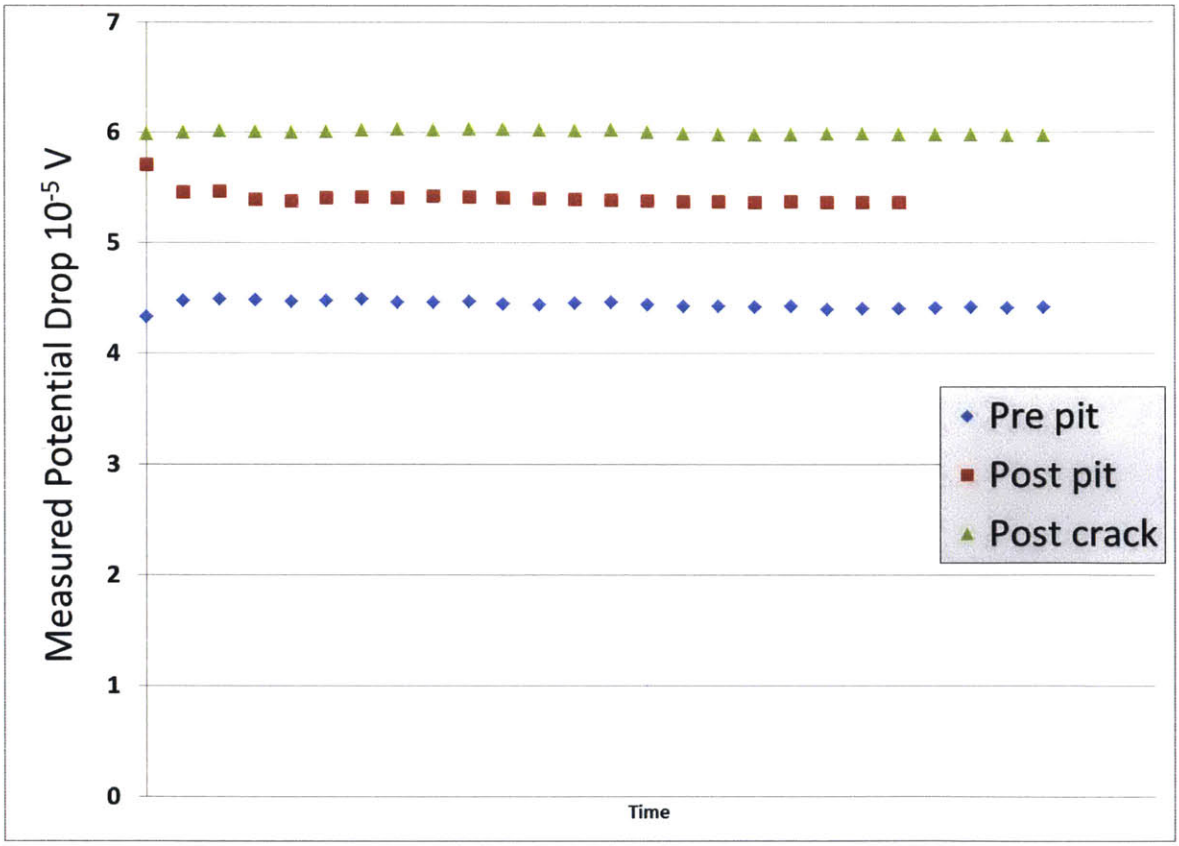

Figure 26: DCPD data for bending sample

5.4 Machine design phase 1 results: BLP

With all of the other modules prepared as developed in Section 4.2, a frame is constructed and all attachments made, as depicted in Figure 27 and in Figure 28. After an unfortunate error in wiring that costs the first power supply, the device is connected and powered, and runs flawlessly, lighting the lamps and pouring water out the shaft access holes in relatively large quantities-but maintaining a water level above the shaft, keeping it submerged. Originally intended only to prove several concepts, when demonstrated, this machine is identified as filling a gap in desired navy testing. Based on its low cost and ease of fabrication with available parts and materials, it is requested that adaptations be made to make it more suitable for use in S-n testing and other applications.

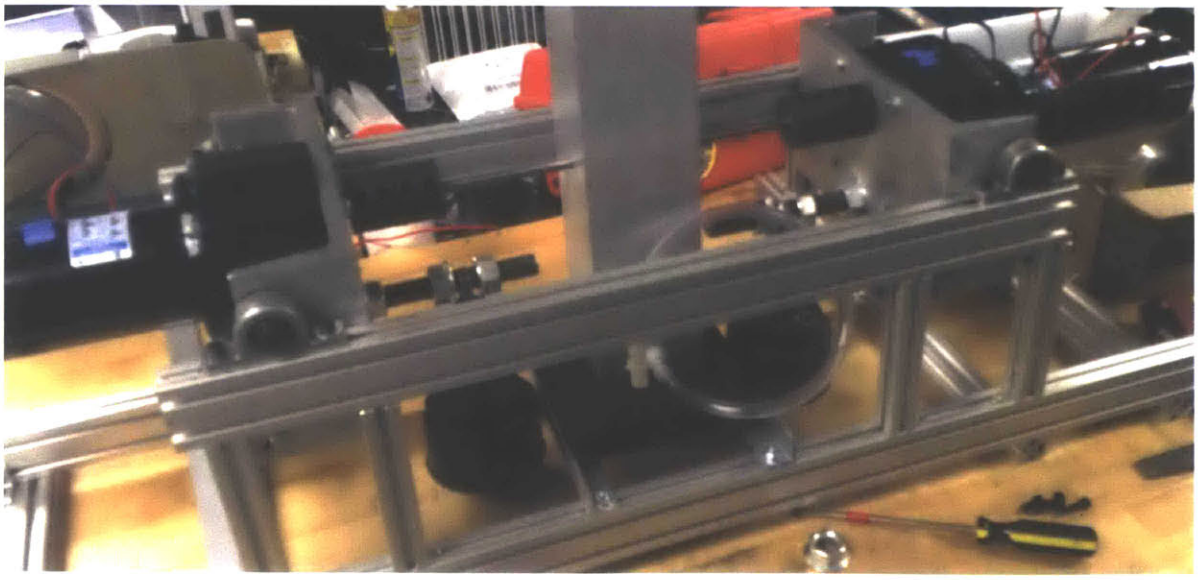

Figure 27: BLP assembly

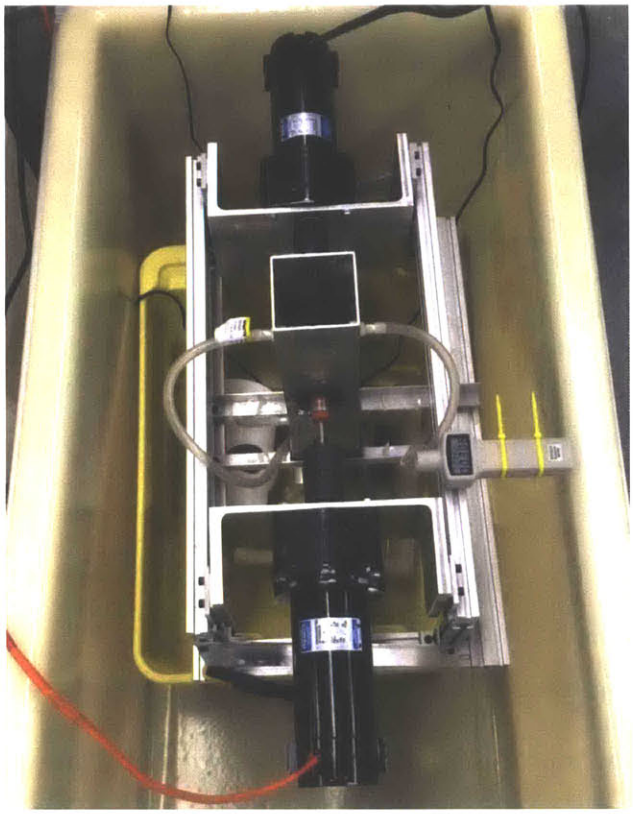

Figure 28: Top view of BLP after several hours of operation

Minor modifications, including the use of a smaller diameter test shaft, allow for a higher stress. The physical arrangement of the weight system, with its proximity to the tank, allow for a 0.200" diameter test specimen to be loaded to approximately 40,000 psi in bending, but that is close to the limit of its capability. The first Class 1 Navy steel shaft, with a pit, tested on this machine fails at about 1.4 million cycles under a calculated load of just under 45,000 psi. This is consistent with the data from Figure 23 and confirms the acceptable use of this device for fatigue testing, with torque. Pictures of the failed shaft appear in Figure 29.

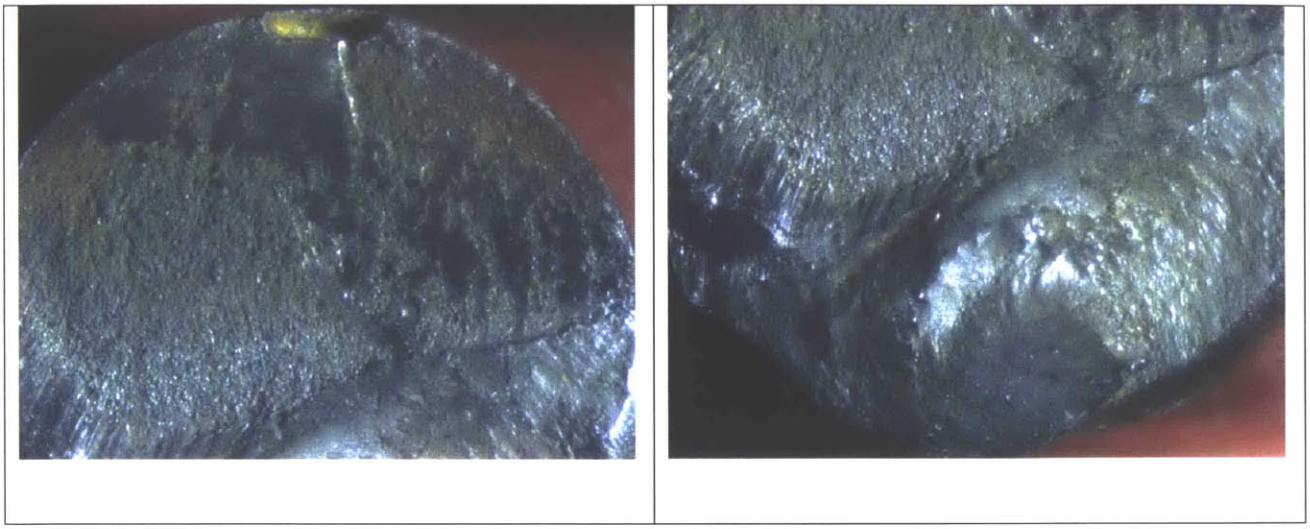

Figure 29: Two images of first shaft broken on BLP

It is worth noting in these images that the fracture facers differ from those seen on simple bending specimens. At the top of the left image, the artificially grown pit is easily identified, with significant coloration from corrosion. Extending from the pit downward, a region of the shaft shows the typical corrosion fatigue surface, a combination of fatigue beach marks and corrosion discoloration/deposits. However, towards the bottom of the left image and in most of the right image (which is the bottom of the same shaft), the clear transition from a Mode I loading dominated corrosion fatigue to a Mode II/Mode III dominated failure is evident. The twisting of the metal is due to the torsional load on the decreasing surface area. There is also less corrosion product evident in this part of the sample, indicating that the fracture may have happened rapidly.

Flexures

During the initial demonstration of the BLP, it was noted that the motors, mounted on simple bushings using standard shoulder bolts, underwent a significant motion. Each motor "rocked" up and down in its pivot with the rotation of the test shaft, with one motor swinging further on each turn than its partner. There was a slight misalignment noted during assembly in one of the shoulder bolts, but the motion was evaluated to primarily come from the runout of the shaft, which had been procured only for demonstration purposes and neither manufactured nor maintained to any specific, tight tolerance. For a perfectly straight shaft, with the two machine collars aligned with an unstressed shaft as in Figure 30a, the system would simple rotate about the axis of the shaft when not loaded. Under bending load, when the shaft is deflected as in Figure 30b, a perfect shaft would still rotate, but it would maintain this bent shape, so that the axis is only clearly defined as the "center" of the shaft at any point along its length, with the motion circular in the normal plane to the instantaneous direction of the shaft. An imperfect shaft, one that exhibits some measurable runout, would behave differently as observed in this work. For convenience, the imperfect shaft is assumed to have an existing bend similar in shape to that of the bent shaft in Figure 30b. Rotating such a bent shaft about the axis between the collars would have it sweeping through a motion more like a jump rope held between two schoolchildren, such as the shape suggested in Figure 30c.

a) Perfect shaft with perfect alignment would rotate around its axis

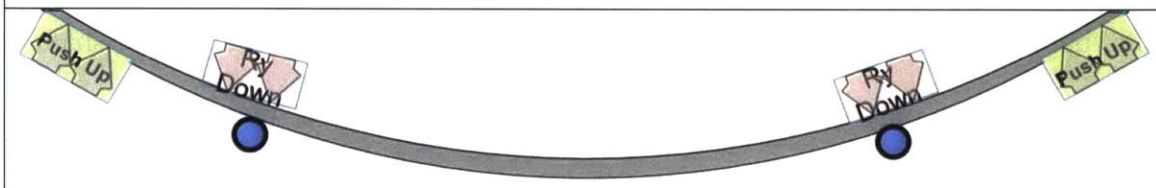

b) Perfect shaft under bending

Also assumed shape of a bent shaft, to allow for explicit calculations

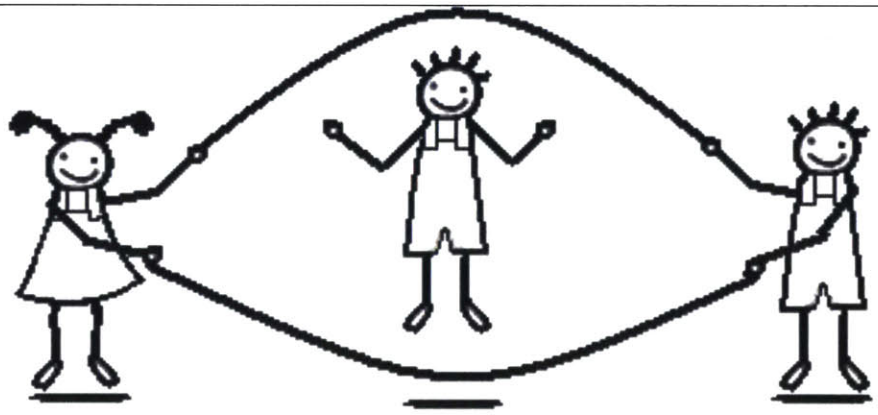

c) Conceptual shape of unimpeded path of an imperfect shaft rotated from both ends

Figure 30: Shaft alignment and imperfection

This motion would require the collars to assume the angle seen at either end of the shaft. When the bend in the shaft is vertical (up or down), the pivots allow for the collars and motor mounts to align with this desired motion. However, when this bend rotates to a horizontal alignment, tending to swing the shaft left or right of the natural axis of the machine, the pivots and motors would not provide adequate compliance, instead resisting the natural bend of the shaft (the bend from the flaw), and applying bending loads to enforce a straighter condition on the ends to accommodate the maximum angular deflection of the collars and motor mounts. To illustrate the loads involved, the demonstration shaft is used as an example. It is ten inches in length, and exhibits a total runout of about 0.015 inches, which is large for such a short shaft. A straight, cantilevered, tip-loaded shaft such as in Figure 31 bends under the load P. For the 10 inch shaft with 0.25 inch diameter (d), the bending load required to give it 0.015 inches of deflection (δ) can be calculated:

$$I_{shaft} = \frac{\pi d^4}{64} = 0.000192 in^4 \quad (20)$$

$$runout = \delta = \frac{PL^3}{3EI} \quad (21)$$

Implies:

$$P = \frac{3\delta EI}{L^3} = \frac{3*(0.015in)*\left(29.5x10^{6lb}/_{in^2}\right)*(0.000192in^4)}{(10in)^3} = 0.25 \text{ lb} \quad (22)$$

According to the principal of superposition, if it takes this load to bend a straight shaft to achieve a runout of 0.015", it can also be assumed that it takes, ideally, this load to bend a pre-bent shaft of the assumed shape to approximately "straight." This means that even with no bending load applied to the shaft, in order to rotate a pre-bent shaft of the assumed shape and runout though a path that forces it straight, ¼ lb of force must be applied by the constraints when the bend is in either of the horizontal positions.

In terms of test parameters, achieving the Navy 6000 psi for example, the required bending force for the test is

$$\sigma = \frac{My}{I} = 6000psi = \frac{M * (\frac{.25in}{2})}{0.000192in^4} \quad 23$$

This determines that M = 9.2 in-lb of internal moment is required, which for the BLP requires about 2.5 lbs of load on the bending arm. The BLP design, with the rigid collars, transfers a moment to the test shaft, as opposed to a force, and this design is intended to maintain a uniform bending load on the test shaft. However, as can now be seen, with the pivot constraints, the bent demonstration shaft experiences additional forces when it is constrained in its motion, giving an erroneous loading up of up to 10% of the desired test loading. Analyzing other approximations of the shape and loading, the parasitic load of the pivots, for the 6000 psi bending test, varies between 2 and 10 percent of the desired load. This percentage would be much lower for high stress loading conditions, as would be done for S-n curve data (and as is done on the BLP in later stages).

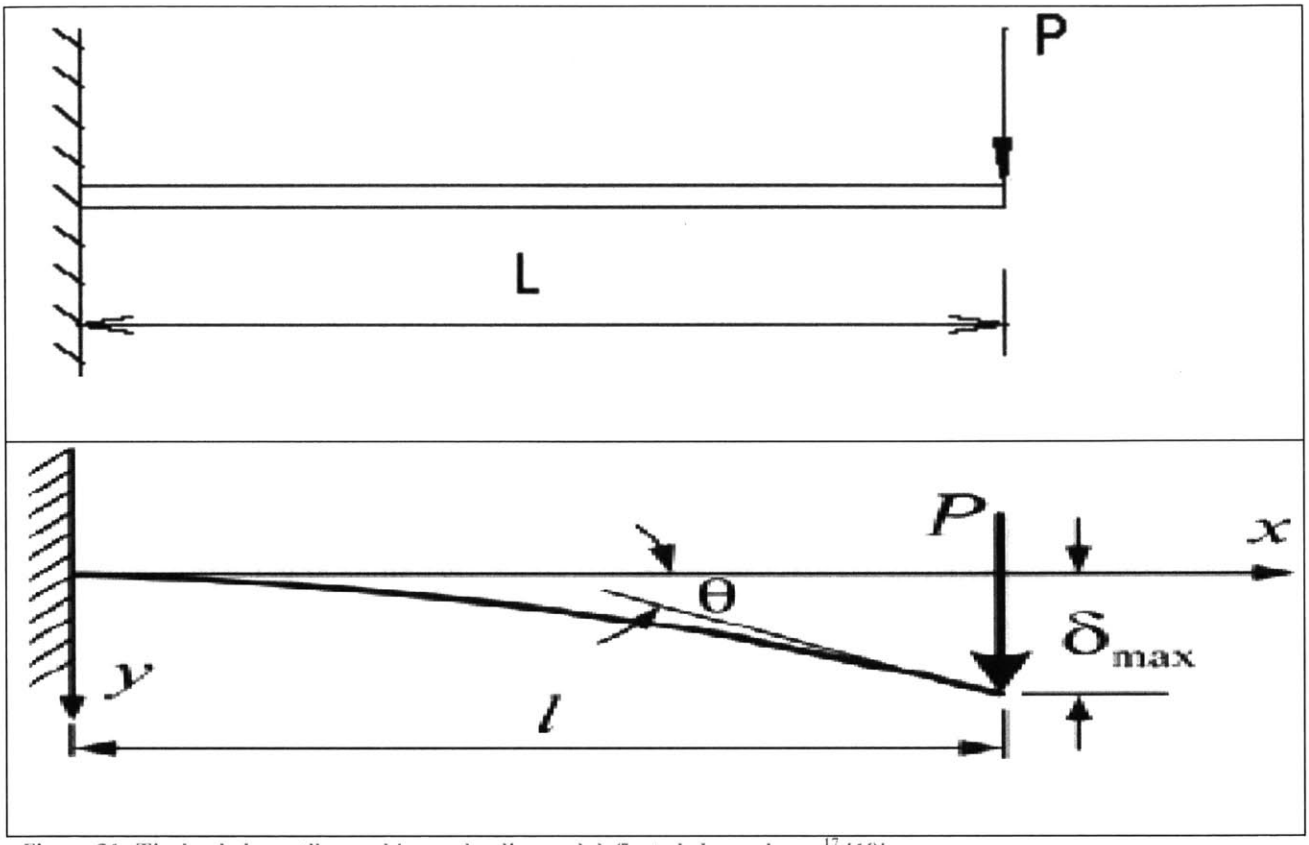

Figure 31: Tip-loaded, cantilevered beam, loading and deflected shape shown[17] [18]

In order to reduce these parasitic loads, flexural bearings are chosen to replace the pivots. The initial design of the flexures can be seen in Figure 32. Figure 33 shows only the key "beam" of the flexure, in detail and with the dimensions defined for reference.

[17] This image excerpted from reference [18].

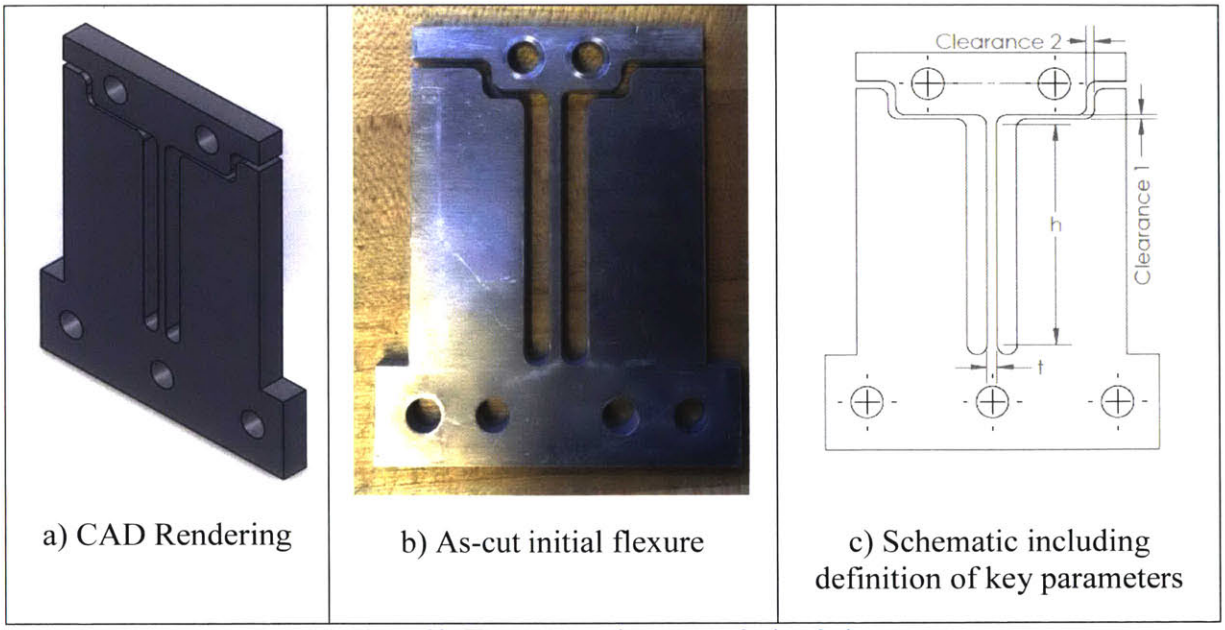

Figure 32: Flexures at various stages during design

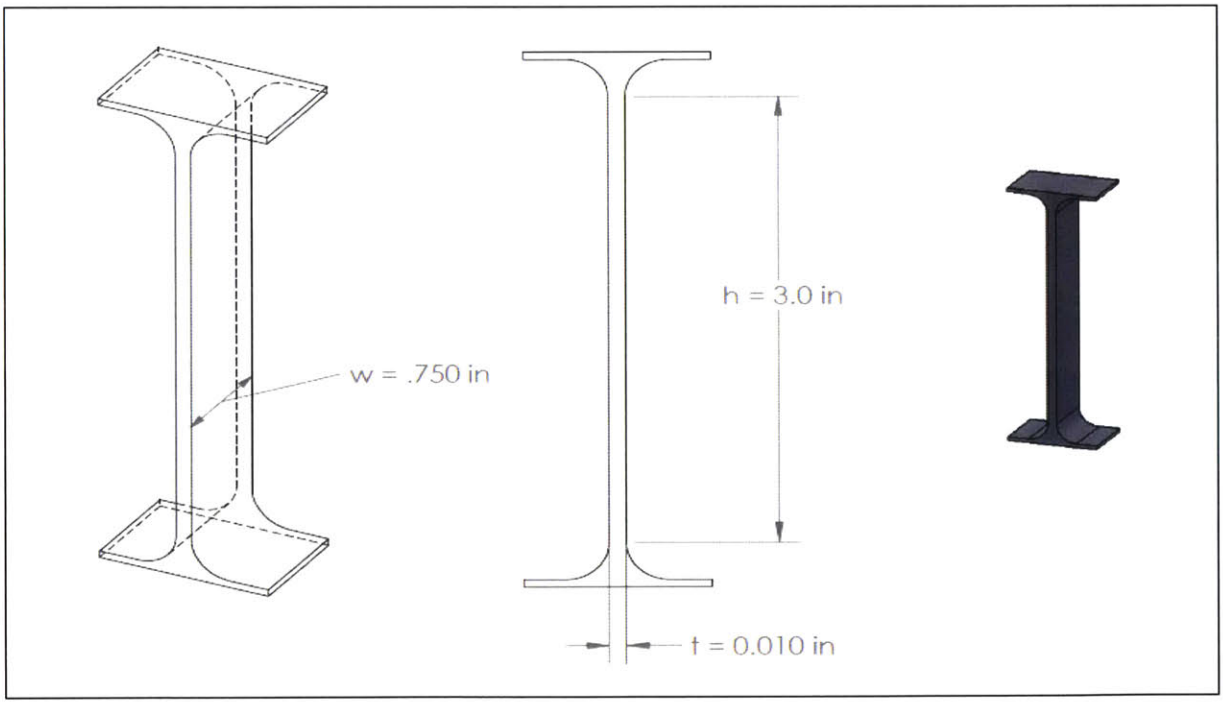

Figure 33: Beam portion of flexure defining variables

Since runouts are expected to be small compared to the length of the beam, the small angle approximation is applied, and the runout demands an angle of

$$\theta = \tan^{-1}\frac{runout}{length} \sim \frac{runout}{length} \quad (24)$$

For the vertical alignment of the pre-bent shaft, the flexural analysis is similar to the bushing analysis, in that the flexures can bend forward or backward (together) to tilt the motor housings in the same way as the bushings are seen to permit motion during the demonstration of the BLP. Now, however, for the horizontal alignment of the bend, the flexures can bend such that one flexure moves forward, and the other moves backward, creating an angle in the axis between them, which is perpendicular to the rigid collar that attaches to the shaft. In this way, the flexures now accommodate motion in all directions, with the resistance (parasitic force) experienced by the shaft only that force required to bend the flexures. Treating the vertical "column" of the flexure in Figure 32 and Figure 33 as a cantilevered beam, the angle at the tip of the beam when subjected to a point force, F, at its tip is [17]:

$$\theta = \frac{Fh^2}{2EI} \quad (25)$$

Equating equations 24 and 25,

$$\theta = \frac{F_{parasitic}h^2}{2EI} = \frac{runout}{length} \quad (26)$$

Which implies:

$$F_{parasitic} = \frac{Runout * 2E_{Al}I_{flexure}}{L_{shaft} * h_{flexure}^{2}} = 0.007\ lb \quad (27)$$

So that the parasitic loads, due to the compliance added to the system, would be reduced by more than a factor of 100. A second term must be considered, however. In addition to moving forward and backward in tandem to accommodate the motion of the motor assembly, the column of the flexure would be required to rotate to match the same angle, θ, due to the rigid attachment of the motors, which are rotating to accommodate the bent shaft, and the flexures. The rotation of a rectangular column under a torque, as seen in Figure 34, can be given by :

$$\emptyset_{torsion} = \frac{TL}{JG} \quad (28)$$

Where G is the shear modulus, and J is a torsional constant approximated by [19]:

$$J = \beta w t^3 \quad (29)$$

And here β, due to the ratio of w to t, is 0.3.

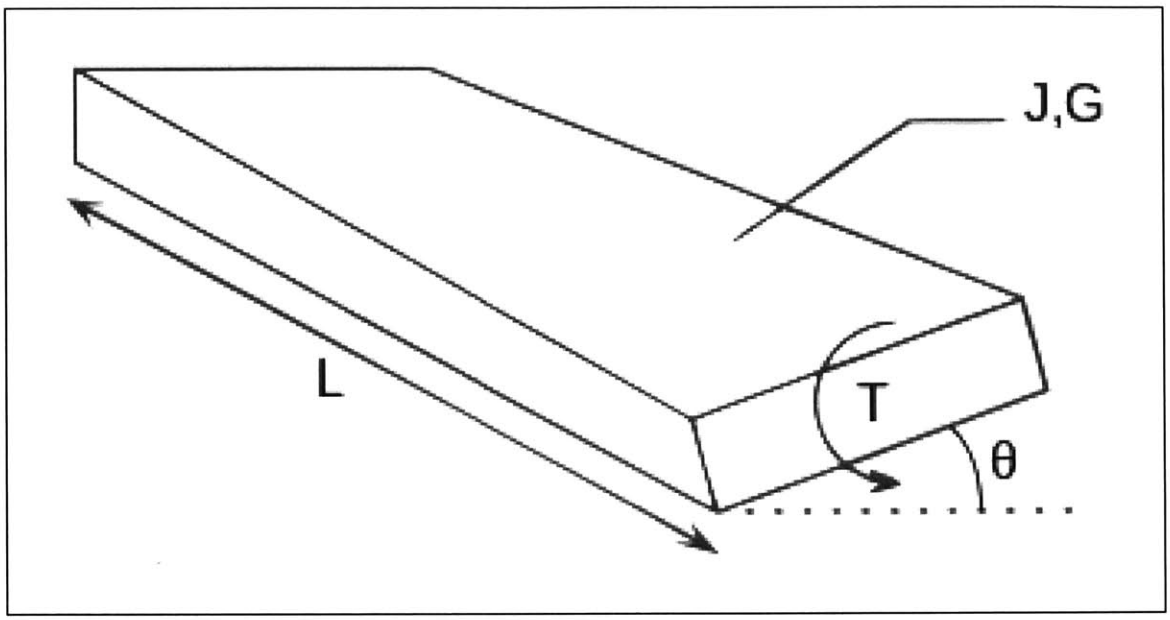

Figure 34: Rotation of a rectangular beam under torque, T [19]

Equating equations 24 and 28,

$$\frac{TL}{JG} = \frac{runout}{length} \tag{30}$$

And the required torque is 0.0014 in-lb. The force on the flexure from accommodating the motion is applied at a distance equal to half the width of the motor, in this case 6 inches, for a parasitic load of 0.00024 lb. While the parasitic load varies slightly with the angle of rotation of the existing bend in the imperfect shaft, the parasitic loads can be seen to be small compared to the test loads.

The aluminum flexures are susceptible to buckling and to fatigue when added to the system as depicted. Suspending the motors from the flexures removes the buckling concern, though to avoid fatigue in high S-n loading scenarios and over the testing of numerous shafts, steel flexures are intended to replace the aluminum. The steel flexure design includes anodized aluminum clamps securing blue spring steel blade flexures.

Torque

Since it is also desired to know the levels of torque being used on the BLP, the machine is disassembled, and the motors and shaft are mounted to a table top. One motor is clamped in place and the other balanced on a pivot bar. Long balancing arms are placed onto the driven motor, and weights added until the system balances, in a configuration per Figure 35. The drive motor is then turned on, with zero, one, or two light bulbs installed to provide resistance. Weights are now moved and/or added until the system is again balanced, with the driven motor turning in generating mode. The change in balance moment is calculated, and this equates to the torque on the system.

Figure 35: Benchtop torque benchmarking

Results are in the following table:

Light bulbs	Torque load (in-lb)
0	36
1	75
2	117

Table 3: Levels of BLP torque loading

The 117 in-lb is near the rated torque of this motor at the desired 110 RPM, consistent with the observed speed of 109 RPM.

5.5 Machine design phase 2 results: Specialized Test Device

The machine performs as desired. Late-breaking discussions with the motor manufacturer led to a modification that connects the DC portions of the motor controllers; the generating motor now provides its power to the driving motor as was initially envisioned. This circuit is placed in parallel with a large resistor to stabilize voltage, and extended operations and testing are required to determine if this configuration will provide the desired longevity. The motor manufacturer, having originally assured that these motors were a fit for the application, now agrees that this configuration is a satisfactory solution to the generating problem. The motor turns at desired speed, and torque can be monitored and verified according to the current witnessed at each machine. Torque is programmable, as desired. The machine also has the capability of being programmed through the motor controllers and disconnected from the computer, allowing multiple repeats of a given set of test parameters without the requirement to keep a terminal at each test device.

The desired magnetic preload system was ineffective in overcoming the forces internal to the motor to keep the rotor, on the shaft, aligned with the stator, housed in the aluminum assembly. The preload collar was removed, and thrust preload was applied manually during the connection of the two housings to the test shaft. While acceptable preload is maintained in this way, as verified through operation and through the ability to maintain resolver alignment to provide position information to the control circuitry, this unnecessarily complicates test article

installation, and it should be corrected. Larger embedded magnets are required in the magnet collar, found in Appendix D.

The resolver did not arrive per manufacturer's drawings. The inner diameter of the resolver rotor was larger than the part drawing specified, resulting in a large gap between the shaft OD at that point and the resolver (a gap of approximately 0.030" radius). This gap is larger than a typical engineered fit for a glued joint (glues used on this thesis are intended to fill up to 0.010" gaps), and inserts were required to make up the difference. The resolvers were successfully fit up and adhered, both on the stator and rotor, and performance was verified during testing.

With initial tests complete, this machine is now the property of the Navy, who will complete testing and evaluation. There are, in addition, two modifications in planning. First, the hanging flexures are aluminum and will not withstand the number of cycles desired for a full life test. These are being replaced with a design that incorporates spring steel as the motion component and anodized aluminum for the mounts to the frame. Second, the tank is being redesigned to sit horizontally with end enclosures to allow for varying diameters, coatings, and geometries of test specimens as the customer requires.

6 Conclusions and recommendations

This thesis seeks to fill some gaps in the knowledge and resources required to design a 12-year shaft for the OHIO Replacement submarine. The model update provides new capability for improving the distributions and for reducing the uncertainty, but this requires new and more relevant data. The data that the Navy has and is currently acquiring do not line up well with the predictive model (tests span several stages or partial stages, for example), but the techniques and machines developed in this thesis can be made to align very well. The Navy's data and data from the newly developed methods can be combined to inform the predictive tool and to inform decisions on the shaft design. The BLP is a capable machine and has demonstrated that a relatively inexpensive device can be rapidly deployed to begin immediate testing. The specialized test device will not suffer from several common failure mechanisms and makes available a new avenue for evaluating corrosion fatigue failure, especially on coated samples expected to demonstrate "full design life." However, the data that it can provide is necessarily slow to come; and in some sense ORP is already past the stage of investment and collecting (and evaluating) data on the time scale that this rig provides.

Along with existing methods of testing, sometimes with the modifications recommended throughout this thesis, it is now incumbent upon submarine designers to embark on a path to fill the knowledge gaps and improve the methods, reliability and uncertainty in setting submarine inspection intervals. It is worth noting at this point that data is not the end goal, though it has been one of the primary goals of this thesis. In order to establish a proper inspection interval,

what is required is systematic evidence that the established interval provides an acceptable level of risk. The model, and its analysis of available data, provides part of this evidence, but it is also advisable to seek expert opinion and historical precedent, as well as other sources of evidence.

6.1 Recommendations for the current machines and OR design

The BLP was originally intended neither for commercial use nor for sustained testing. It was a proof-of-concept prototype, and consequently many of the decisions in its design should be re-evaluated in light of its adoption by the Navy. Its opposed motors were chosen because the symmetry allowed for many common parts between the "drive" and "brake" sides of the machine. Common motor mounts, flexural bearings, shaft collars, and cabling alleviated much work in the design and in the assembly, and the gear motors were selected primarily for their availability and the ease with which they were able to be set up to provide the appropriate test speed, at approximately the correct torque. There are other options for providing a brake and therefore the torsional resistance required to achieve desired test shaft torque loading. The first step in evaluating braking systems is for the Navy to determine the desired torque profiles or ranges of torque for future testing. This decision will help inform the analysis of the cost and complexity of changing the BLP to have a longer-lasting and more adjustable brake (including the cost and complexity of mounting and maintaining), compared to continuing with the existing system.

The simplest option for adjusting the brake would be to remove the discrete loading of the light bulbs and to add a rheostat or other variable resistance. Brakes of many kinds also exist and could be applied to this system; in the torque range required, many applications for bicycle trainers or small motorcycles would be immediately adaptable, including band brakes, magnetic particle brakes, and others. Since the system requires a pump, it would also be possible to provide the resistance, or part of it, by driving a pump directly. Sizing the pump to account for added flow resistance (an adjustable orifice would be an example of a variable resistance system) could be accomplished, although the bearing system and submersion of the pump might require more substantial changes in the rest of the machine than are desired.

The flexures have already been redesigned and replaced, but that change should be verified and incorporated into the parts drawings. The recommendation is to transition to steel blade flexures to avoid fatigue problems with the monolithic aluminum flexures as test cycles accumulate on subsequent test shafts. The pump and tank system should be evaluated for changes to make them more similar to the suspended design of the primary rig, to simplify the water management and to reduce the splash and wastage. This is also in process, but it has not yet been proven.

More pointedly, it is evident that the Navy needs to create a baseline data set that expands upon the work presented in this thesis and elsewhere by the project; specifically they need to create S-n curves for the full spectrum of metals from which they wish to select, across a suite of sample and treatment options as was done in this thesis, for comparison. The BLP is not designed for the high loading of low cycle fatigue testing; it is designed for submarine operational loading, which is quite limited in bending. The Navy needs to make available one of the large prolongs,

or preferably stock from such, to allow for the weight system modification that will make the BLP an S-n level fatigue device.

Whatever the final design, the Navy has adopted this machine to perform immediate testing. Its longevity and design are most appropriate for testing uncoated shafts to failure, primarily to supplement the creation of S-n data on shafts of various designs and treatments, data that includes torque. Much like was done on the bending test machines, a suite of BLPs should be used to create curves for shafts with and without pits, for comparison. It would also be of value to the Navy and to the community of researchers to perform tests that quantify the effects of various levels of torsion, to determine conclusively how this loading should be incorporated into shaft design. This information may also inform decisions on the profiles and levels of torsion to be tested. Steady torsion would lend itself to critical plane analyses, while variable torsion is much more representative of operational use and loading. Consistent with the first results shown in Figure 29 (Section 5.2), an analysis should be done regarding the effects of Mode I vs Mode II/Mode III loading. This analysis should determine under what conditions the torsional loading takes over to fracture a sample, and whether or not this effect should be considered for submarine shafting.

Longer tests, especially verification testing of proposed and even finalized designs, are most appropriate for the STD. Its design does allow for much higher loading, especially on larger specimens, and it can therefore supplement BLP testing to provide the highest loading for S-n curves as necessary. The purchase of fewer of these machines is envisioned, although probably at least three to perform parallel testing to confirm the final design at full cyclic life while the

first full-scale shafts and submarines are manufactured. Once perfected, though, a large bank of these machines are the ideal test bed for putting fresh design ideas or materials into comparative testing for future designs and classes.

6.2 Recommendations for test adaptation

Though no torsional S-n curves were developed as part of the current work, this thesis does recommend a comparison be performed, using the LFE-150 or another suitable platform to create a series of tests in bending, and then another series in torsion, and then a set of samples tested on the rigs designed in this thesis under combined bending and torsion, and analysis done to quantify the effects of torque. Such a study needs to make a recommendation to the Navy on whether torque needs to be considered in future design analyses and testing.

The demonstration of DCPD as a method for detecting transition should be completed and matured. The ability of DCPD or perhaps ACPD to monitor the condition of a specimen during testing provides key data to inform the model as it is written. Once proven and calibrated, coated specimens could be run on one of our machines and monitored in real time. Time to water ingress, in the form of the initial PD detection of corrosion, could be measured for the first time, on a sample that does not have to be removed from the test device. The corrosion rate could be measured in situ, and perhaps even some characterization of the formation of pits could be accomplished, (similar work is being proven in parallel in the corrosion lab associated with this thesis). Next, the step jump of transition could be logged, marking the change to cracking, and

then crack growth and impending failure monitored much as it is in industry with these techniques. The analysis of this data set would create a truly probabilistic model, with distributions and variance, for each phase and specific to the Navy materials and operations. This would remove significant uncertainty and would solidify where improvement efforts are best targeted.

In parallel with developing PD techniques, the adaptation of the machines and tests that have been completed to coated samples is the next step for the test program. This needs to be done both from the standpoint of gathering data that more fully informs the navy and the model about the least understood and characterized piece, water ingress, and from the standpoint of understanding the fundamentals of how the coatings fail, and how the interfaces at critical joints interact with bending, flexure, and combined loading. This work could very easily translate into methods to prove and verify the new polysulfide paint that has been fielded but not evaluated by the Navy, as well as to quantify the level of protection of the systems and changes already in place, for which users otherwise must wait for five years until the next scheduled inspection provides data.

6.3 Recommendations for further submarine design

This thesis and the preceding project documented in the appendix, if nothing else, call into question the engineering body of evidence to extend the life of an OHIO-like shaft to 12 years.

The Navy does have experience with shafts that remain in the water for extended periods, and for extended cycles, although almost exclusively on surface ships. While surface shafts are not entirely analogous to submarine designs and operations, many materials and characteristics are common. OHIO has not failed a shaft in its decades of operation. Several changes have been implemented, if not rigorously tested and verified. From the shipyard perspective, several areas that were the emerging "worst offenders" are now being coated that previously were not, which provides significant reduction of risk. The new coating may solve the water ingress problem wholly or in part, but inspection data on shafts with that system are years away and will accumulate only very slowly. The problem may indeed be solved, in full or in part, but the Navy does not yet have a strong, arguable body of evidence to present to the decision makers and to the community at large to make their case for such a long life extension.

The gaps and concerns that led to this research can be avoided in the future. Navy designers often distinguish between evolutionary and revolutionary changes. The existing shaft system on the OHIO class represents a victory for evolutionary propulsion design. By eliminating each successive limiting failure mode, a shafting system is now in place that adequately meets the design requirements for a 6-year shaft life. Work to reduce the risk of corrosion fatigue, including this thesis, can extend that life another increment, but it is not yet clear that such improvements will provide a 12-year operational life with an acceptably low risk of failure. Only through the extended testing made available by the primary rig, and through fielding the class and evaluating its performance and the data from shaft inspections can designers gain confidence that another failure mode won't produce a limit of 8 or 10 years, or perhaps simply reduce the confidence in the 12-year risk. Doubling the shaft life was an aggressive goal, and

such changes might be better served with a revolutionary approach. Some designers are already indicating interest in "solving the problem altogether" and fielding a life-of-ship shaft that has no requirement for periodic removal and inspection.

In order to achieve this, a new approach is recommended. Future classes of marine vessels, including submarines, may leverage methods of producing thrust that do not include a primary shaft. Such devices are less applicable to the interests of this thesis, and the discussion that follows therefore does not focus on these systems; however the concepts and approaches presented would largely be applicable to such devices, at least in spirit.

In the Navy's own "Integrated Product and Process Development Handbook", Integrated Product Teams are collectively responsible for delivering a product, and they are defined to include, "all of the functional areas involved with the product-all who have a stake in the success of the program, such as design, manufacturing, test and evaluation (T&E), and logistics personnel, and, especially, *the customer*" (emphasis added) [20]. Designers should adhere more strictly to this and sit down with the end users as customers in order to rigorously define the requirements of the next propulsion system, instead of continuing with the current process of "how much can I get for how much?" For the significant changes being demanded (doubling shaft life or even life-of-ship-shafts), it is appropriate to clearly define UP FRONT the need and its justification, so that designers can begin with the correct end-goal in mind.

Knowing the correct time requirement for shaft life, an exhaustive search should then begin to identify the materials and geometry that can best meet this need. Too many assumptions and derived requirements exist in the current system. This project team demonstrated, for example,

that materials exist that do not pit in the marine environment, meaning their use could completely eliminate the corrosion fatigue problem. When proposed, a previously unspoken and unknown requirement to select only from a limited number of steels "with which the shafting community had experience" was revealed. These barriers must be removed, or at the very least shared from the beginning.

Coatings may provide similar effects, as mentioned, but these also were not methodically evaluated across the spectrum of pros and cons; rather an expert was brought in as part of a Tiger Team and designed this coating. Its pre-installation testing was, in his own words, just a way to show that it stuck to steel at least somewhat, but there is again neither a body of evidence to mandate its selection, nor one to evaluate its performance [21].

Given the full set of requirements and constraints, a sequence of tests should be performed. Candidate materials should be uniformly tested in order to make direct comparisons between them in terms of resisting damage mechanism modes like corrosion, fatigue, wear, and corrosion fatigue. Interactions of these materials with all other materials in the shafting, propulsion, and ballasts tank systems must be tested and verified. Propulsors, specifically, have recently opened the aperture to include a large number of metals that have not been specifically coupled with shafting materials.

In parallel, the geometry and other requirements of the shafting system should be developed, so that ideas and decisions can be incorporated into the testing to help insure against competing and interacting physics. While doing this, designers should also be more agile in selecting which method provides the most accurate and ready information: analysis, modeling, or

experimentation. As one example, the failure of the adapter shaft at the Bearing Test Facility brought to life a stress concentration factor that was significantly higher, verified through post-crack finite element analysis (FEA), than the design had assumed. An FEA model is time consuming and costly, but once developed it can be reasonably versatile as designs are adjusted, often justifying an early cost with unforeseen returns on investment. More importantly, simple FEA can be done on each part and assembly as part of the CAD process, similar to what is done in Professor Slocum's lab. Although not as detailed, the rapid information obtained from ANSYS helps guard against these types of surprises by showing where more focus-or even gross changes- are required from very early in design. When the parts are not as developed as required, an alternative is to create a benchtop test that will inform the key parts of the decision, similar to the blade flexure that was manufactured from a scratch piece of tin in twenty minutes to get a qualitative feel for the response to circular orbits.

In these ways, the knowledge gaps that exist and will exist for future shaft designs can be filled, starting from the component and interface levels and building all the way to a conclusive, reliable predictive model that has quantifiable and controllable uncertainty. This is the engineering OQE that the Navy desires to have before they select, approve, and field revolutionary designs that make the kinds of leaps in shaft life that are desired. Evolutionary methods have not bridged the dangerous transition from interpolation to extrapolation, and therefore shaft life extensions of orders of magnitude require new and more robust techniques.

Bibliography

[1] W. E. King, A. Arsenlis, C. Tong and W. L. Oberkampf, "Uncertainties in Predictions of Material Performance using Experimental Data that is Only Distantly Related to the System of Interest," in *Uncertainty Quantification in Scientific Computing*, Boulder, 10th IFIP WG 2.5 Working Conference, WoCoUQ 2011, 2012, pp. 294-311.

[2] G. Chen, K.-C. Wan, M. Gao, R. Wei and T. Flournoy, "Transition from Pitting to Fatigue Crack Growth - Modeling of Corrosion Fatigue Crack Nucleation in a 2024-T3 Aluminum Alloy," *Materials Science & Engineering,* vol. A219, pp. 126-132, 1996.

[3] R. Melchers, "Probabilistic Models for Corrosion in Structural Reliability Assessment - Part 2: Models Based on Mechanics," *Transactions of the ASME,* pp. 272-280, 2003.

[4] B. Fang, R. Eadie, M. Elboujdaini and W. Chen, "Transition from Pits to Cracks in Pipeline Steel in Near-Neutral pH solution," in *12th International Conference on Fracture*, Ottawa, 2009.

[5] Naval Sea Systems Command, *Military Specification: Steel Forgings, Carbon and Alloy, for Shafts, Sleeves, Propeller Nuts, Couplings, and Stocks (Rudders and Diving Planes),* Washington, DC: IHS, Inc., 1990.

[6] Department of Defense, "Propulsion Shafting (Section 243-1)," in *Design Methods for*

Naval Shipboard Systems, Carderock, MD, IHS, 1994, p. 11.

[7] D. Harlow and R. Wei, "Probability Approach for Corrosion and Corrosion Fatigue Life," *AIAA,* vol. 32, no. 10, pp. 2073-2079, 1994.

[8] D. Harlow and R. Wei, "A Probability Model for the Growth of Corrosion Pits in Aluminum Alloys Induced by Constituent Particles," *Engineering Fracture Mechanics,* vol. 59, no. 3, pp. 305-325, 1998.

[9] ASM International, "Chapter 14 - Fatigue," in *Elements of Metallurgy and Engineering Alloys (#05224G)* , Materials Park, OH, ASM International, 2008, pp. 243-246.

[10] W. Werchniak and E. J. Czyryca, "Effect of Prior Corrosion Fatigue Cycling on the Fatigue Strength of Restored Propulsion Shaft Steel," David W. Taylor Naval Ship Research and Development Center, Bethesda, MD, 1985.

[11] R. E. Link, "Evaluation of a Quenched and Tempered Alloy Steel for Main Propulsion Shafting Applicatoins - Final Report," David Taylor Research Center, Bethesda, MD, 1990.

[12] Matelect Ltd, "The Potential Drop Technique & its Use in Fatigue Testing," Matelect, London, UK.

[13] ASTM International, "Standard Test Method for Measurement of Fatigue Crack Growth Rates," ASTM International, West Conshohocken, PA, 2015.

[14] New Way Air Bearings, *Air Bearing Application and Design Guide, Revision E,* Aston, PA: New Way Air Bearings, 2006.

[15] R. Burcher and L. Rydill, Concepts in Submarine Design, Cambridge, UK: Cambridge University Press, 1994.

[16] Wikipedia, "OHIO-Class submarine," 3 April 2016. [Online]. Available: https://en.wikipedia.org/wiki/Ohio-class_submarine.

[17] S. P. Timoshenko and J. M. Gere, Mechanics of Materials, vol. Fourth Edition, Boston, MA: PWS Publishing Company, 1997.

[18] D. Ami, "Cantilever Beam Deflection," 2014. [Online]. Available: http://7qa.danaami2.top/cantilever-beam-deflection/. [Accessed May 2016].

[19] Wikimedia Foundation, Inc., "Wikipedia," 11 April 2016. [Online]. Available: https://en.wikipedia.org/wiki/Torsion_constant. [Accessed May 2016].

[20] Office of the Secretary of Defense (Acquisition and Technology), "DoD: Integrated Product and Process Development Handbook," Office of the Secretary of Defense (Acquisition and Technology), Washington, DC, 1998.

[21] T. Juska, Interviewee, *Conversation with Inventor of New Coating System.* [Interview]. 15 July 2014.

[22] P. Pitner, "Statistical Analysis of Steam Generator Tube Lifetime of Probabilistic Method for Tube Bundle Inspection," *Reliability Engineering and System Safety,* pp. 271-292, 1988.

[23] R. Tryon and T. Cruse, "A Reliability-Based Model to Predict Scatter in Fatigue Crack Nucleation Life," *Fatigue & Fracture of Engineering Materials & Structures,* vol. 21, pp. 257-267, 1998.

[24] Dechema, "Corrosive Agents and their Interaction with Materials," in *Corrosion Handbook*, vol. 11, G. Keysha, Ed., New York, VCH Publishers, 1992.

[25] R. Melchers, "Probabilistic Model for Marine Corrosion of Steel for Structural Reliability Assessment," *Journal of Structural Engineering,* pp. 1484-1493, 2003.

[26] R. Melchers, "Probabilistic Models of Corrosion for Reliability Assessment and Maintenance Planning," in *Proceedings of the Offshore Mechanics and Arctic Engineering Conference (CD-ROM)*, Rio de Janeiro, 2001.

[27] P. Shi and S. Mahadevan, "Damage Tolerance Approach for Probabilistic Pitting Corrosion Fatigue Life Prediction," *Engineering Fracture Mechanics,* vol. 68, pp. 1493-1507, 2001.

[28] T. Goswami and D. Hoeppner, "Pitting Corrosion Fatigue of Structural Materials," in *Structural Integrity in Aging Aircraft*, New York, ASME, 1995, p. 45.

[29] Y. Kondo, "Prediction of Fatigue Crack Initiation Life Based on Pit Growth," *Corrosion,* vol. 45, no. 1, pp. 7-11, 1989.

[30] R. Tryon and T. Cruse, "Probabilistic Mesomechanical Fatigue Crack Nucleation Model," *Journal of Engineering Materials and Technology,* vol. 119, pp. 65-70, January 1997.

[31] A. Coppe, M. J. Pais, R. T. Haftka and N. H. Kim, "Using a Simple Crack Growth Model in Predicting Remaining Useful Life," *Journal of Aircraft,* vol. 49, no. 6, pp. 1965-1973, 2012.

[32] N. Yamamoto and K. Igegami, "A Study on the Degradation of Coating and Corrosion of Ship's Hull Based on the Probabilistic Approach," *Journal of Offshore Mechanical Architectural Engineering,* vol. 120, no. 3, pp. 121-128, 1998.

[33] Wikipedia Commons, "Pareto Distribution," 24 April 2014. [Online]. Available: http://en.wikipedia.org/wiki/Pareto_distribution#Relation_to_Zipf.27s_law.

[34] M. L. Gross, "Investigation of the Fatigue Properties of Submarine Hull Steels," US Naval Engieering Experiment Station, Annapolis, MD, 1961.

Appendix A: Mil-Handbook-2189 Requirements[18]

Equations and conditions dictated:

Table I. Mechanical properties of shafting and sleeve materials.

Material Specification	Density lb/in³	*E* x 10⁶ Elastic Modulus lb/in²	*G* x 10⁶ Shear Modulus lb/in²	*UT* Ultimate Tensile Strength lb/in²	*YP* Yield[1] Strength lb/in²	*FL* FATIGUE[2] LIMIT (in air) lb/in²
Steel, forged						
class 1 MIL-S-23284	0.284	29.5	11.75	95,000	75,000	47,500
class 2 MIL-S-23284	0.284	29.5	11.75	80,000	55,000	40,000
class 3 MIL-S-23284	0.284	29.5	11.75	75,000	45,000	34,000
class 4 MIL-S-23284	0.284	29.5	11.75	60,000	35,000	27,000
class 5 MIL-S-23284	0.284	29.5	11.75	105,000	75,000	47,500
K Monel, forged						
QQ-N-286 (UNS N05500)	0.305	26.0	9.50	140,000	100,000[1]	50,000
Nickel aluminum bronze, forged						
ASTM B150 alloy C63000	0.274	17.0	6.40	80,000	40,000[4]	26,000
Ni-Cr-Mo-Cb, alloy 625						
cast (centrifugally): MIL-C-24615	0.305	26.9	10.50	70,000	40,000[1]	20,000[3]
forged:	0.305	30.0	11.50	120,000	60,000[1]	51,000[3]
welded inlay MIL-E-22200 and MIL-E-22200/3 type MIL-IN12 MIL-E-21562 type MIL-EN625	0.305	25.0	9.60	110,000	60,000	25,000[4]
Copper-Nickel (70-30), cast ASTM B 369 alloy C96400	0.323	22.0	8.50	60,000	32,000[4]	13,000
CPP oil, 2190	0.031	0	0	0	0	0
Sand	0.064	0	0	0	0	0

[1] 0.10 percent offset [2] 0.20 percent offset [3] In seawater and air
[4] At 10^8 cycles [5] 0.50 percent extension under load [6] In seawater (also used for in-air)

Table 1 includes the list of material property values to be used in design.

Maximum bending stress shall not exceed 6000 lb/in^2 (12,000 for alloy 625 clad weld materials).

This is to be calculated as the product of the stress and the stress concentration factor, (K_b x S_b).

---

[18] This entire appendix is from Mil-Handbook-2189. This material is primarily quoted directly from the source, and no further citations are provided.

Bearings are treated as point loads at the center of the bearing, with the exception of the aftermost bearing, which acts at the larger of the shaft diameter or one-quarter of the bearing length.

An allowance of an additional 20 percent of calculated torque shall be applied to account for increased resistance during ship maneuvers.

Torsional Load:

$$Q = \frac{63025\ x\ SHP}{RPM}$$

Total torsional load with increased load for turning:

$$Q_t = 1.2\ x\ Q$$

Steady shear stress:

$$S_s = \frac{Q_t x OD}{2xJ}$$

$$S_s = \frac{5.1 x Q_t x OD}{OD^4 - ID^4}$$

Bending stress:

$$S_b = \frac{10.2 x M_t x OD}{OD^4 - ID^4}$$

$$S_a = 0.05\ x\ S_s$$

Appendix B: Thesis for Engineer's Degree

Submarine Propulsion Shaft Life: Probabilistic Prediction and Extension through Prevention of Water Ingress

By

Douglas E. Jonart

M.S. Systems Technology (C3)
Naval Postgraduate School, 2008

B.S. Mathematics
University of Wyoming, 1995

SUBMITTED TO THE DEPARTMENTS OF MECHANICAL ENGINEERING AND MATERIALS SCIENCE AND ENGINEERING
IN PARTIAL FULFILLMENT OF THE REQUIREMENTS FOR THE DEGREES OF

NAVAL ENGINEER'S DEGREE IN NAVAL CONSTRUCTION AND ENGINEERING
AND
MASTER OF SCIENCE IN MATERIALS SCIENCE AND ENGINEERING

JUNE 2014

Signature of Author:_____

Department of Naval Construction and Architecture
May 9, 2014

Certified by:_____

Alexander H. Slocum
Neil and Jane Pappalardo Professor of Mechanical Engineering
Thesis Supervisor

Certified by_____

Ronald G. Ballinger
Professor of Nuclear Science and Engineering, and Materials Science and Engineering
Thesis Supervisor

Accepted by:_____

David E. Hardt
Ralph E. and Eloise F. Cross Professor of Mechanical Engineering
Chairman, Graduate Committee

THIS PAGE INTENTIONALLY LEFT BLANK

Submarine Propulsion Shaft Life: Probabilistic Prediction and Extension through Prevention of Water Ingress

by

Douglas E. Jonart

Submitted to the Departments of Mechanical Engineering and Materials Science and Engineering in Partial Fulfillment of the Requirements for the Degrees of Naval Engineer's Degree in Naval Construction and Engineering and Master of Science in Materials Science and Engineering

ABSTRACT

Submarine propulsion shafts have demonstrated acceptable reliability performance when inspected and refurbished at least every 6 years. Designers wish to extend the inspection interval to 12 years without sacrificing reliability. This interval is unprecedented, as no known submarine shafting system is currently operated with this inspection cycle, nor are any known commercial vessel shafts. Experience and improved design have eliminated many threats to the life of a submarine shaft, but inspections of existing shafts show a high percentage with signs of wetting, leaving designers with less-than-acceptable confidence to approve this longer inspection interval due to the possibility of corrosion fatigue failure.

This thesis uses probabilistic models from literature for pitting and cracking of wetted shafts, along with Monte Carlo simulations, to predict results of shafts inspections. Each possible water ingress distribution is analyzed by simulating shafts under 6 years of exposure to the water ingress, pitting, and cracking models in order to estimate the effects of corrosion fatigue. A water ingress distribution that predicts inspection results closest to actual inspection results is identified. Some information about water ingress is inferred from this distribution. Next, using the same literature models, a water ingress distribution that predicts similar performance at 12 years is identified. It is shown that the time a shaft is in service prior to becoming wetted must increase substantially. Predicted failure rates are low, but they are still higher than acceptable. This thesis recommends that inspection procedures are updated to provide more robust information for future analyses, which would better identify the appropriate distributions and greatly reduce uncertainty.

Thesis Supervisors: Alex Slocum
Title: Neil and Jane Pappalardo Professor of Mechanical Engineering, and Ron Ballinger
Title: Professor of Nuclear Science and Engineering, and Materials Science and Engineering

Contents

List of Figures

List of symbols

Symbol	Name	Units
a	Pit size (depth)	m
a_0	Initial pit depth	m
c	Characteristic pit or crack size	m
ΔH	Activation enthalpy	kJ
ΔK	Stress intensity factor (range)	$MPa/m^{1/2}$
$\Delta\sigma$	Stress (range)	MPa
f	Frequency	Hz
F	Faraday constant	J/(v g)
Hz	Measure of frequency	Cycles/sec (1/s)
I_{P0}	Initial pitting current	mA/cm^2
k	Number of particles	
M	Molecular weight	g/mol
n	Valence	
N	Number of cycles	
φ_k	Aspect ratio	
r	Pit size (radius)	
ρ	Density	Kg/m^3
R	Universal gas constant	J/(mol K)
t_{pg}	Time for pit growth	days

1.0 Introduction

Of critical interest to many industries is the reliability of components and systems. Reliability and service life prediction are inherently cross-disciplinary and complex topics. In general, engineers are able to design in adequate margins to deter known and anticipated failure modes. However, failures continue to occur that necessitate further changes to designs and systems. All too often, unanticipated failure mechanisms are discovered after parts and machines are in service, and reliability analysis tends to be a business of hindsight and lessons learned.

The world of ships and submarines, including those of the military, is not immune to the occurrence of failures. The submarines of many countries rely on a single propulsion shaft, making this shaft vital to the missions and effectiveness of these vessels. Moreover, a shaft failure that allows gravity or drag to unseat the broken shaft and remove it from the vessel creates a large diameter flooding penetration that is effectively impossible to plug, ensuring destruction of the submarine, and in a timeframe likely to claim the lives of all aboard, even if the vessel had been operating on the surface.

In spite of the best efforts of designers, there have been a number of submarine shaft failures. Designs have been continuously improved, and recent classes all but eliminate the possibility of shaft ejection, even if it fractures. The number of historical failures is a statement

about the complexity of the design and operations of these components: multiple modes of failure exist simultaneously, creating a very constrained design space. These mechanisms of failure are most often the result of complex interactions between geometry, materials, environment, loading, and many other factors, and therefore anticipating and quantifying their effect on systems is difficult. Establishing service life is often based on information and data from sources other than physical operation of the shaft in the ocean environment. Fitness for service analysis therefore requires extrapolating from a non-operating (laboratory data, simplified experiments, etc.) domain where experimental data is available or can be taken, to an application domain where there is little to no data. Often, obtaining application level data is prohibitively difficult or expensive [1]. In the case of submarine propulsion shafting, the size of the components, the length of time in service of the systems, and the highly variable operational environment all complicate, or outright prevent, direct testing. Scaled and simplified tests are performed instead, in an attempt to gain understanding of the issues, and the results are extrapolated to operating conditions. This is especially true in the areas of corrosion effects and corrosion testing.

Test results are very often used to develop models, which in the case of corrosion testing must be calibrated against extensive corrosion data, either with known environmental conditions or in situations where designers are capable of having these conditions established retroactively. [3]. Such data is not always readily available, and the business of extrapolation is more of a physics endeavor than a statistics endeavor, requiring in some ways even more depth

of understanding of the processes involved [1]. Another method might be to integrate existing data from other sources, but that also is not without its pitfalls. A review of attempts to pool models for corrosion indicated that such pooling produces poor-quality models exhibiting large amounts of scatter. [3]. Further, extrapolation methods do not deal with missing physics, and it is a common experience that solving one problem only reveals previously unknown couplings, physics, or failure modes [1]. This has been witnessed in submarine shaft maintenance and design, where repeated solutions have failed to provide the full expected increase to service life, as new failure modes – previously masked by modes with shorter time scales – come to control the service life and failure rate.

1.1 Existing Limit on Shaft Life

Past shaft failures on submarines have been systematically evaluated and their causes addressed throughout the history of the submarine service. Several reviews, often at design decision points for new classes or improvements to existing submarines, have been performed, each isolating the primary mechanism or mechanisms responsible for failures that limit the service life of the shaft. However, solutions to these limiting phenomena have served often to expose additional underlying mechanisms and failure modes – new physics as predicted by King et al., above. Notwithstanding this history, the navy currently has a class of submarines with 30

years of operating experience with no shaft failures. There have, however, been many cases where a shaft has developed precursors to failure by corrosion fatigue (pits, small cracks, etc.). Shafts are removed and inspected during scheduled maintenance periods in a drydock, with a 6-year maximum operational time on a shaft. At the end of each operational period, the shaft is removed from service for refurbishment and then returned to the rotating stock of propulsion shafts. Refurbishment consists of removal of all protective coatings and wear sleeves, followed by inspection through non-destructive testing and repair of all unacceptable conditions (defects and indications) identified. This 6-year limit is driven by concerns about corrosion fatigue, a process initiated by water gaining access to the carbon steel of the shaft to cause corrosion. Inspections of these shafts, though free of failures, confirm that corrosion fatigue does progress and needs to be monitored, particularly in the regions of concern indicated in Figure 1, which is a simplified schematic of the current propulsion shafting arrangement. In this figure, the shaft configuration aft of the dry, pressurized engine room is illustrated. The shaft passes through two bearings, each with an alloy 625 (an Inconel) sleeve. These sleeves exhibit exceptional corrosion performance, and are used as the wear surfaces in contact with the lubricated bearings. The stern tube bearing, on the right in the figure, is the transition point from the dry engine room to the wet ballast and mud tanks. Aft of this bearing (towards the left in the drawing), all spaces in the illustration are free-flood spaces, exposed to sea water at submergence pressure. The propeller, in the far left of the figure, is attached to the shaft. From the propeller bearing aft, the remaining length of shaft and propeller are suspended with no further supports, creating a strong bending force, often modeled as a

cantilevered beam. Each revolution of the shaft for propulsion, however, changes the orientation of this bending moment, relative to any point on the surface of the shaft, through a full cycle of bending (from maximum tension to maximum compression and back). Though the shaft is almost completely encased in a glass-reinforced plastic (GRP) coating, the figure indicates that at each waterborne end of each of the sleeves, water sometimes gains access to the shaft steel, and combines with this cyclic bending load (as well as the torsional load of propulsive forces) to create the conditions that lead to corrosion fatigue.

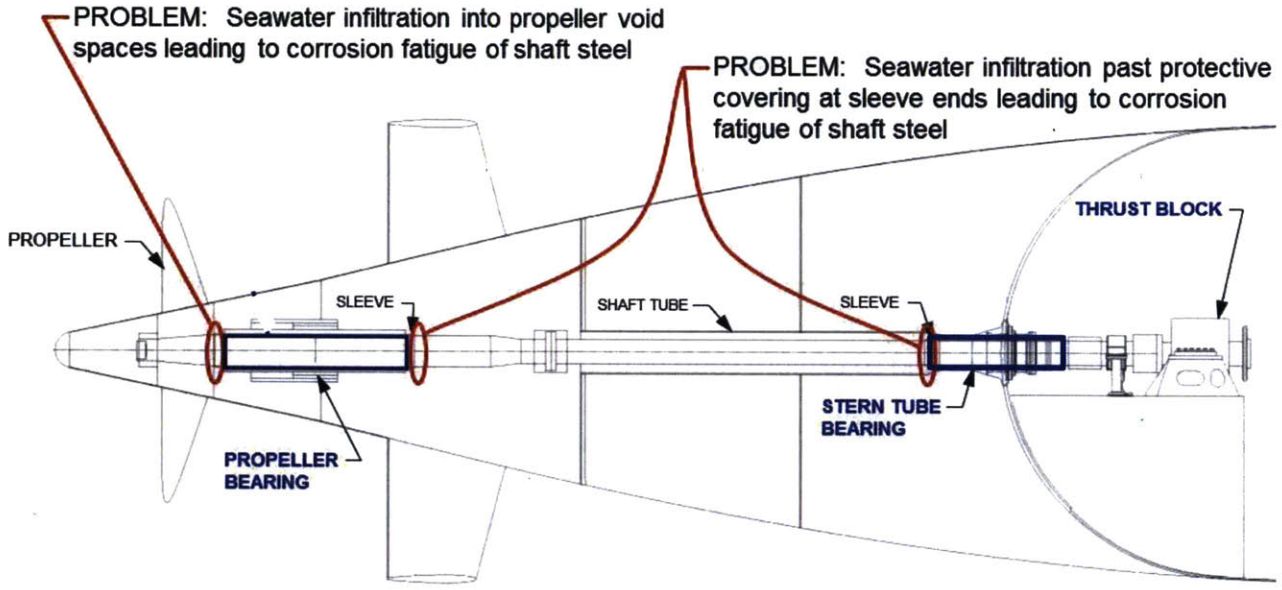

Figure 1: Schematic of submarine shafting indicating regions of corrosion fatigue concerns[19]

[19] Taken from "Shaft Life Advancements", W. H. Needham, Presentation at Shaft Life Advancement Industry Day at MIT, October 13, 2011.

The submarine community has elected to increase the propulsion shaft inspection interval for the next class of submarines, now in the beginning stages of design, to have scheduled availability in a drydock every 12 years, instead of 6. This requires a substantial increase in the service life of the propulsion shaft, but it is a key to saving billions of dollars in the procurement, operations, and maintenance of the vessels. To achieve this goal, the navy needs to better understand and design against corrosion fatigue of these components. One researcher gives a summary which captures the difficulty of this task:

> *"In practice corrosion is not an independent issue. Corrosion interacts with applied stresses, fatigue, mechanical damage, and most importantly, with protective systems such as cathodic protection, paint coatings, and management practices. The interaction with each of these phenomena or materials is generally complex and the interactions are not fully understood in most cases. There is considerable scope for further fundamental and applied corrosion research. Eventually this will need to be translated into engineering design rules and guides for the "protection" of ageing infrastructure, including the development of probabilistic models."*[20]

The submarine community finds itself looking for precisely this kind of probabilistic model to evaluate design options and to explore sources of uncertainty that can be reduced that will help achieve its aggressive shaft service life goal. Shi and Mahadevan (2001) identify three methods to ensure component reliability: a "safe life" method requiring the structure to survive under a given loading for a specific number of service cycles, essentially a mechanics only condition; the "fail safe" approach that requires the entire structure be capable of damage without

---

[20] Melchers, "Probabilistic Model for Marine Corrosion of Steel for Structural Reliability Assessment," 2003. P 1492.

catastrophic failure of the entire structure; and a "damage tolerance" approach assuming an initial flaw or defect that grows, but the growth of which is not adequate to endanger the structure during the design or service life and can be found by inspection and repaired. The third approach is most applicable here, with corrosion damage and pit formation filling the role as the initial damage, with the potential of transitioning into cracks that must not be allowed to grow until they endanger the shaft.

An example of this process is found in the reliability analysis of steam generators in nuclear power plants. Analysis of steam generator tube failure data reveals that failures were derived from multiple sources, including stress corrosion cracking, fretting, and damage from foreign objects. The most prevalent source of failures, however, was cracks in the roll transition region of the tube sheet-a situation analogous to the shaft degradation process and the challenge of the submarine force, primarily concerned with corrosion leading to cracking [22]. In the case of these nuclear steam generators, there is a large and expanding database from inspections that allows for ever-improving statistical and engineering analysis. Instead of a large database of failure history, shaft inspection data is available from only approximately 60 shaft inspections. Unfortunately, the quantity and quality of data available are both considerably less than Pitner was able to obtain. A single, comprehensive analysis of data is not an accessible solution, so the problem of corrosion pits and inspection intervals to preclude failures from corrosion pitting and fatigue cracking must be tackled through other methods.

1.2 Complexity of the Problem

The problem of corrosion fatigue failure that faces the submarine community is not uncommon: after conducting a thorough review across many applications, corrosion pitting was found by one group of researchers to be responsible for nucleating fatigue cracks in a wide range of metals (Chen, Wan, Gao, Wei, & Flournoy, 1996). Expanding on both the ubiquity and complexity of the problem, another pair of researchers declared that fatigue crack initiation and growth had been found to degrade reliability of many structures subjected to repeated loadings. They further state that the data on this process exhibits considerable scatter, creating a significant challenge for the design for reliability, which needs to recognize appropriate extreme value behavior (3-sigma reliability or other metrics giving a small probability of failure) [23].

Corrosion fatigue requires a series of events, sometimes referred to as a failure chain or event tree, to proceed in succession. Each step involves different physics and is controlled by different parameters and interactions of the many variables involved. Figure 2 depicts the corrosion fatigue sequence of events that limits the submarine shaft service life, and lists a few of the challenges that complicate each step. Though the shaft system has a number of protective systems and features in the design, much of the system is submerged in seawater, as shown in Figure 1, and water eventually reaches the mild steel of many shafts, beginning the corrosion fatigue process. The mild shaft steel, when exposed to this seawater environment,

corrodes, and that sometimes leads to the formation of pits. These pits act as stress concentrators for the various loads on the shaft, and sometimes cracks form, then propagate, leading to one failure mechanism.

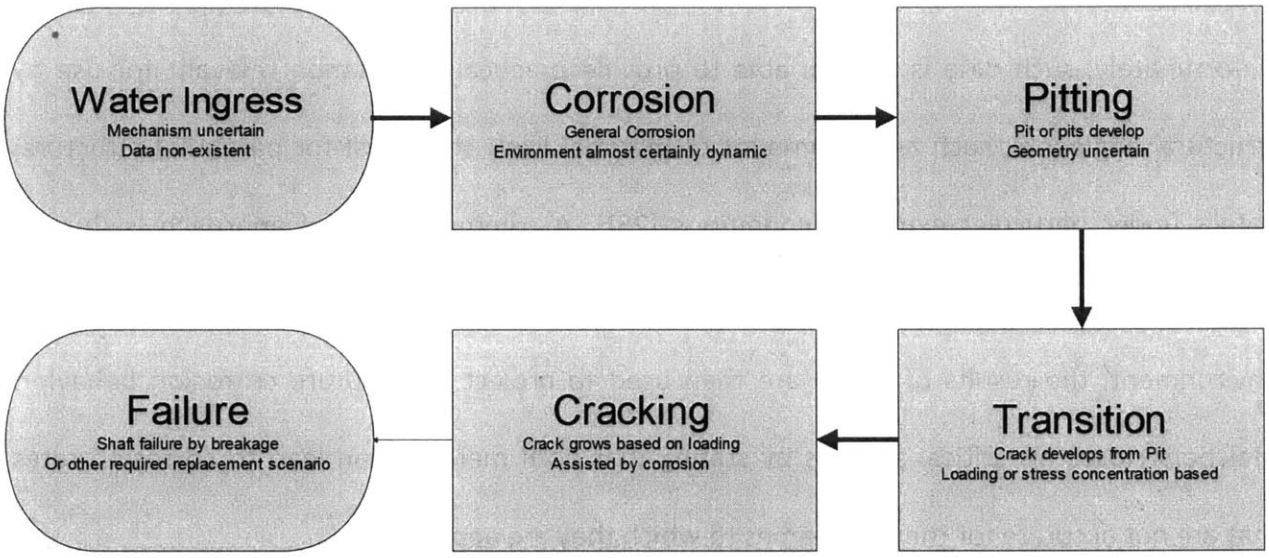

Figure 2: Corrosion fatigue process

The focus of this thesis is the development of a model that provides information to help estimate the required inspection interval for shafting. Water ingress, and its timing, is critical to the analysis of shaft life. By modeling each of the subsequent steps, possible distributions of water ingress may be analyzed. Due to the many combinations of materials, environments, environmental factors, and types of corrosion, only limited data is usually available for a given material exposed to a particular environment. This is the case for mild steel under marine conditions [24] including submarine propulsion shafting. Melchers (2003), a structural

engineer, states that much of the data that is available comes from short-term tests under laboratory conditions. He goes on to state that, though the literature on corrosion is extensive, conventional corrosion theory consists mainly of general principles and electrochemistry and is applicable mainly to short-term corrosion tests under specific and often ideal conditions. Unfortunately, such data is seldom able to provide practical information relevant for use by structural engineers, such as the amount of material likely to be lost for particular structural details under particular exposure conditions [25]. A common practical approach is thus to consult compendia based on experience [24] or to conduct coupon exposure tests in a specific environment, the results of which are then used to project likely future corrosion behavior. Melchers closes his critical analysis by stating that both methods can lead to corrosion rates that are not accurate for the timeframes to which they are applied [25].

Examining the areas of concern for corrosion pitting, there are additional complexities with which to contend. Figure 3 provides a more detailed view of one of these areas. This figure illustrates the aft portion of the shaft as it exits the stern tube bearing. There is an alloy 625 (Inconel) sleeve, used as a wear surface for the bearing interaction, as seen in the drawing. This bearing is placed on the shaft using a shrink-fitting technique, and then a GRP protective layer is applied covering the sleeve-shaft interface and the length of the shaft. The area labeled as a typical corrosion area indicates where inspections have revealed many defects, typically referred to only as "indications" on an inspection report. The path the water takes to access this area is not yet known. It is also not known if there is free exchange of fresh seawater into

the area once penetrated, or if the water stagnates in the small geometry created. It is therefore unknown if this region under attack is an aerobic environment, an anaerobic environment, or possibly one in which the intitally available oxygen becomes depleted, each of which would have a different corrosion response. Other work by this project has revealed that water in this region may complete a galvanic circuit between the sleeve material and the shaft steel, which would indicate a very high corrosion rate that might be brief or might endure long enough to create significant damage. Each stage of the event tree in Figure 2 has similar complications, making the modeling of the corrosion fatigue process in this case difficult.

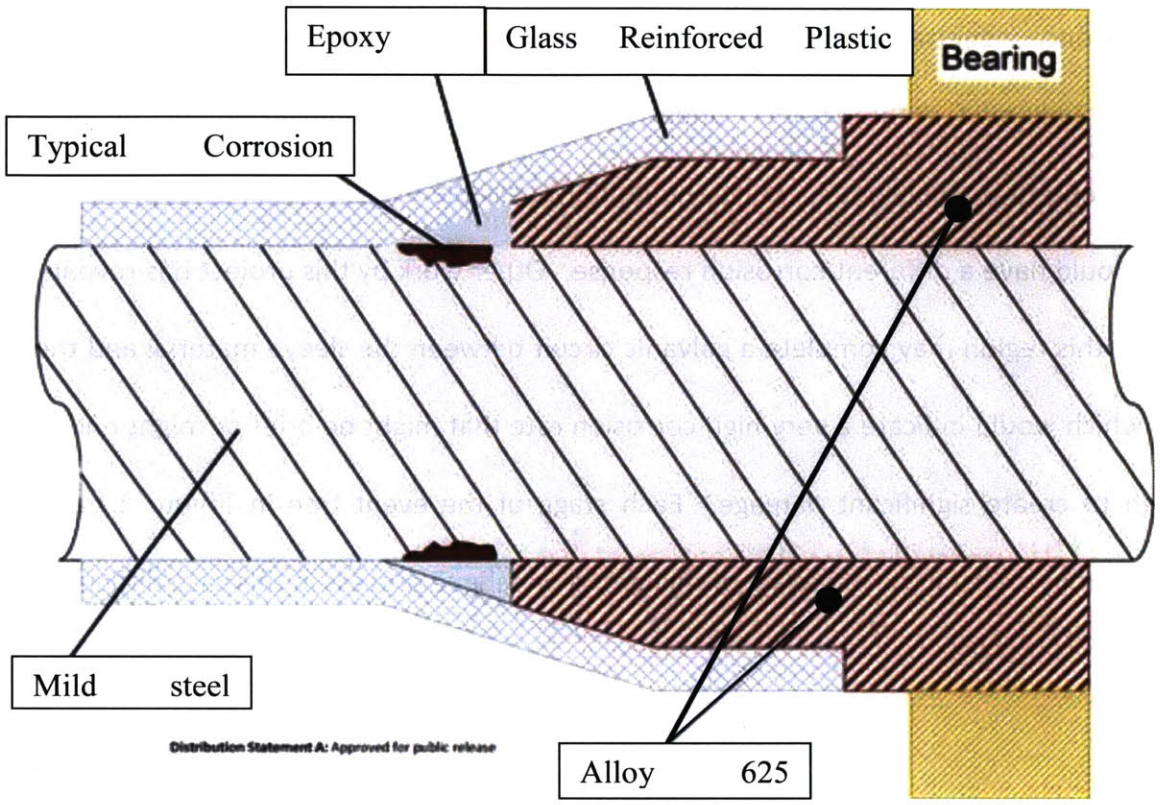

Figure 3: Detail of shaft/sleeve interface, highlighting region of concern[21]

1.3 Possible Solutions

Due to the above considerations, the task faced by submarine designers to mitigate environmental degradation of the shaft material is difficult. There are a number of possible solutions, each of which might partially or completely achieve success. For example, increasing

[21] Taken from "Maintenance Free Technologies Overview", Dr. Airan Perez and Edward Lemieux, Presentation at Shaft Life Advancement Industry Day at MIT, October 13, 2011.

the detail of the inspections to provide more robust information would give designers a stronger footing from which to predict performance of the existing shaft system. For example, it is not currently known if a particular "indication" is a pit, a pit with a crack, a machining artifact, or another of several possibilities. The ability to characterize the distributions of indications may allow designers to develop more robust life prediction models to evaluate the likely time to failure for the existing system. As will be discussed, however, the limited data available gives little promise that this method alone will provide confidence in the current shaft design with a 12-year shaft inspection interval.

According to the information provided by the submarine community, the current design has accounted for and effectively eliminated all purely mechanical sources of failure known to have previously affected propulsion shafts. If the shaft can be kept dry with high confidence, therefore, the longer shaft life will likely be achieved. Designers, unfortunately, have little information regarding the current time or mechanisms of water ingress, and essentially no existing data on effectiveness of current or proposed systems to prevent water from accessing the shaft metal. However, preventing water ingress is an attractive solution for achieving a longer service life, as it requires few significant changes to the design of the shaft itself, and interrupts the failure chain depicted in Figure 2 at the earliest possible point.

There are other solutions; the shaft design itself could be changed in ways that interrupt the failure chain elsewhere. Incorporating materials that are less susceptible to corrosion, or perhaps immune to pitting in the operational environment, would reduce or eliminate the

likelihood of corrosion fatigue failures. Research on pipelines shows that, after the transition from pits to cracks has occurred in the field, tiny, elongated, blunt cracks are often seen in very large numbers and frequently in crack colonies. The majority of these cracks become dormant, but if they surpass a threshold depth, around 0.5mm, they can propagate and may lead to pipeline rupture if not detected and removed. [4]. It might be possible to design a shaft that causes even more cracks to become dormant, or in which the threshold is higher. As the scale of design changes grows, however, a conflict quickly arises between making changes believed to solve the current problem and the added risks of new problems being exposed, alluded to by King et al. (2012) and previous shaft life experiences.

Submarine designers have revealed that, in order to progress through the procurement process on schedule, there is an immediate need to establish confidence in the ability to achieve a 12-year maintenance cycle. For this reason, solutions requiring less expansive testing and validation are preferred over solutions requiring longer programs of study and analysis. Major design changes, and truly exotic solutions such as shaftless propulsion, are therefore beyond the scope of this project, although their long term pursuit is recognized as having value for subsequent classes of submarines, where the design and testing windows might better facilitate them. To that end, this project has also performed a limited investigation into the feasibility of developing a cladding material that would largely preclude pitting, and which could be evaluated and tested in a time frame for the future submarine classes. However, the focus of the project, and this thesis, is on the immediate needs of the class currently being designed.

This thesis infers information about water ingress for the existing design by coupling models for subsequent steps of the failure chain with summary data from the shaft inspections performed to date. It then makes a first order prediction of the failure distribution for the existing shaft design, if they were to be left in service without refurbishment. Finally, the same models will be used to evaluate the required water ingress distribution that must be achieved, assuming no other major changes in the shaft design, such that a 12-year service life yields similar predicted inspection performance.

2.0 Existing Models and Life Predictions

To develop the models needed for this study, literature on the subject and on each phase in the failure chain is considered. The information available to engineers about marine corrosion, for example, is largely anecdotal, not well organized, and of limited use even for simple applications, according to Melchers. Although classification societies and a number of navies regularly collect plate thickness measurements as estimates for corrosion loss, little of the data has been published for a variety of reasons [25], though a review of published corrosion statistics for ships is available [26]. More specific to the immediate concern of corrosion fatigue, field evidence suggests that corrosion pits might be a common site for crack initiation. In one laboratory study, the earliest cracks appeared to initiate at corrosion pits forming around non-metallic inclusions; later cracks grew from corrosion pits that formed randomly on the surface [4]. The models of these researchers and others are considered in this section.

A distinction must be drawn between corrosion pits, of concern here, and pitting corrosion. In mild steels in a corrosive environment, anodic and cathodic areas tend to move around on the surface to create the impression of uniform corrosion often referred to as "general corrosion" [3]. However, the level of uniformity is subjective, and various localized surface geometries may develop. In stainless steels, aluminum alloys, and several other corrosion-resistant metals, this general corrosion is significantly resisted by the formation of passive, protective layers, often oxides. In locations where the protective layer is breached, corrosion may be rapid and

highly localized, burrowing deeply into the metal, creating a pit with a very high depth-to-diameter aspect ratio. This is called pitting corrosion, and is not of primary interest here, as the shaft is a mild steel. Even for the general corrosion of mild steel, buildup of a complex corrosion product film on the surface of the corroding metal will soon control the behavior by inhibiting the supply of oxygen to the corrosion interface even for fully aerated waters [3]. In this environment, local areas with higher corrosion rates may develop, creating depressions in the surface that often take the form of shallow, low-aspect ratio pits, called corrosion pits. It should also be noted that galvanic couples between the shaft steel material and more noble metals can cause highly localized corrosion. In fact, as indicated in Figure 3, the region of the shaft immediately adjacent to the alloy 625 bearing sleeve is one such area, and such a couple is suspected based on other work by this project, though that work is not detailed in this thesis. Under load, especially a cyclic load, these corrosion pits may affect the stress concentration and response of localized regions, including the formation of cracks. This is the pitting that is of concern in the current research, as one of the steps in the corrosion fatigue failure chain depicted in Figure 2.

In the remainder of this chapter, several views of the entire process of corrosion fatigue will be discussed, followed by a more detailed review of existing treatments in the literature for each step in the failure chain. Finally, as it will be shown to be of deep concern, a general treatment of uncertainty as it relates to the development of models and to predictions from those models will be evaluated.

2.1 Selection of a Framework

Fatigue cracks are very often observed to nucleate and propagate from corrosion pits [27]. Many researchers have studied this important phenomenon, with varying methods and resulting conclusions. One paper concluded that, "in the field, it generally takes years for pits to grow and initiate cracks, and the pit growth may proceed under intermittent exposure conditions" [4]. Another group contended that there is a competition between time spent in pit growth and crack growth, citing the results in Figure 4, which show that longer times spent growing (larger) pits correspond to greatly reduced growth times for the cracks that initiate from these pits:

The effect of pit size on the corrosion fatigue life

Transition size from pitting to crack nucleation c_{ci} (mm)	Pit growth time (days)	Short crack growth time (days)
0.05	69	6690
0.1	554	3860

Figure 4: Demonstration of effect of larger pits on crack growth duration[22]

[22] Taken from Shi and Mahadevan, "Damage Tolerance Approach for Probabilistic Pitting Corrosion Fatigue Life Prediction," 2001, p. 1499.

In Kondo (1989), who is very often referenced as a starting point for other models, the author assumes that failure occurs in three stages: pit initiation and growth, crack initiation from the pit, and crack propagation. In another example, researchers first performed a then-exhaustive review of models and solutions [27]. This pair then built on work from several authors: a three-stage model from one source [7], a seven-stage model proposed but not numerically developed [28], Harlow and Wei's probabilistic pit corrosion model (reviewed in several sections of this thesis), a development of Kondo's transition model by Chen et al. (also detailed in this thesis), and a series of other studies. Shi and Mahadevan, who define both short and long crack stages, conclude that short crack growth rates exceed those of long cracks – thereby necessitating the separation of the two in their model [27].

Some of the most comprehensive work is done by Australian Robert Melchers, who informs his readers that future models must be probabilistic, to account for uncertainties caused by: modelling approximations; variability in environmental conditions and in modeling them; and variations in material [3]. In the analysis of this thesis, the goal is to make use of the best probabilistic models, heeding Melchers's instruction. Melchers goes on to state that variability is due to a number of sources, but unfortunately there are very few suitable data available, going on to say that even for variability between coupons at the same site, most published reports give insufficient information for its estimation, typically reporting the mean of (usually only) two coupons and not even the individual results [25]. Evaluation and selection of models for this paper, then, must consider treatment of variability, as well.

Returning to the summary work of Shi and Mahadevan, they conclude that the fatigue life of a component in a system is the sum of four critical phases: time to pit nucleation, time for pit growth leading into short crack nucleation, time for short crack growth, and time for long crack growth. Their model also includes transitions between these times as additional stages, as illustrated in Figure 5 [27].

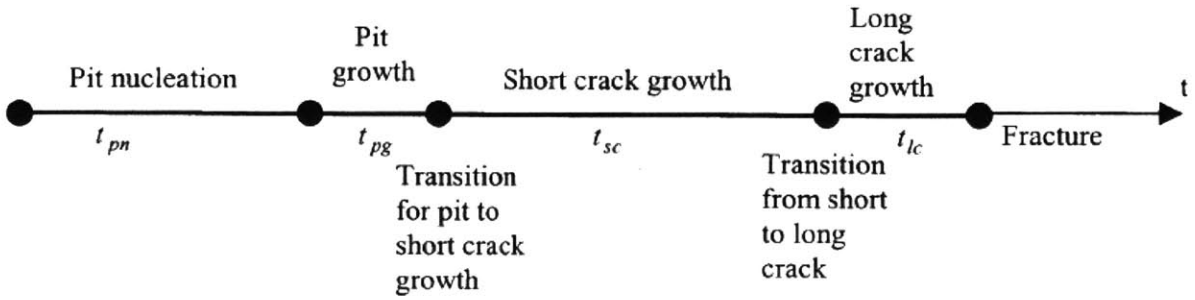

Figure 5: One model considering 7 stages, four discrete phases in time and three transitions[23]

Evaluation of the sometimes anecdotal information from the submarine shaft inspections reveals that few cracks have developed, none of which have propagated to failure. While good news from the standpoint of reliability, this also means that very little information is available for the calibration and/or validation of detailed crack modeling results. For this reason, detailed consideration focuses on the following phases, consistent with the chain presented earlier: corrosion, primarily as it becomes a source of uncertainty; pitting, both nucleation and

---

[23] This figure is taken from Shi & Mahadevan, "Damage tolerance approach for probabilistic pitting corrosion fatigue life prediction," pp 1495.

growth; and transition from pits to cracks. A simplified crack growth model is used for first order failure predictions once water ingress distributions are identified for both 6 and 12 year service lives.

2.2 Corrosion and Corrosion Rate

Melchers's review of published corrosion loss data for structural steel coupons in immersion conditions immediately reveals that corrosion is not linear in time, and shows very large scatter. He concludes that "corrosion rate" has limited meaning and that a rate measured over a short time may be quite misleading in predicting longer-term corrosion. It also follows (due to the observed scatter) that any probabilistic models based on such data will have a high level of uncertainty and be of limited use [25]. In later work, Melchers proposes a more complex model for corrosion based on review of many studies. The general model is schematically depicted in Figure 6:

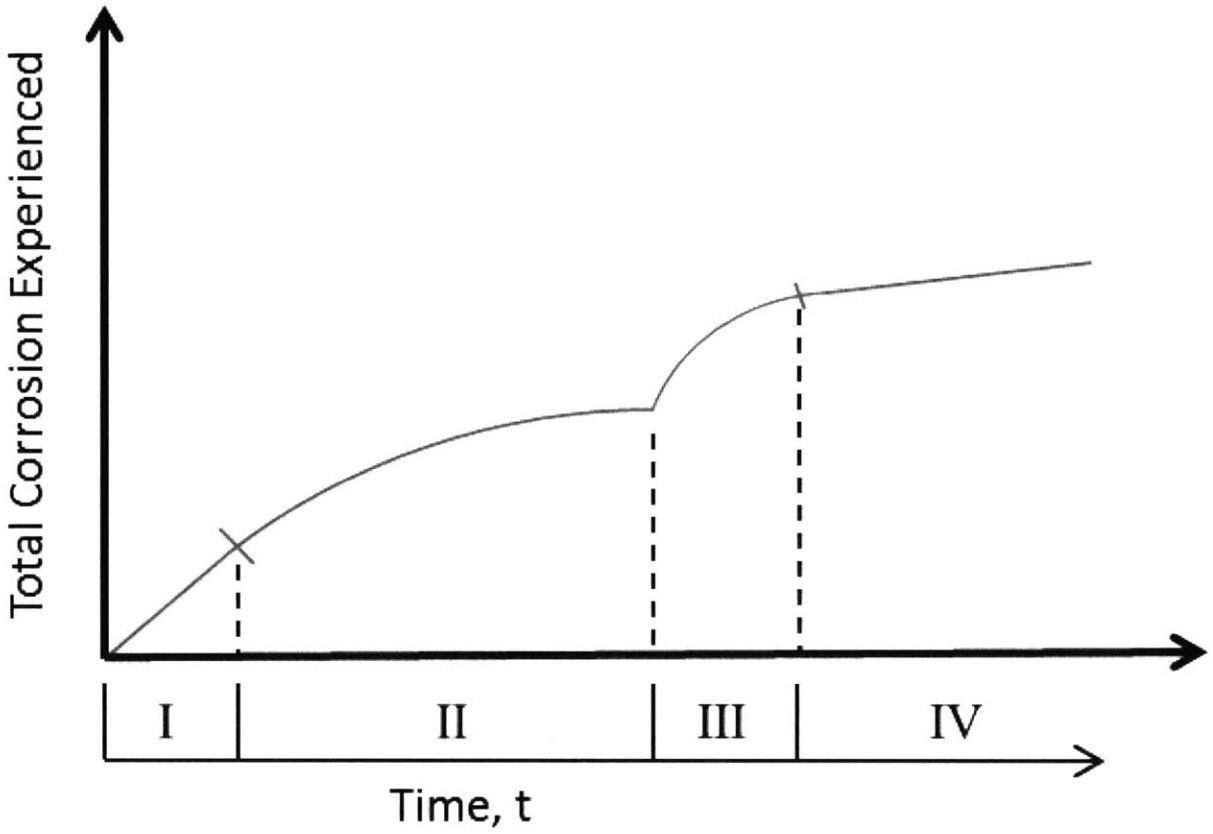

Figure 6: Melchers's model for corrosion over extended periods of time[24]

A detailed description of the model, paraphrasing the author's longer explanation, follows. Phase 1 in his model is called the kinetic phase, and consists of the time immediately following immersion. Initially, a rapid increase in corrosion rate (from zero) quickly leads to a steady rate of corrosion, which is indicated by the slope of the observed linear region. Usually under

[24] Although he references this model in many of his works both before and afterwards, this depiction was taken from his second 2003 paper, partially titled "Part 2: Models Based on Mechanics," p 273.

oxygen concentration control, this rate is the value commonly referred to and tested as the "corrosion rate." Phase 2 develops as a buildup of film (corrosion products) limits the diffusion of oxygen to the base metal, such as diffusion control through rust in the mild steel case. Phase 3 is when biological organisms and other organic processes, especially sulfate reducing bacteria (SRB), take over to again increase the corrosion rate. He notes that no models exist for this non-linear region that is dependent on numerous parameters. Phase 4 is the asymptotic, long term corrosion behavior. Commonly, Phases 1 and 2 are of the greatest practical interest. However, he also notes that Phases 3 and 4 may be of primary interest in tropical waters. [25]. Developing this model, he does note that SRB regions are likely to be under activation control, as these bacteria operate independent of oxygen; hence the long term rates are often dependent on metal composition and temperature more than other factors [3].

Acknowledging these complications, the analysis in this thesis uses published rates and statistics on variability, but recommends side-by-side experiments using natural and artificial seawater environments for future work.

2.3 Pit Nucleation and Growth

Much of the research that deals with pitting in detail is concerned exclusively with pitting corrosion (discussed/defined in the beginning of this chapter), and is therefore of limited

applicability to the mild steel of submarine shafts. Additionally, pit nucleation distributions are often simply assumed or treated deterministically. Kondo, for example, "develops" pits according to the deterministic model that the radius of observed pits is given by: $r = t^{1/3}$. This model, then, implies that a virgin surface nucleates minute pits as soon as it goes into service [29].

A probabilistic method was used by Shi and Mahadevan. In their model, consisting of seven stages, they stated that time to pit nucleation depends on numerous factors which were not yet well understood. They therefore treated the time to pit nucleation and the size of initial pits as random variables, and then tested several possible distributions of each. By comparing the results with these various nucleation distributions to field experiences, they were able to infer which distributions might be likely [27]. As this method is similar to the water ingress method used in this thesis, the analysis of this thesis uses the distributions that the authors identified as most consistent with experimental data for pit nucleation, rather than trying to distinguish from among the effects of several simultaneously changing distributions.

The question of geometry is central to many discussions on pits and pit growth. Almost all authors assume a somewhat idealized geometry. Kondo (1989), for example, assumes hemispherical pits. Harlow and Wei (1998) derive their growth formula assuming ellipsoidal pits, and they take three approaches to handling aspect ratio as each pit grows. Their first method is to assume a fixed aspect ratio, from which they derive the following pit growth model, equivalent to those of several other authors:

$$\frac{2}{3}\pi\emptyset_k^2(a^3 - a_0^3) = \frac{MI_{p_0}(k)}{nF\rho} exp\left[-\frac{\Delta H}{RT}\right] t \quad (1)$$

where k is the number of constituent particles initiating a given pit, $\emptyset_k$ is the aspect ratio, a is pit depth, a_0 is initial pit depth, M is molecular weight, $I_{p0}(k)$ is the initial pitting current (a function of k), n is the valence, F is Faraday's constant, ρ is the density, ΔH is the activation enthalpy, R is the universal gas constant, T is temperature in kelvin, and t is time. The other two treatments of aspect ratio provide complex solutions and are not considered in detail in their analysis, so they are omitted here [8].

Equation 1 appears in several papers reviewed for this research, though this is the most general form. In this formulation, taking $\emptyset_k$ = 1 yields the hemispherical assumption, which is used often by other authors. In a study using an accelerated method to generate pits, it was clear after inspection that the pits generated were nearly circular on the surface, and semi-circular in cross-section, giving support to the simplest geometry [4]. After some work, even Harlow and Wei assume hemispherical pits, but note that their sample of more than 1500 pits gave an average aspect ratio, $\emptyset_k$, of 1.57, with a range of 1.0 to 4.2, so they intended to consider ellipsoidal pits in future work [8]. More complex geometries might be justified in the future if further details become available from better shaft inspection data, but as stated earlier, only somewhat vague counts of "indications" are available for the analysis in this work. For this reason, and due to its ubiquity and acceptance for first-order evaluations, hemispherical pits are assumed in this analysis. Additionally, a strong argument can be made for treating $\emptyset_k$ itself

as a random variable, but pragmatism leaves it being treated deterministically in almost all published modeling [8], as it will be treated here.

There are few pit growth models in the literature that differ substantially in form from the model developed by Harlow and Wei (1998). These two authors begin with a probabilistic distribution of constituent particles based on scanning electron microscope images of titanium. Their pit growth model has a probabilistic initial current dependent on the clusters of these particles, modeled as a Pareto distribution (see Appendix A for discussion of this distribution). Referring to pits as initial damage, they assume this damage nucleates on the bare surface as a pit due to a localized galvanic corrosion cell surrounding exposed constituent particles in the alloy. Their work includes an argument that only cathodic particles need to be evaluated, as well as derivations of the models they invoke. It is also of note that their concern was aluminum, although their distribution was based on titanium samples, and their work is applied to other metals by other authors [8]. This probabilistic growth was deemed to be the most appropriate for the analysis in this work.

2.4 Transition from Pit to Crack

Many researchers conclude that pits transition into cracks. Fang et al. (2009) found that blunt cracks initiated around corrosion pits, which the authors stated were acting as stress concentrators. Though they didn't directly deal with a transition model, they did state that pits

were the principal sites for crack initiation [4]. In general, the transition from pitting to cracking is handled by either a critical pit size model or a pitting/cracking growth competition model. In each, the pit is handled as a surface crack with growth described by pitting kinetics [2].

In the critical pit size model, the fatigue crack nucleates when the pit is large enough for local mechanical conditions to allow for crack growth. This is most often defined in terms of the pit producing a stress intensity factor equivalent to the factor that would be produced by a crack of equivalent depth, shown in its simplest form in Equation 2 [2]. Harlow and Wei, for example, state that pit growth continues until a critical size is reached, at which time a small corrosion fatigue crack nucleates with high probability [8]. Note that assumptions made to simplify pit and crack geometry must be applied with care in this criterion, as transition is critical in determining the relative lengths of growth phases, and therefore service life.

$$(\Delta k)_{pit} = (\Delta k)_{crack} \tag{2}$$

On the other hand, fracture mechanics dictate transition in the competition model, with transition occurring according to Equation 3, when the pit growth rate is first exceeded by the growth rate of a crack with similar geometry, often an assumed sharp crack with the same depth [2]. Again, oversimplification can be a danger, as can assumptions on which dimension of the pit is used for the initial crack geometry.

$$\left(\frac{dc}{dt}\right)_{crack} \geq \left(\frac{dc}{dt}\right)_{pit} \quad (3)$$

One paper gave results suggesting that both transition models can be valid. In aluminum alloys, pit size for corrosion fatigue crack nucleation was found to be dependent on loading frequency, as shown in Figure 7. In this graph, the horizontal axis is 1/f, so frequency increases from right to left. Examining the data and trends, then, it can be seen that the stress intensity at transition decreases with increasing frequency, and then seems to stabilize and become independent of frequency. This research found that critical pit size is independent of frequency for high frequency loading, but for loading below about 5 Hz, the growth competition model criteria must also be met before a crack will nucleate [2].

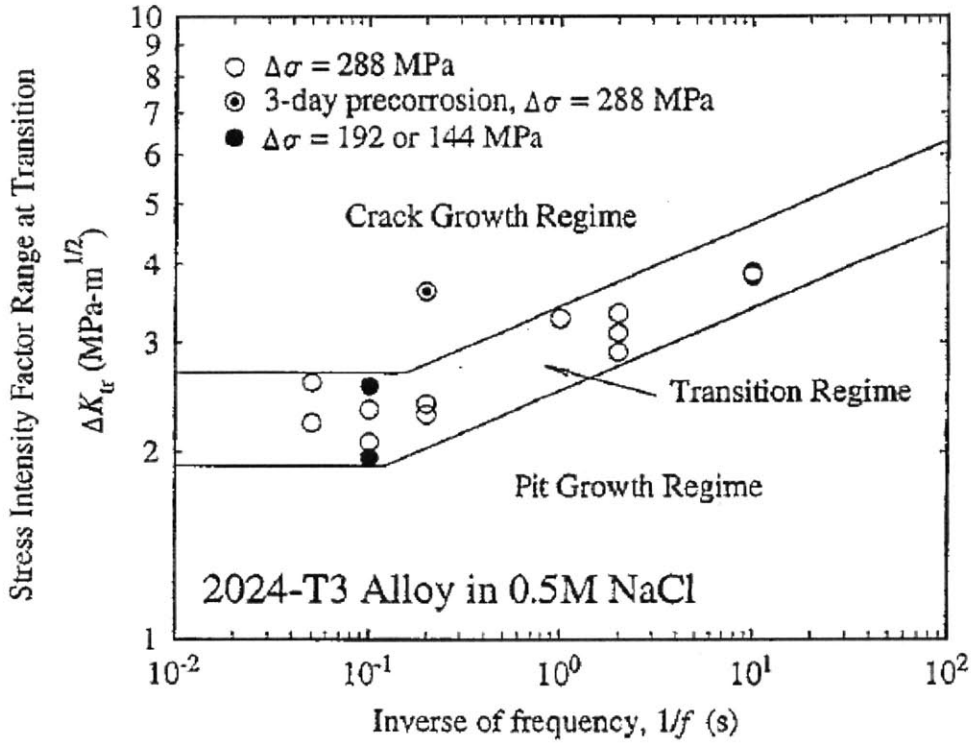

Figure 7: Stress intensity factor vs. load frequency for corrosion fatigue crack nucleation[25]

Developing this set of transition criteria further, these authors also produced Figure 8, in which increasing frequency is depicted by a line, and a series of individual frequencies. In this construct, it can be seen that for lower frequencies, pits grow for less time, transitioning quickly, due to the very high crack growth rates at these frequencies, indicated by the high slope of the f_1 line at a, for example. However, for higher frequencies, the crack growth would be lower, and the pit growth rate would dominate for a longer period, meaning that until the pit had grown sufficiently large, and its growth slowed considerably, that the crack would not form. For this reason, at high frequencies, transition would be dominated only by the necessity

[25] This figure is excerpted from Chen et al., "Transition from pitting to fatigue crack growth – modeling of corrosion fatigue crack nucleation in a 20204-T3 aluminum alloy, pp 130.

for a sufficiently large pit. At point a, the rapid crack growth would dominate, and the overall growth rate would increase when a crack formed, whereas for b and c, the crack and pit growth rates are equal at transition.

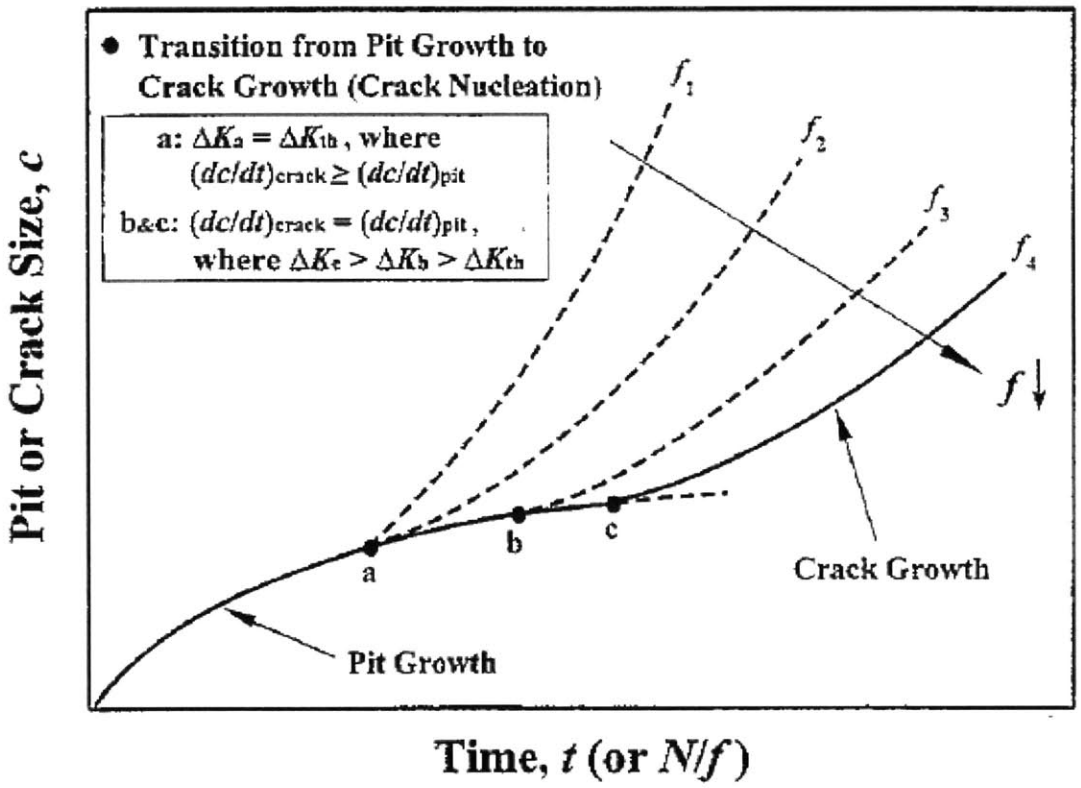

Figure 8: Conceptual framework for the damaging process of corrosion fatigue[26]

In this thesis's analysis, it is known that submarine shafts are cyclically loaded at many different frequencies, and almost exclusively below the 5 Hz transition point indicated in Figure 7. The

[26] This figure is excerpted from Chen et al., "Transition from pitting to fatigue crack growth – modeling of corrosion fatigue crack nucleation in a 20204-T3 aluminum alloy, pp 131.

work presented by Chen et al. (1996) was for aluminum, so it is possible that steel could transition at a different frequency, or potentially not at all. Typical submarine operations would have the shaft rotating considerably slower than 5 Hz, so it was reasonable to consider the growth rate criteria for submarine shafting. Loading is highly variable in the three regions of interest illustrated in Figure 1, with torque loading changing as the submarine changes speeds and maneuvers, and the bending frequency changing with the frequency of the shaft rotation. As loading affects crack growth rate, and therefore any transition criteria based on competition models, some consideration was given to the ramifications of assumed loading. As previously stated, investigation of cracking for this analysis is first-order only, and it was not desired for a somewhat arbitrary rate competition criterion to overshadow other factors. Each of the transition models was tested in several preliminary analysis paths, and it was found that using the simple 0.5 mm criteria from Fang et al. (2009) was quite conservative, especially with varying loading. This transition criterion is therefore applied as a mean for critical pit size.

2.5 Crack Growth and Failure

In modeling the failure process, one pair of authors advise that a model must recognize the multiple stages of fatigue damage accumulation such as crack nucleation and long crack growth. The authors further declare that each stage is driven by different mechanisms and

requires distinct modeling characteristics, as well as quantitative links that match the progression of defects from one stage successively onward [30]. Up to this point in the chapter, the current analysis has evaluated the treatment of the processes that lead to cracks. Several sources agree that these processes may account for the larger portion of the service life of components. In one example, Fang et al. (2009) found that the main fraction of pipeline life is consumed in the crack initiation process. Other research disagreed; as mentioned, the model of Shi and Mahadevan had a long short crack growth phase and a much shorter long crack phase, and their results suggest that if small pits transition into cracks, the time for short crack growth is much longer than the time for pit nucleation and growth, as was illustrated in Figure 4 [27]. For Fang et al. (2009), growth of cracks in three stages was observed. Early, blunt transition cracks became sharp cracks which grew based on proposed hydrogen interaction. The growth of these two stages consumed a majority of pipeline life compared to the long crack growth in stage three that threatened rupture and pipeline leakage, implying that crack precursors took the most time, followed by the combination of the first two phases of crack growth, and finally the terminating phase of crack growth was shortest [4].

In 1997, two researchers argued that most fatigue crack models are based on macrostructural variables, without accounting for the microstructural inhomogeneity that governs small crack growth. They stated that, in such models, propagation of cracks was reduced to the use of parametric functions of macro-level stress and strain. The challenge precluding better work was that too many micromechanical processes operated simultaneously and randomly [30].

Elaborating on this complexity, other researches declared that many models describe crack growth as a function of stress-intensity factor. This factor is a complicated function of loading, boundary conditions, crack position, and geometry, such that except for very simple or idealized geometries, significant computational difficulties arise, requiring numerical techniques including finite-element analysis that become computationally expensive [31]. Considering this challenge, and the debate in the literature about whether most of service life is spent on crack precursors and initiation or in crack growth, the current analysis evaluated the information available regarding cracking in the shaft inspection data, and found that very little data was available to select or calibrate a cracking model. Discussion with the submarine community did reveal that they traditionally use very conservative crack modeling-meaning that they design under the assumption that cracks quickly grow and lead to failure, not allotting large portions of service life to be spent in the crack growth phase.

For these reasons, a simplified crack growth model that is used by the military to predict service life was adopted. Since this thesis calculates an initial size for cracks at transition, the initial size and critical size are easy to define, and the work of Coppe et al. is readily applied. This model, based on the very popular Paris's Law, has been successful and provides information on uncertainty. The model simplifies the localized stresses to create first order approximations for remaining service life. The researchers have been able to continue to monitor the same components, updating their model and using Bayesian inference techniques to refine the model and evaluate successive iterations of predictions [31]. This has produced an effective, well-

understood model that will be used in this paper for first-order approximations. It is recommended that future work updates the model in the same manner.

2.6 Uncertainty

It is widely understood that modeling often deviates from reality, in sometimes substantial ways. These deviations may result from simplifications or approximations that are well understood, but which bound the problem or make it somehow more tractable. In some cases, though, and of particular concern in this thesis, is that there can be uncertainty in whether or not the model accurately reflects and predicts the real processes and effects. A few examples of the first kind of uncertainty are provided by Melchers, in his work to consolidate data and bound the variability in it. He states that uncertainty may be due to differences in physical and chemical environments; differences between nominally similar exposures; differences between specimens under nominally identical exposures; and errors in data observation and recording [25]. Another group, addressing the scatter in empirical models, identifies that sources of scatter can also be unknown or unaddressed, i.e. the second type of uncertainty, and must be attributed to things like incomplete data and missing model parameters. They go on to point out that that the large scatter seen in fatigue testing demands that many specimens must be tested in order to establish confidence [23]. In general, uncertainty from scatter must be

tracked and managed, and its effect on predictions taken into account in order to provide estimates and ranges of confidence in the reported results. This form of uncertainty has, as will be seen, a profound effect on predictions and the level of work that must be accomplished in order to establish restrictions on water ingress that are adequate to confidently approve a 12-year shaft service life. In other cases, though, there are types of uncertainty that are unknown or unmeasurable and that may invalidate the model and its predictions. One has already been mentioned in the missing physics discussion of King et al. Continued experience, confirmation and Bayesian updating of the model with increasing amounts of inspection data, and additional data that confirm the assumptions and decisions made in producing the model are the correct protections for these uncertainties. The current analysis must then address uncertainty in each of its modeling phases.

On one hand, Melchers contends that the models (especially corrosion models) currently available are largely empirical with wide uncertainty, which requires caution in their use [25], yet on the other hand even he points out that relatively small differences in the composition of the steel and its heat treatments theoretically should have little bearing on its corrosion properties under conditions similar to those experienced by submarine shafts, demonstrated both in short-term laboratory experiments and numerous long-term field observations [3]. For example, for aerobic and early anaerobic conditions, Melcher's found the coefficient of variation was between 3% and 7% for a range of coupons in waters believed to be a reasonable approximation for at-sea conditions for variability testing [25], indicative of less scatter from

this particular part of the modeling problem. Coefficient of variation, or COV, is a method for reporting variation, in which instead of standard deviation being reported directly, it is reported as a percentage of the associated mean, e.g. with a mean of 50, reporting a standard deviation of 10 or a COV of 20% would be equivalent. The analysis in this thesis therefore uses published information on rates and the uncertainty associated with those rates, instead of detailed immersion or coupon test results from which the published rates have been derived.

Pit size distributions have been studied in depth, and many distributions have been shown to predict pit sizes accurately. Harlow and Wei cite previous work from Engelhardt and Turnbull on a method shown to predict depth of pits down the major axis of ellipsoidal pits with < 10% error [8]. As the method is independently available in Harlow and Wei's paper, a discussion of the work of Engelhardt and Turnbull is not repeated in this paper.

Fatigue data, however, was found to have significant scatter. The coefficient of variation (COV) of fatigue life testing ranged widely, depending on material and loading. Even well-controlled laboratory testing saw a range of COV from less than 10 percent to over 500 percent for different steels [30]. In the analysis presented here information was taken from (dated) fatigue tests performed by the submarine community. In one paper, the authors note that a thorough investigation of the scatter in fatigue life had not been performed for most alloys. One notable exception, the work of Bastenaire, demonstrated that scatter increased with strength. The COV for mild steels ranged from 20% for low cycle fatigue to 50% for high cycle fatigue. Higher strength materials exhibited much larger scatter in fatigue life, with corresponding COV values

of 25% and 90% [23]. Due to the large scatter in fatigue data, the parameters of the crack growth method were set conservatively, and tested during sensitivity analysis.

The analysis in this thesis acknowledges that high uncertainty can lead to very large amounts of conservatism and thus necessarily increased margins, adversely affecting cost, schedule, and performance (King, Arsenlis, Tong, & Oberkampf, 2012). Unfortunately, in the present case a paucity of validation data leaves few options except to include in the modeling all of the sources of uncertainty discussed above and to continue to look for sources of information or other methods to reduce the uncertainty. Suggestions for further work in this area include recommended inspections and tests to reduce the uncertainty, thereby improving the accuracy and reliability of predictions made.

3.0 Research Methods

A number of models and probability distributions are being combined for the analysis in this thesis. As stated, this thesis follows the work of Shi and Mahadevan, using a log normal distribution for pit nucleation. The mean was set to 1500 days and COVs of 5%, 50%, and 95% were used. A summary of all random variable inputs is shown in Figure 10. Initial pit size modeling is also according to Shi and Mahadevan, using a normal distribution with a mean of 1.98 micrometers and the same set of COVs. To calculate initial pitting current, k is taken as a Pareto distribution in accordance with Harlow and Wei. Several values were used for each of the scale and shape parameters, in order to perform sensitivity analysis. The values of 4, 8, 10, 20 made up the set for scale parameters and 1, 3, and 5 were used as shape parameters. Detailed analysis of these distributions showed that the combination of shape equal to 1 and a scale of 4 gave results most similar to the data they reported [8]. Critical pit transition size was taken as Fang et al.'s 0.5 mm, but modeled as a normal distribution with COVs of 5%, 50%, and 95% for sensitivity analyses. This criterion gives an initial crack size, assumed to be of same length as the width of the pit, and the crack growth model of Coppe et al. is applied to calculate remaining lifetime. Hemispherical pits are assumed, which is reasonable given the expected low aspect ratio of corrosion pits, as opposed to the high aspect ratio of pitting corrosion as previously discussed. The pit growth model, covered previously as Equation 1, is:

$$\frac{2}{3}\pi\emptyset_k^2(a^3 - a_0^3) = \frac{MI_{p_0}(k)}{nF\rho} exp\left[-\frac{\Delta H}{RT}\right]t$$

The time to grow a critical pit, i.e. a pit that transitions into a crack, is:

$$t_{pg} = \frac{2\pi nF\rho}{3MI_{P_0}(k)}(a_{ci}^3 - a_0^3)e^{\Delta H/RT}$$

(4)

where t_{pg} is the time for critical pit growth, a_{ci} is the critical pit size, and the other variables are as previously defined for Equation 1. Once transition had occurred, growth of the crack was modeled using Coppe et al.'s version of Paris's Law:

$$\frac{da}{dN} = C(\Delta K)^m.$$

(5)

Here, a is the crack size, N is the number of cycles, and ΔK is a range of the stress intensity factor. C and m are crack growth parameters, in this analysis established by estimating the average time between transition and inspection, and setting these parameters to grow visible cracks approximately the size of those reported (anecdotally) in inspections.

Water ingress was modeled using a two parameter Weibull distribution. Using these distributions, the modeled version of the failure chain from Figure 2 is illustrated in Figure 9. Here, the distributions are listed for each stage; corrosion is included as part of the pit

nucleation, and failure is defined as a crack that grows until it spans the circumference of the shaft.

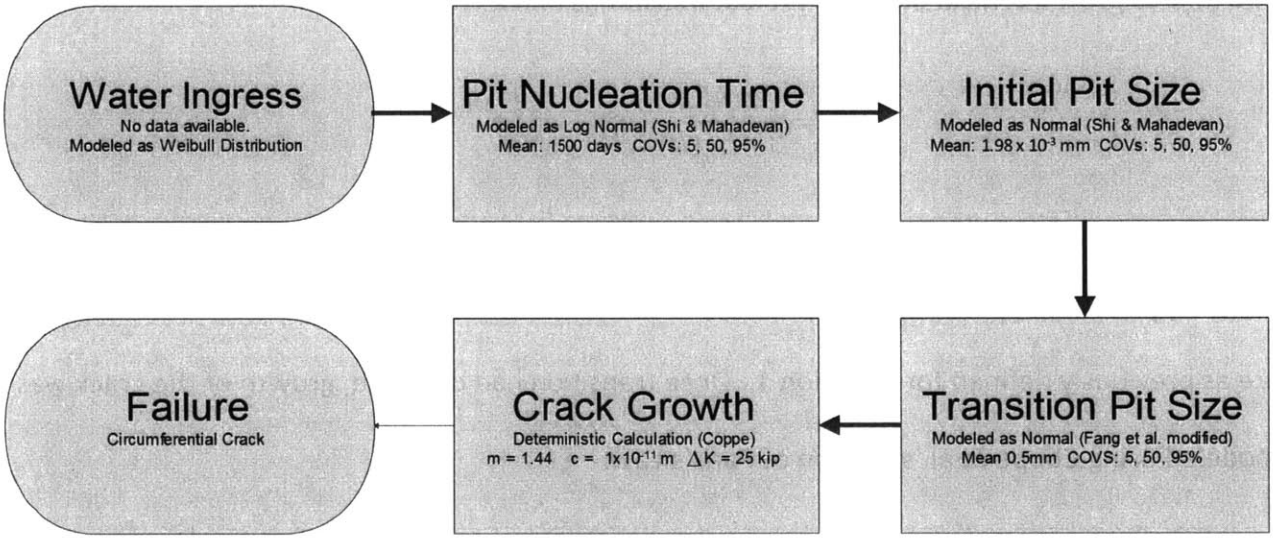

Figure 9: Summary of the failure chain as modeled

With these models in place, a Monte Carlo simulator was constructed to select all random variables and calculate the times and events of interest. A summary of the random variables and distributions is given in Figure 10.

Parameter	Symbol	Distribution	Source	Values	COVs tested (%)
Time to pit initiation		Log Normal	Shi & Mahadevan	1500 days	5, 50, 95
Initial pit size	a_0	Normal	Shi & Mahadevan	1.98×10^{-3} mm	5, 50, 95
Critical pit size	a_{ci}	Normal	Fang et al. (modified)	0.5 mm	5, 50, 95
Cluster size	k	Pareto	Harlow & Wei	Scale: 4, 8, 10, 20	Shape: 1, 3, 5

Figure 10: List of probabilistic distributions and parameters in use

Other parameters utilized in the modeling are listed in Figure 11.

Loading (each side of cycle)	25,000 psi
Cycles per month	1,000,000

Valence	2
Faraday's Constant	96,485 J/volt-gram equivalent
Density of steel	8000 kg/m^3
Molecular weight (Iron assumed)	55.845 g/mol

Figure 11: List of parameters for modeling

Once established, the values listed were held constant during investigation of potential water ingress distributions. Values were changed for sensitivity analysis later. The scale and shape parameters for the Weibull water ingress distribution were manipulated as the independent variables.

Using these distributions and parameters, the simulator calculated times to water ingress, then additional time to pit initiation, followed by time to growth until transition into a crack, and finally time for cracking to lead to failure.

Outputs of the simulator were the percentages of simulated shafts that had wetted shafts, pitted shafts, cracked shafts, and failed shafts after 6 simulated years of exposure and operation. Based on the actual shaft inspection results, target values were:

Condition	Inspection Summary Value

Wetted	70%
Pitted	40%
Cracked	4%
Failed	0

Figure 12: Summary statistics, used as target values

For each potential water ingress distribution, a distance metric was calculated from the target values. The deviations between the output values and the target values were taken, squared, and summed. The distance metric was the square root of this sum, i.e. the definition of the L2 norm with 4 variables. No weighting was applied, with the exception that water ingress distributions that consistently gave failures were rejected. This distance metric was minimized by successive changes to the two Weibull parameters and tracking of statistics on the norm and standard deviation of the metric.

Next, a similar procedure was followed for investigating the allowable level of water ingress to produce acceptable 12-year inspection results. It was determined that wetting and pitting are much more indicative of the states of processes than desirable metrics of performance, when compared to cracking and failures. That is, the submarine community is arguably much more concerned about having a very low probability of a failed shaft than it is about whether a given percentage of those shafts are wetted. For this reason, the target values for the 12-year

simulations changed. Water ingress distributions were manipulated in much the same way as before, with the new goal of producing zero failures on a consistent basis, while allowing for some small percentage of cracks to develop. Pitting and wetting were tracked for reporting purposes, but these values were allowed to deviate as necessary from any target values.

For each distribution and parameter selected, the uncertainty is handled in one of several ways. When distributions have been directly selected, the parameters have been chosen to be consistent with information available on uncertainty in the data that drove the selection of the distribution. In several cases, a set of COVs has been utilized to broadly capture some relatively unknown scatter in the data, with the varying levels of the COV intended to help quantify the effect of the parameter and its scatter on the overall model and predictions. Finally, in a few cases a parameter was simply set to several values, and the effect of the changes was tracked on the results of the simulation. In all cases, the range of results have been reported back to the submarine community for their consideration, though direction for the project has mostly provided focus, and dictates the results shared in the current paper.

THIS PAGE INTENTIONALLY LEFT BLANK

4.0 Results and Discussion

4.1 6-Year Allowable Wetting Distribution

The minimum L2 metric for allowable water ingress to achieve the 6-year inspection result was given by a Weibull distribution with shape parameter 0.75 and scale parameter 1600. The probability density function (pdf) is shown in Figure 13. The high level of positive skewness is very evident in this image. This would be indicative of shafts having a relatively high probability of getting wet early in life, here peaking around the end of the first year, near the 300 day point.

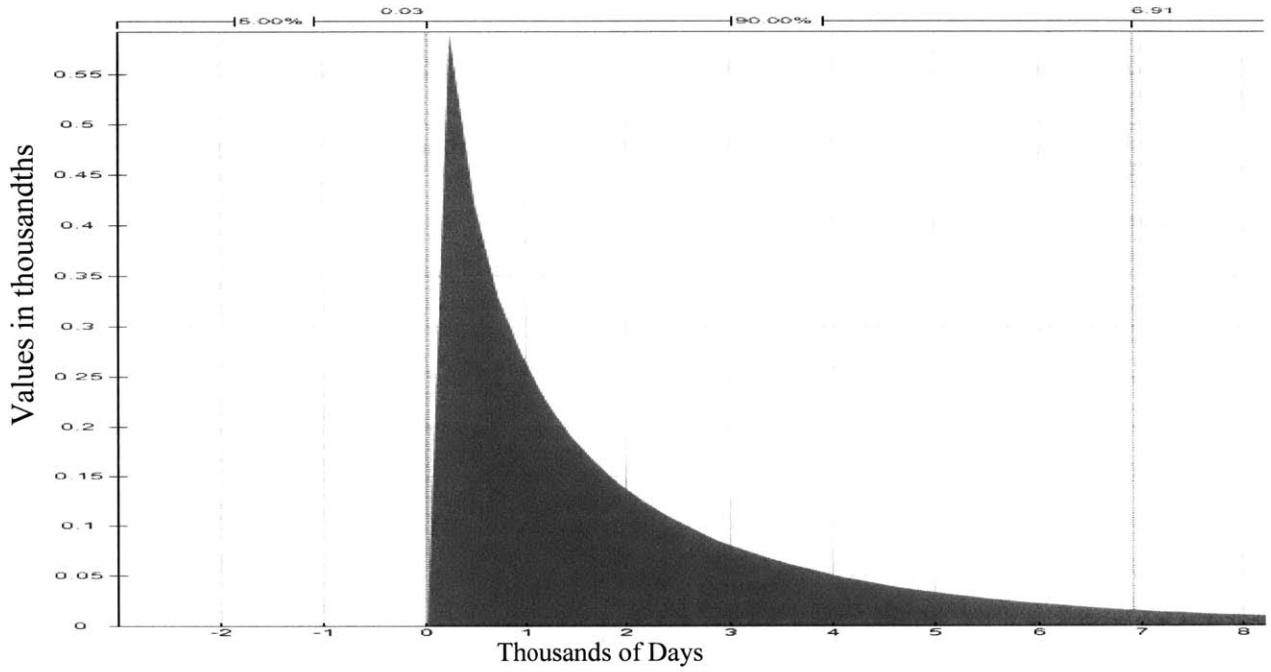

Figure 13: PDF of 6-year allowable wetting showing high skew

The cumulative density function (cdf), shown in Figure 14, illustrates the total number of shafts wetted as a function of time. The vertical lines indicate the 6 and 12 year points for reference (2190 and 4380 days). Note this distribution accurately predicts a value of approximately 70% wetted shafts at 6 years, consistent with the target value.

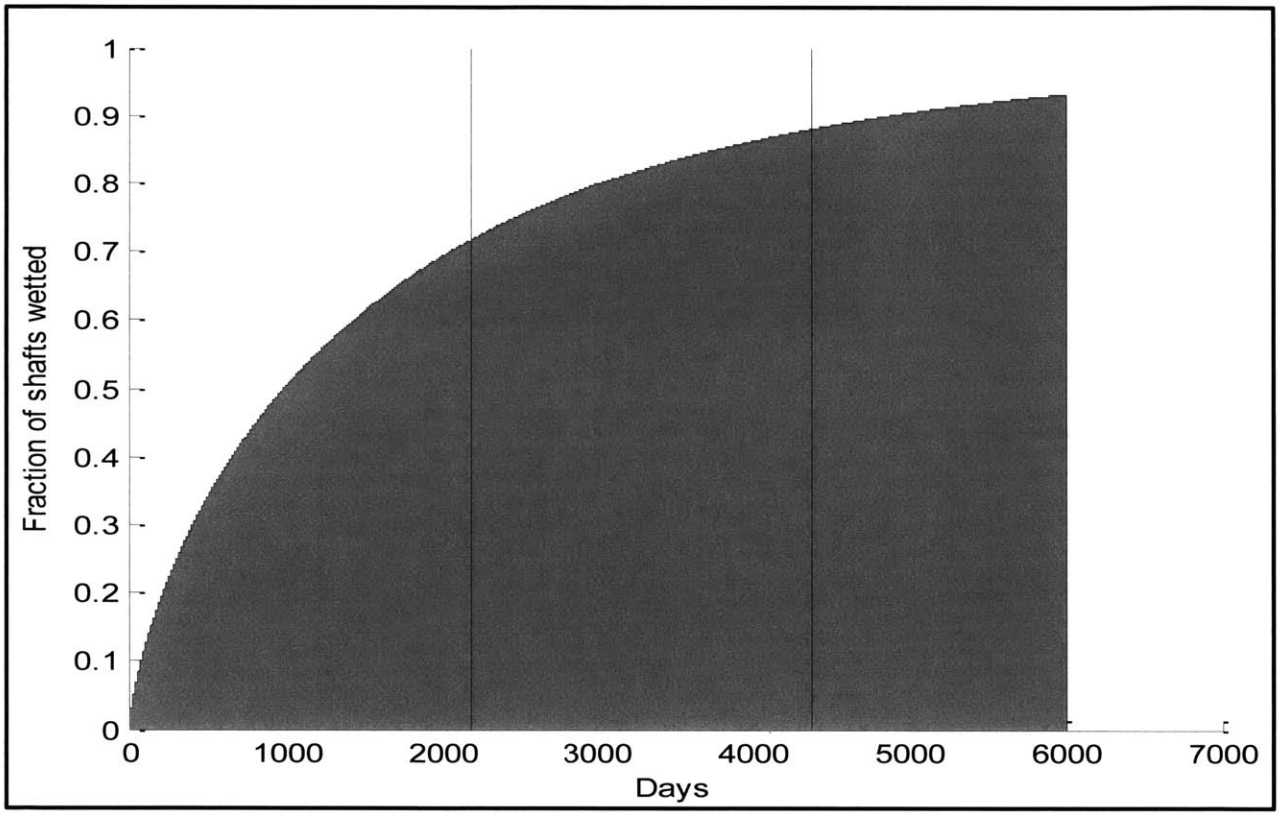

Figure 14: CDF of 6-year allowable wetting

The high probability of wetting early in operational life must be correlated to physics that are reasonable. Several cases are plausible. First, it is possible that on some shafts, the glass-reinforced plastic cover wears in rapidly, and experiences separation from the underlying metal

and/or painted coatings early in life, allowing water to wick down the separation and onto the metal shaft. A second possibility is that the GRP or an O-ring fails almost immediately upon entry to service, and the water then takes some time to migrate through the paint coating, or the motion of the shaft cracks the paint over time, to allow the water to reach the bare metal. In this scenario, it is also possible that the true distribution of water ingress is bimodal, with some percentage of very fast or instantaneous failures, and the remaining shafts being provided much more dry operational time by the protective systems. Investigation into this possible bimodal distribution is recommended for future efforts.

While the specific number of actual inspections upon which the inspection summary values are based was not provided, there have been between 50 and 100 inspections completed. Through successive runs of the Monte Carlo model, the prediction was that in a sample size of 60, there was actually about a 10% chance of having experienced a single shaft failure. This result became the basis for defining "similar performance" for a 12-year inspection interval.

4.2 12-Year Allowable Wetting Distribution and Comparisons

The minimum L2 metric for allowable water ingress to achieve these 12-year inspection results was given by a Weibull distribution with shape parameter 2.14 and scale parameter 32,000. The pdf for this distribution is shown in Figure 15. The scale of this distribution must be noted;

for the 6-year distribution in Figure 13, a period of 8,000 days covered the distribution, excepting the final tail, while the 12-year distribution can only be illustrated on a scale closer to 80,000 days. The skew is also substantially less, meaning that not only must the dry time increase significantly for shafts, but there is much less allowance for some shafts to get wet very early in life. Whatever the physics driving the very early failures is proven to be, that problem must be identified and mitigated.

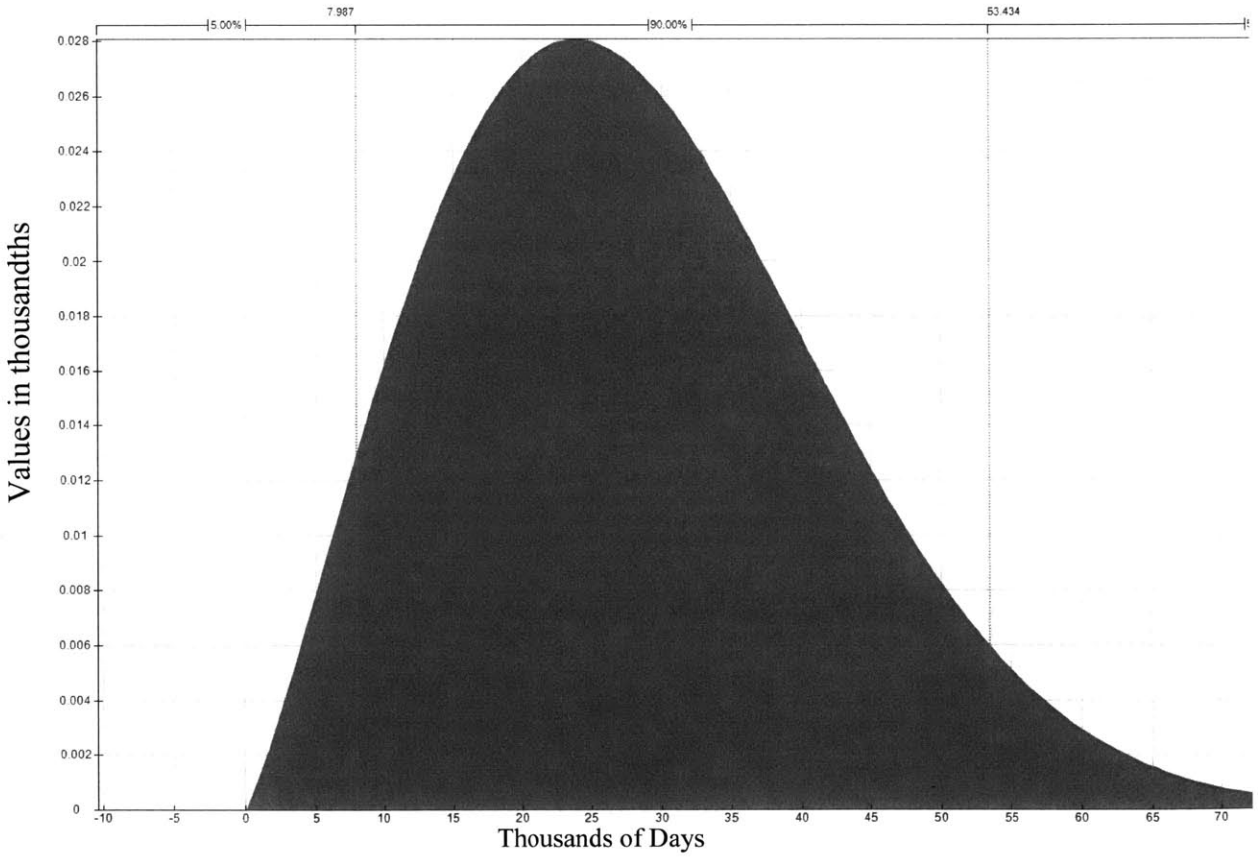

Figure 15: PDF of 12-year allowable wetting

The associated cdf in Figure 16 again shows the difference in scale between the two requirements for water ingress prevention. The vertical lines still shows the 6-(and 12-) year points for reference, but the 6-year point now correlates with a small percentage of shafts being wetted by this time, instead of nearly 70%. The stark contrast in the two distributions is better illustrated in Figure 17, where the two distributions are illustrated together, with the 6-year in blue and the 12-year in red. The magnitude of the change is evident, and illustrates a significant challenge to the design of the improved water ingress prevention.

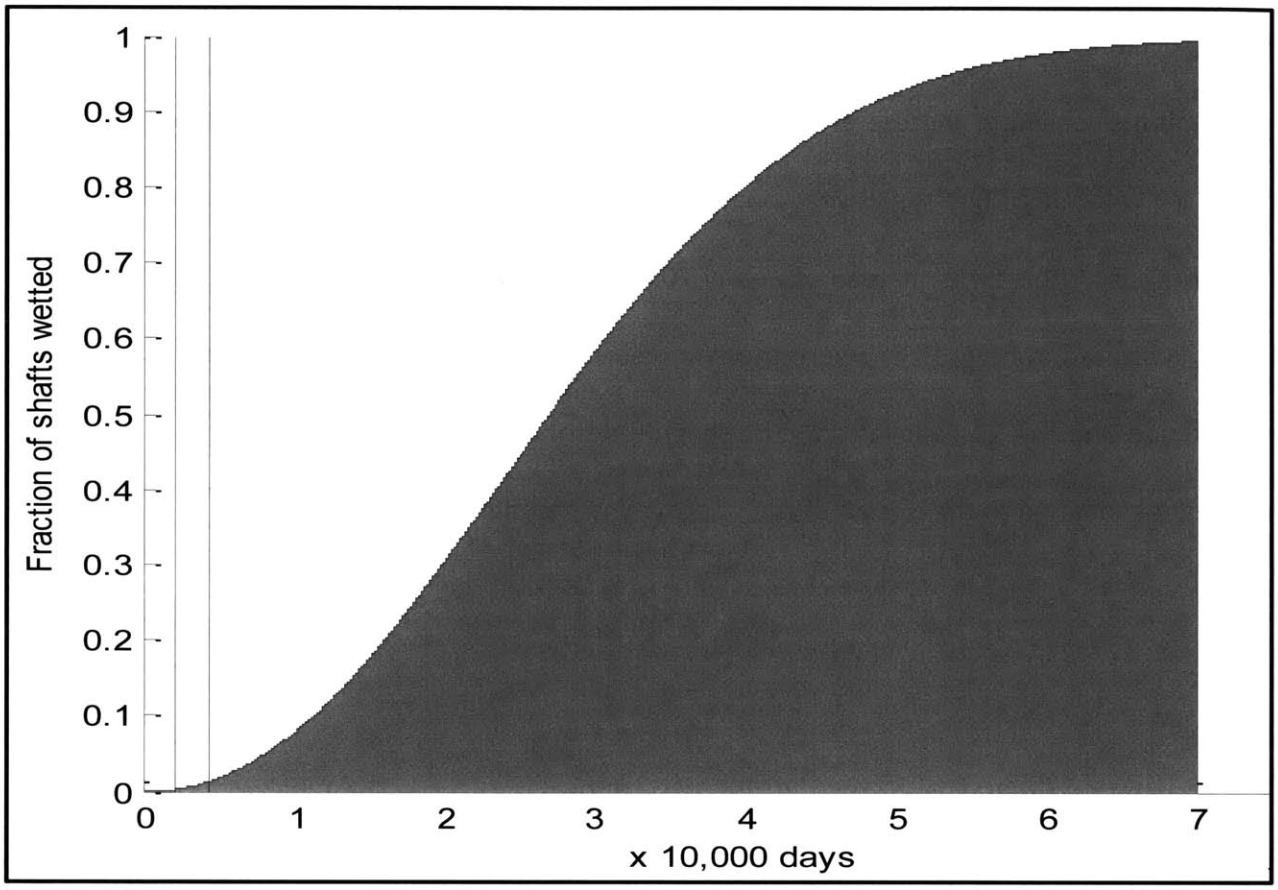

Figure 16: CDF of 12-year allowable wetting

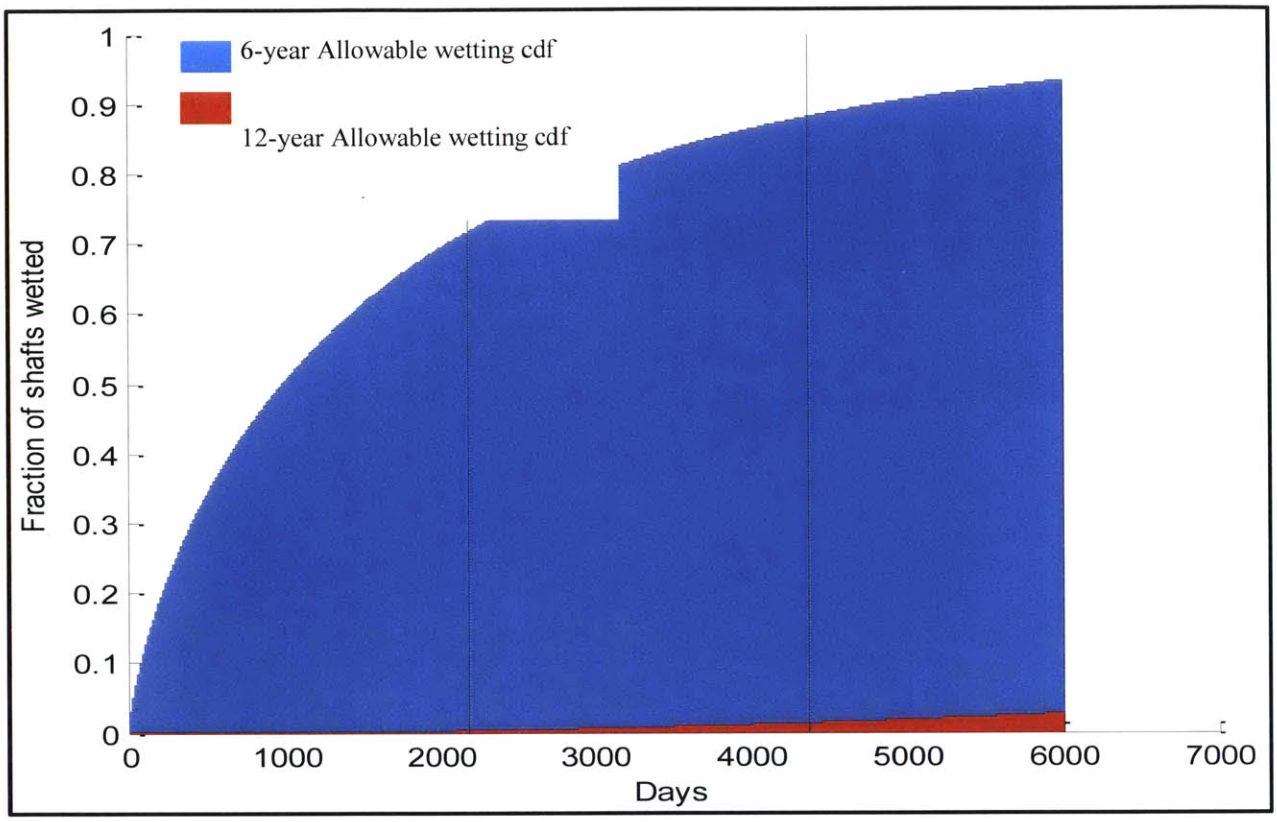

Figure 17: CDFs for 6-year (blue) and 12-year (red) allowable wetting

More detailed comparisons of the allowable wetting for satisfactory 6 and 12 year inspection intervals are provided in the tables in Figure 18 and Figure 19. Each table provides the

Evaluated at 6 Years	Allowable Wetting Profile for 6 Year Service Life	Allowable Wetting Profile for 12 Year Service Life
Wetted	71%	2.3%
Pitted	39%	0.04%
Cracked	5%	0
Failed	0*	0

Figure 18: Prediction of inspection results at 6 years for each water ingress distribution

predicted inspection results for shafts for each of the water ingress distributions covered. Figure 18 gives the inspection results if shafts are inspected at the 6 year point. Note that for the 6 year allowable

ingress distribution, with 6 years between inspections, there is an estimated 10% chance of breaking a shaft before the inspection and refurbishment interval is reached. The same is true for the 12-year allowable water ingress distribution when inspections are set to 12-year intervals.

Evaluated at 12 Years	Allowable Wetting Profile for 6 Year Service Life	Allowable Wetting Profile for 12 Year Service Life
Wetted	87%	5.6%
Pitted	69%	0.3%
Cracked	59%	0.16%
Failed	45%	0*

Figure 19: Prediction of inspection results at 12 years for each water ingress distribution

Examination of these tables indicates that keeping shafts dry greatly reduces the risk from corrosion fatigue, and the percentages listed are consistent with the order of magnitude increase in dry time required, according to this analysis. If water ingress is prevented according to the requirements for 12-year inspection intervals, but shafts are allowed to stay in service until failure, the predicted failure distribution is shown in Figure 20. Total years in service until failure is noted on the x-axis, and the vertical axis on the left lists the number of shafts failing in a corresponding 10-year period (e.g. from 111-120 years, at the 120 datum). The shape of this graph is dominated by the very long times before wetting can be tolerated, seen by the similarity in shape and scale between Figure 15 and Figure 20.

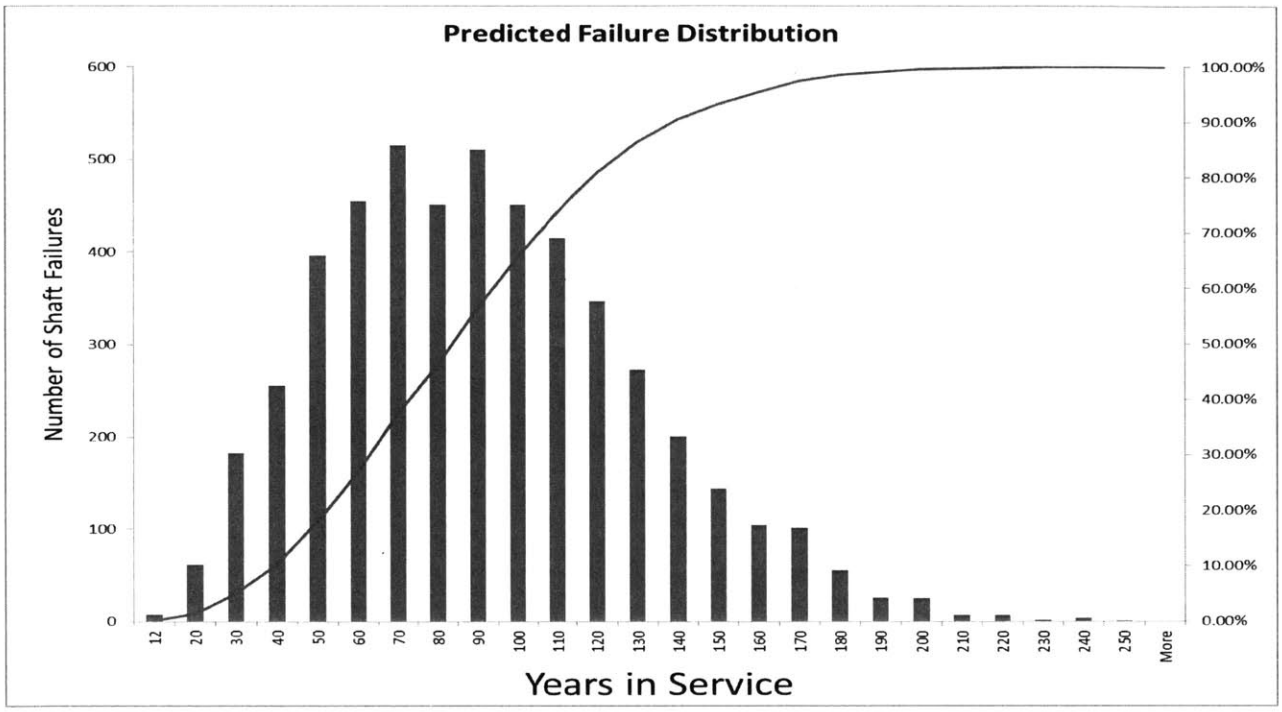

Figure 20: Predicted failure distribution (one representative simulation)

The cumulative frequency of predicted failures, a close approximation to the cdf of this distribution, is overlaid on the chart in Figure 20 in the red line, with the percentage scale on the right of the figure. These two depictions each indicate that, at the 12-year inspection point, there is a low probability of failure. Though the distribution of failures is defined by samples and frequencies, the shape of the curve suggests that it, too, could be approximated by a Weibull distribution, which is not uncommon for failure analyses. Additional detail is provided in Figure 21, which expands the information in the early years of the histogram presented in Figure 20. Two year bins are used for the first 20 years, detailing the times of failure. In this individual simulation of 5,000 shafts, it can be seen that 3 were predicted to fail before the 10 year point, with an additional 3 by the 14 year point. Successive simulations gave similar

results, revealing a predicted failure probability of about 0.14%, in terms of shafts that fail prior to the 12 year inspection interval. It is worth noting that this probability, if accurate of the true process, is unacceptably high; typical Navy risk management goals for a component failure of this magnitude would require 0.0001%, or closer to 1/1000th of the estimated probability. There is, however, considerable uncertainty in this estimate, and this uncertainty requires some consideration.

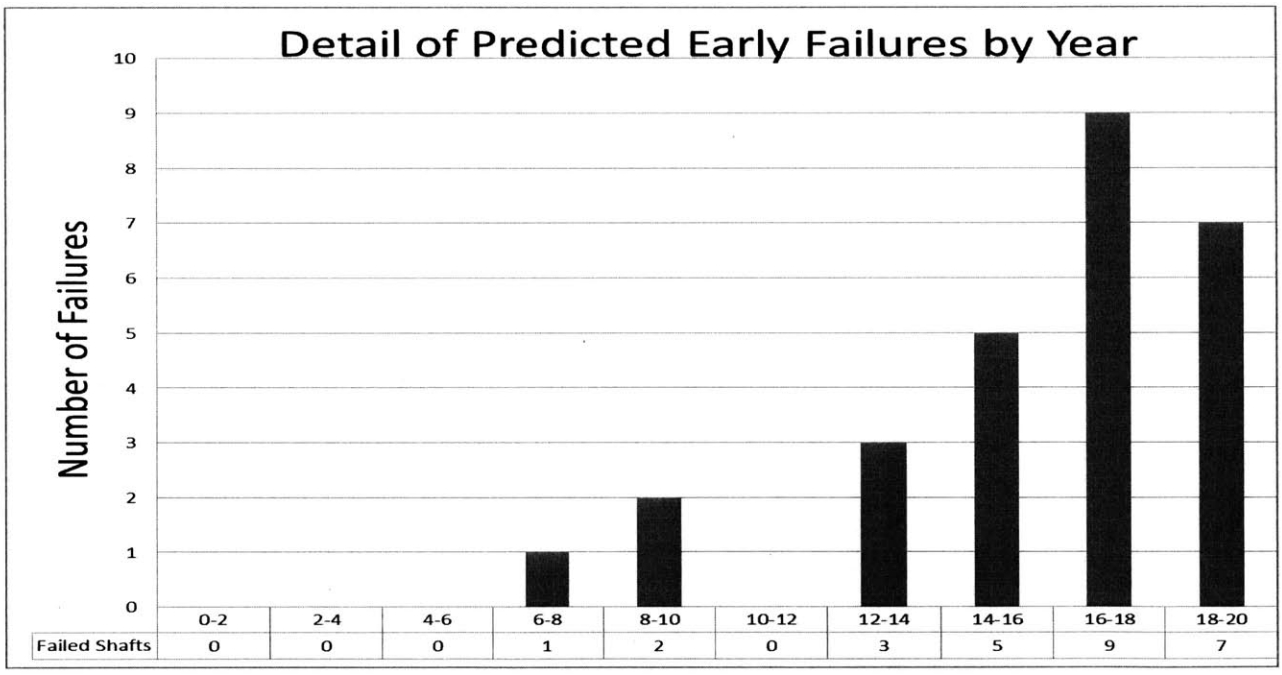

Figure 21: Detail of shafts predicted to fail early (one representative simulation)

4.3 Uncertainty

King et al. (2012) declare that predictions are most useful in the presence of quantified uncertainties. As discussed previously, this analysis includes a number of sources of uncertainty. Figure 22 illustrates the effect of this uncertainty. In this figure, the two-tailed 95% confidence interval on the mean is illustrated with the braces. As stated in the figure, this span is nearly 180 years, due to the large uncertainty in the estimates. This broad uncertainty has the effect of pushing the mean far to the right, forcing overdesign and undue conservatism. In this case designers would be required to design a shaft system producing a mean time to failure of approximately 100 years in order to have the predicted (not quite acceptably) low probability of a failure in the 12 year operational cycle.

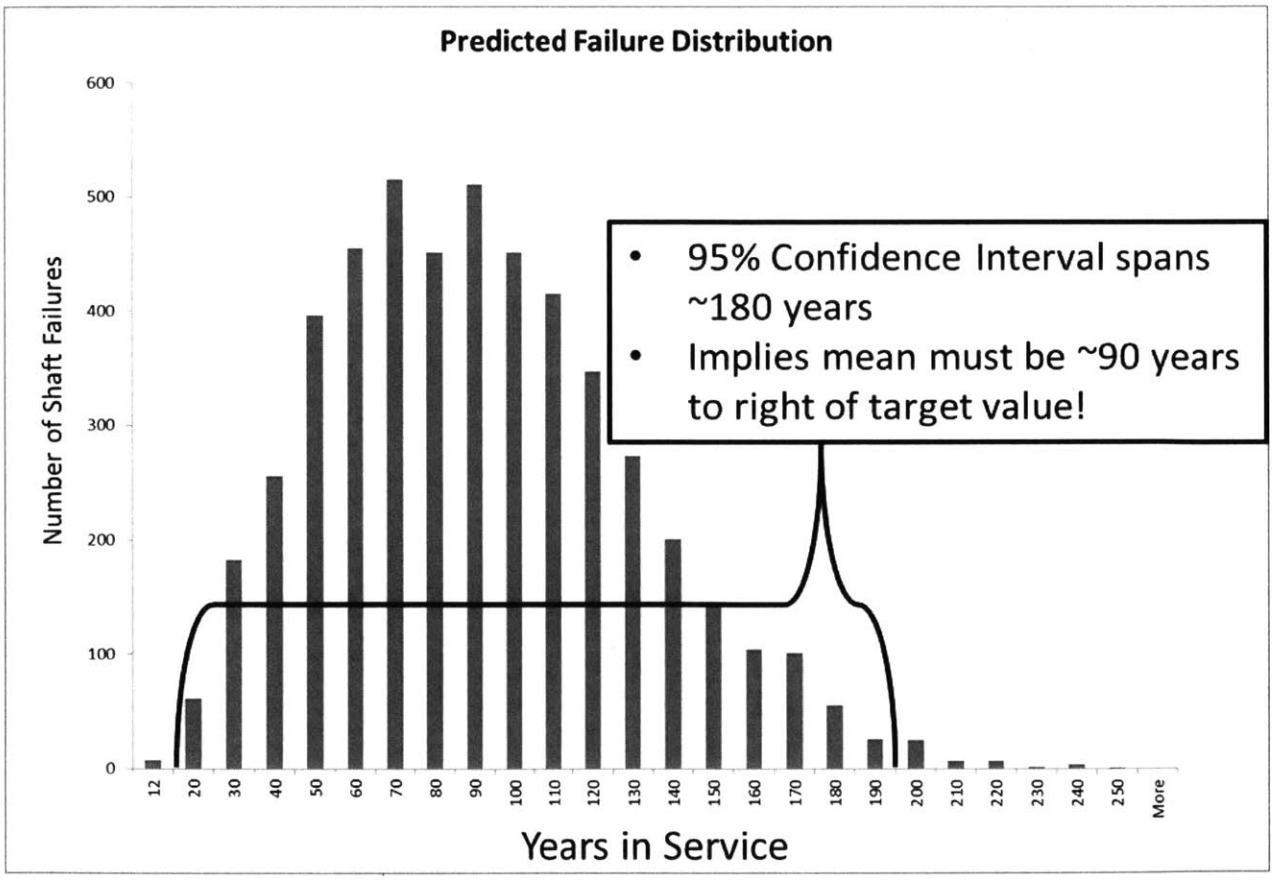

Figure 22: Sample failure distribution showing effect of high uncertainty

Reducing this uncertainty would have a number of benefits as discussed, and there are many methods to accomplish this. Improved inspection data is one of the key recommendations of this thesis, to include characterization of the types of indications and details about the distribution of their sizes, shapes, and locations. Targeted testing could also replace some of the COV dispersion estimates with specific values. Reducing uncertainty is doubly important when one considers that little data or testing exists on the effectiveness of the current and proposed systems for preventing water ingress. Claiming (or assuming) that these improvements will achieve the goal of a 12 year inspection interval is therefore tentative at best, at least for the foreseeable future while data is accumulated, and it will be difficult to build a strong case that the target probabilities have been reached. The effects of each parameter on this uncertainty, and on the estimates of shaft life, are investigated in Appendix B: Sensitivity Analysis.

5.0 Conclusions and Recommendations for Future Work

This thesis has utilized modeling methods from literature to evaluate the corrosion fatigue failure process of the submarine propulsion shaft. Using these models, this thesis was able to infer information about the unknown, precipitating water ingress distribution, and about the level of changes necessary in preventing water ingress in order to achieve a reliable 12-year inspection interval. Although preventing water ingress is a desirable method for improving

shaft life, as it interrupts the failure chain at the earliest possible point, the level of uncertainty in modeling this process complicates and calls into question the level of improvement required. This thesis also made first order estimates of the failure distribution of propulsion shafts, noting that the predictions do not quite achieve typical levels of confidence for navy risk management.

In order to achieve the 12-year inspection interval, shafts must stay dry for considerably longer, defined in this thesis in the terms of an order of magnitude longer. Uncertainty drives much of this time, and reductions in uncertainty would greatly improve the reliability of these results, as well as reduce the level of water ingress prevention shown to be necessary.

Improved inspections have been emphasized as a necessary step to achieving the desired levels of confidence, both in the reliability and in the predictions being used to justify the inspection interval. A broader canvassing of the literature is further recommended, that additional methods and models might be tested, to create a more complete picture of the predictions that might be made by different methods. A recommendation based on King et al. (2012) would be to manufacture one or two additional shafts, allotting resources later in the class life to take these shafts out of service for detailed analysis, treating them as application tests. This would both reduce the difference in the period of prediction and improve the quality of data available. As mentioned earlier, an investigation of the corrosion rates of interest would benefit designers for all future designs. Natural seawater, as pointed out several times by Melchers, contains biological and chemical components that affect the corrosion behavior. Additionally, these constituents may affect the initial oxidation potential and therefore corrosion rate. Controlled

experiments are recommended that use specimens exposed to natural seawater, to approved artificial seawater, and to an emerging seawater substitute that uses artificial seawater augmented by enzymes that mimic the effects of the components that so concern Melchers (2003). Another investigation recommended in an earlier section is analysis similar to that of this thesis, but using bimodal distributions simulating some failures upon entry-to-service. Testing that reveals the water ingress path or paths is also recommended. Finally, it is recommended that methods to interrupt the corrosion fatigue failure chain at other points be investigated. As mentioned, other work by this project, not addressed directly in this thesis, has investigated a cladding material that exhibits corrosion properties which may preclude pitting. This was a material of opportunity, exhibiting some of the traits desirable in a cladding for the shaft, but a more detailed analysis would need to be performed to design a material with the full suite of material, mechanical, and corrosion properties that would be desired in this application.

Two interesting results were also identified during sensitivity analysis. Due to the long time that shafts must be kept dry to achieve the desired results, above, very few of the other parameters tested had a large effect on the final failure distribution, which was primarily driven by the "safe" dry time of each shaft. However, the pitting current was seen to have a substantial effect, especially interesting given the likelihood of a galvanic couple and high corrosion current, discovered as mentioned by other work from this project, which is not the focus of this thesis. Second, the transition criterion in use had a significant effect on which

predictions showed the greatest deviation from the target values, for cases with minimized L2 norms. Testing is recommended to confirm the critical pit size and transition criteria from a pit to a crack.

List of Abbreviations

CDF cumulative density function, also sometimes cdf

COV Coefficient of Variance

FMEA Failure mode and effects analysis

GRP Glass reinforced plastic

PDF probability density function, also sometimes pdf

SRB Sulfate reducing bacteria

Bibliography

Chen, G., Wan, K.-C., Gao, M., Wei, R., & Flournoy, T. (1996). Transition from Pitting to Fatigue Crack Growth - Modeling of Corrosion Fatigue Crack Nucleation in a 2024-T3 Aluminum Alloy. *Materials Science & Engineering, A219*, 126-132.

Coppe, A., Pais, M. J., Haftka, R. T., & Kim, N. H. (2012). Using a Simple Crack Growth Model in Predicting Remaining Useful Life. *Journal of Aircraft, 49*(6), 1965-1973.

Dechema. (1992). Corrosive Agents and their Interaction with Materials. In G. Keysha (Ed.), *Corrosion Handbook* (Vol. 11). New York: VCH Publishers.

Fang, B., Eadie, R., Elboujdaini, M., & Chen, W. (2009). Transition from Pits to Cracks in Pipeline Steel in Near-Neutral pH solution. *12th International Conference on Fracture* (pp. 12-17). Ottawa: Curran Associates, Inc.

Goswami, T., & Hoeppner, D. (1995). Pitting Corrosion Fatigue of Structural Materials. In C. Chang, & C. Sun, *Structural Integrity in Aging Aircraft* (p. 45). New York: ASME.

Harlow, D., & Wei, R. (1994). Probability Approach for Corrosion and Corrosion Fatigue Life. *AIAA, 32*(10), 2073-2079.

Harlow, D., & Wei, R. (1998). A Probability Model for the Growth of Corrosion Pits in Aluminum Alloys Induced by Constituent Particles. *Engineering Fracture Mechanics, 59*(3), 305-325.

King, W. E., Arsenlis, A., Tong, C., & Oberkampf, W. L. (2012). Uncertainties in Predictions of Material Performance using Experimental Data that is Only Distantly Related to the System of Interest. In A. Dienstfrey, & R. Boisfert, *Uncertainty Quantification in Scientific Computing* (pp. 294-311). Boulder: 10th IFIP WG 2.5 Working Conference, WoCoUQ 2011.

Kondo, Y. (1989). Prediction of Fatigue Crack Initiation Life Based on Pit Growth. *Corrosion, 45*(1), 7-11.

Melchers, R. (2001). Probabilistic Models of Corrosion for Reliability Assessment and Maintenance Planning. *Proceedings of the Offshore Mechanics and Arctic Engineering Conference (CD-ROM).* Rio de Janeiro: ASME.

Melchers, R. (2003). Probabilistic Model for Marine Corrosion of Steel for Structural Reliability Assessment. *Journal of Structural Engineering*, 1484-1493.

Melchers, R. (2003). Probabilistic Models for Corrosion in Structural Reliability Assessment - Part 2: Models Based on Mechanics. *Transactions of the ASME*, 272-280.

Pitner, P. (1988). Statistical Analysis of Steam Generator Tube LIfetime of Probabilistic Method for Tube Bundle Inspection. *Reliability Engineering and System Safety*, 271-292.

Shi, P., & Mahadevan, S. (2001). Damage Tolerance Approach for Probabilistic Pitting Corrosion Fatigue Life Prediction. *Engineering Fracture Mechanics, 68*, 1493-1507.

Tryon, R., & Cruse, T. (1997, January). Probabilistic Mesomechanical Fatigue Crack Nucleation Model. *Journal of Engineering Materials and Technology, 119*, 65-70.

Tryon, R., & Cruse, T. (1998). A Reliability-Based Model to Predict Scatter in Fatigue Crack Nucleation Life. *Fatigue & Fracture of Engineering Materials & Structures, 21*, 257-267.

Wikipedia Commons. (2014, April 24). *Pareto Distribution.* Retrieved from wikipedia.org: http://en.wikipedia.org/wiki/Pareto_distribution#Relation_to_Zipf.27s_law

Yamamoto, N., & Igegami, K. (1998). A Study on the Degradation of Coating and Corrosion of Ship's Hull Based on the Probabilistic Approach. *Journal of Offshore Mechanical Architectural Engineering, 120*(3), 121-128.

Appendix A: Discussion of Pareto Distributions

Though many will be familiar with other concepts from his work, Italian economist Vilfredo Pareto is the namesake of a less commonly known distribution function, or more accurately a family of distribution functions. One of the primary concepts typifying these distributions is that, though possible, the likelihood of high values of the object or parameter being studied becomes increasingly small. The well-known "80-20" rule actually comes from this distribution, and is often associated with the accumulation of wealth; that the upper 20% of people own 80% of the wealth. Alternatively, in process engineering and process improvement, this rule states that only a few types of problems, around 20%, make up 80% of the improvement that can be gotten-indicating that classifying and numerically analyzing the faults in a system will rapidly identify which solutions to target first.

The distribution is defined as a survival function, such that it maps the probability for a random variable X with a Pareto distribution, that a given value of X is larger than some number x, and the distribution is defined including the (positive) lower bound of X, x_m. The pdf for the Pareto distribution is given by:

$$f_x(x) = \begin{cases} \alpha x_m^{\alpha} & x \geq x_m \\ 0 & x < x_m \end{cases}$$

Which gives a cdf of:

$$F_x(x) = \begin{cases} 1 - \left(\frac{x_m}{x}\right)^{\alpha} & x \geq x_m \\ 1 & x < x_m \end{cases}$$

Graphically, the pdf for is a monotonically decreasing function, here shown for four values of α:

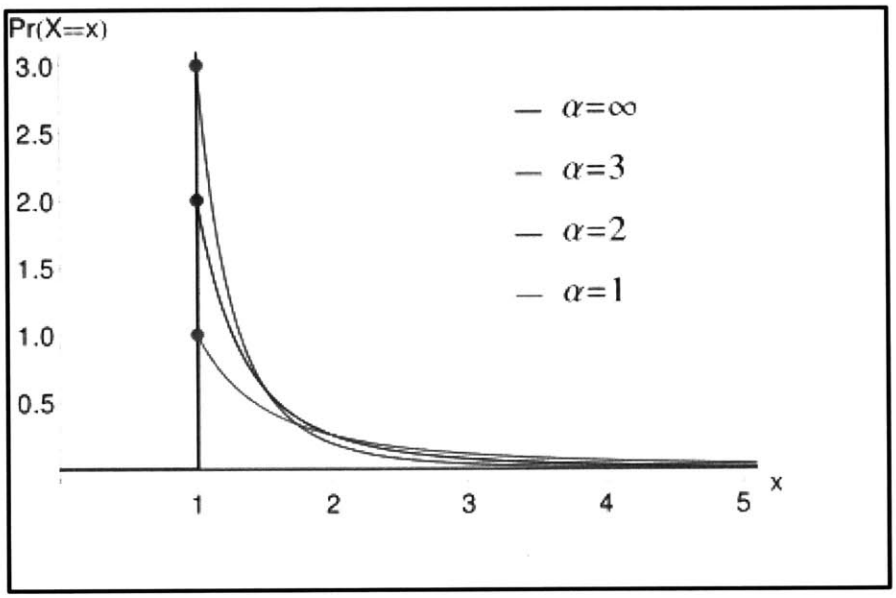

The cdf then becomes:

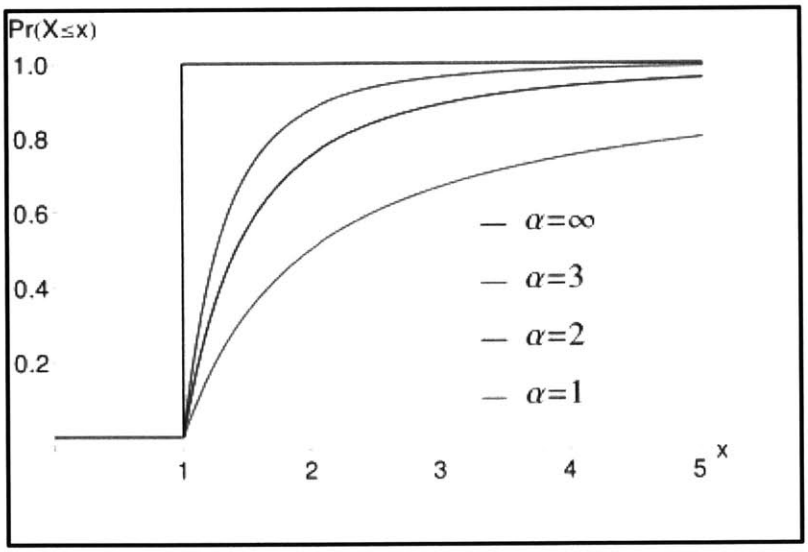

The discrete Pareto, used by Harlow and Wei, is more commonly referred to as Zipf's law, and its cdf is seen to be similar, approximating the continuous distribution:

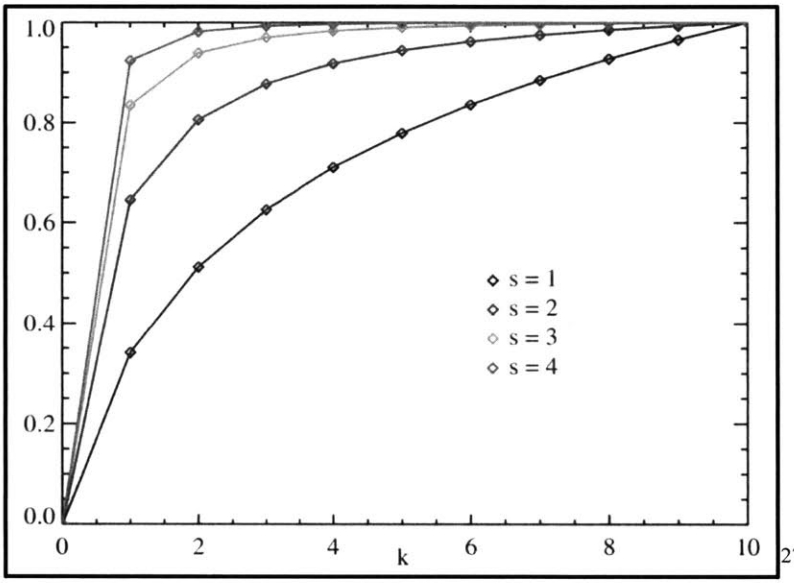

[27]

[27] These graphs were taken from the Wikipedia page; a similar discussion is also available there [33]

Appendix B: Sensitivity Analysis

Parameters investigated for sensitivity analysis included the COV for the log normal pit initiation time distribution, taken from Shi and Mahadevan (2001), the COV for the normal initial pit size distribution taken from Shi and Mahadevan (2001), and the shape and scale parameters of the Pareto clustering distribution taken from Harlow and Wei (1998). The base case was the case that was coupled to the 12-year allowable wetting distribution detailed in this thesis, which had shape parameter 2.14, and scale parameter 32,000.

Parameters for the base case were:

Pit Initiation Time Mean	Pit Initiation Time COV	Pit Size Mean	Pit Size COV	Pareto Shape	Pareto Scale
1500	0.5	.00000198	0.5	1	4

After 20 runs of 5,000 iterations of the Monte Carlo each, the mean failure time for shafts was 127 years, with a standard deviation of 48.9. The effects of altering the parameters were:

		Mean Fail Time	Standard Deviation
Pit Initiation Time COV	Decreased to 0.05	Negligible	Negligible
	Increased to 0.95	Negligible	Negligible
Pit Size COV	Decreased to 0.05	0.5% increase	Negligible
	Increased to 0.95	Negligible	0.4% decrease
Pareto Scale	Increased to 8	Decreased 15% (108.7)	Decreased 8%
	Increased to 10	Decreased 18% (104.7)	Decreased 9%
	Increased to 20	Decreased 25% (96.0)	Decreased 11%
Pareto Shape	Increased to 3	Increased 12% (142.4)	Decreased 6%
	Increased to 5	Increased 16% (148.2)	Decreased 8%

These results show that the pitting current, driven by the size of the initiating cluster, is the key parameter for determining the length of time spent during pitting. This makes physical sense, as the discussion in Harlow and Wei indicates that the largest clusters do the most damage, and are most likely to transition into cracks, and all the tested increases make larger clusters more likely. Analysis showed that the base case with shape 1 and scale 4 gave results that best matched those described in their study [8]. These results indicate that more accurate and reliable predictions might be facilitated through a more in-depth study of the distribution of particles found in shaft steel.

Because the models tended to underpredict cracking, although results from the L2 norm perspective were acceptable, a second analysis was done using the distributions coupled with the 6-year allowable wetting distribution, in order to investigate further. Varying the parameters for the transition criteria revealed that using a normal distribution for the size of the pit that transitions into a crack, with mean 0.3 mm and standard COV of 0.95 made the 4% cracking criteria more accurate when coupled with a slightly different wetting distribution. When "calibrating" this criterion in this way, a new minimum L2 norm was found, with a set of distributions that predicted results even more similar to the target values of the actual inspections. The new water ingress distribution had shape parameter of 0.75, and scale increased to 1750 (from the previously reported 1600). This combination tended to slightly underpredict the number of shafts exhibiting wetting, while providing consistent results very close to the 40% pitted and 4% cracked shafts, with no failures at the 6-year point. It is recommended that a study be done to validate the transition criterion for submarine shafting.

Appendix C: BLP drawings

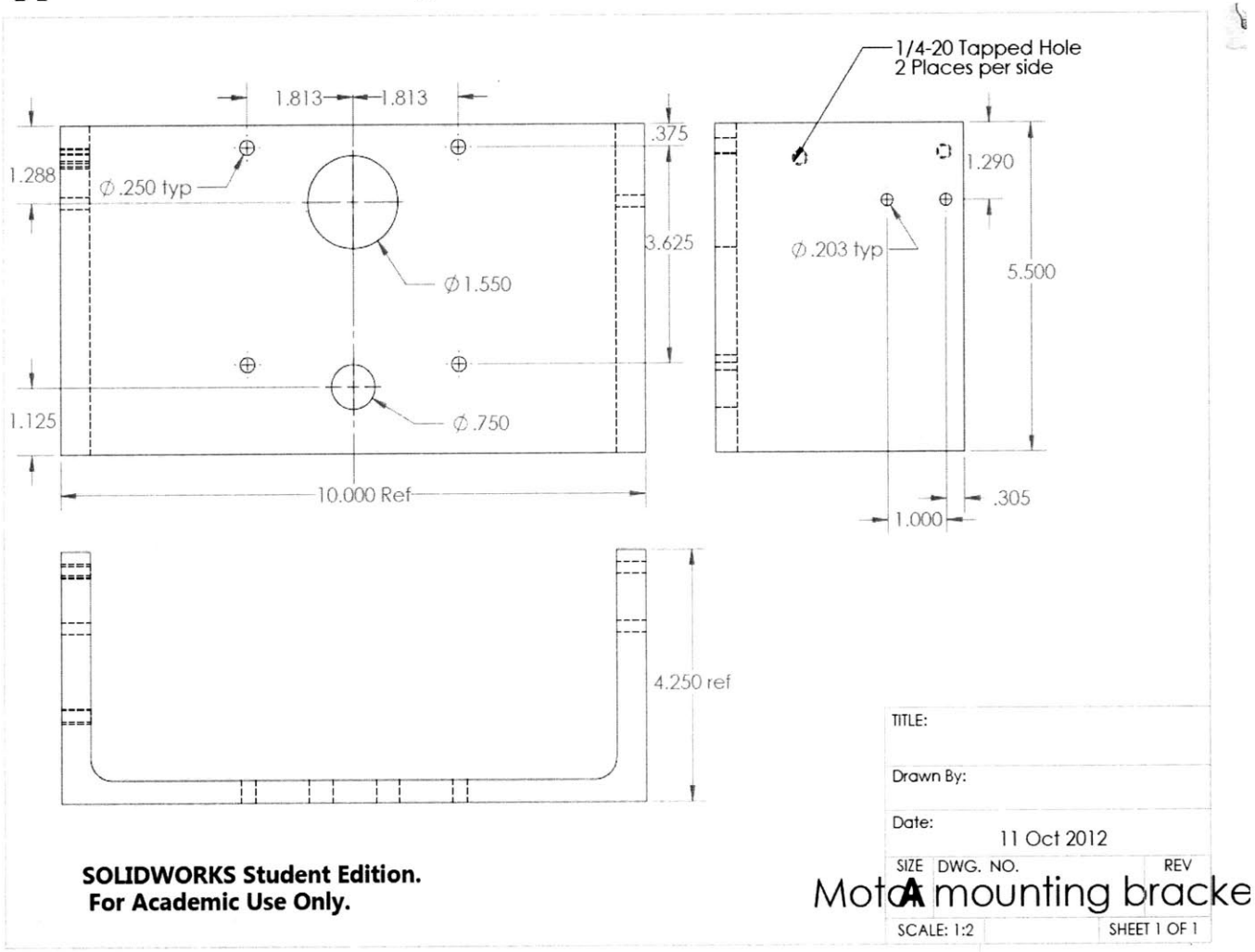

Appendix D: Drawings for Specialized Test Device

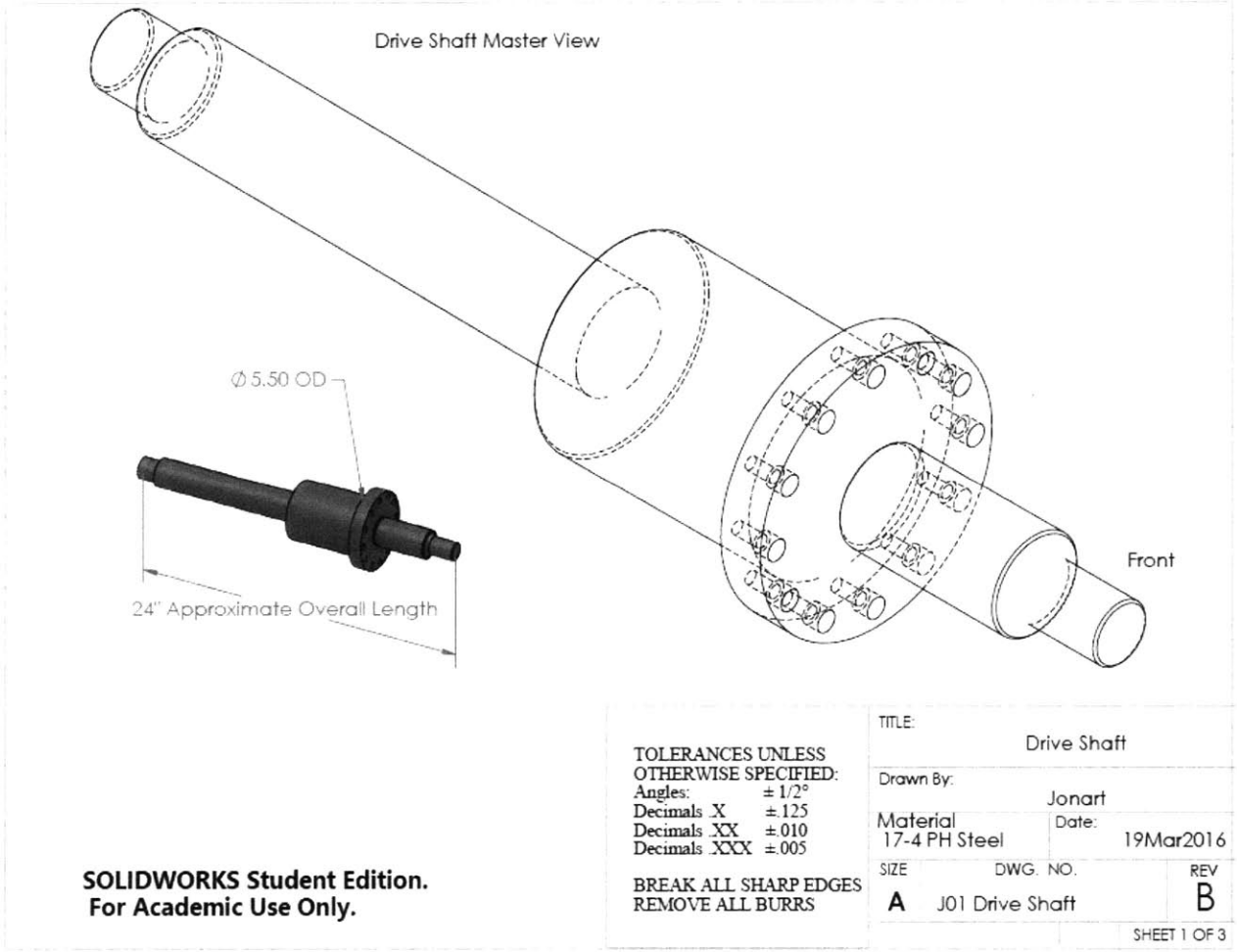

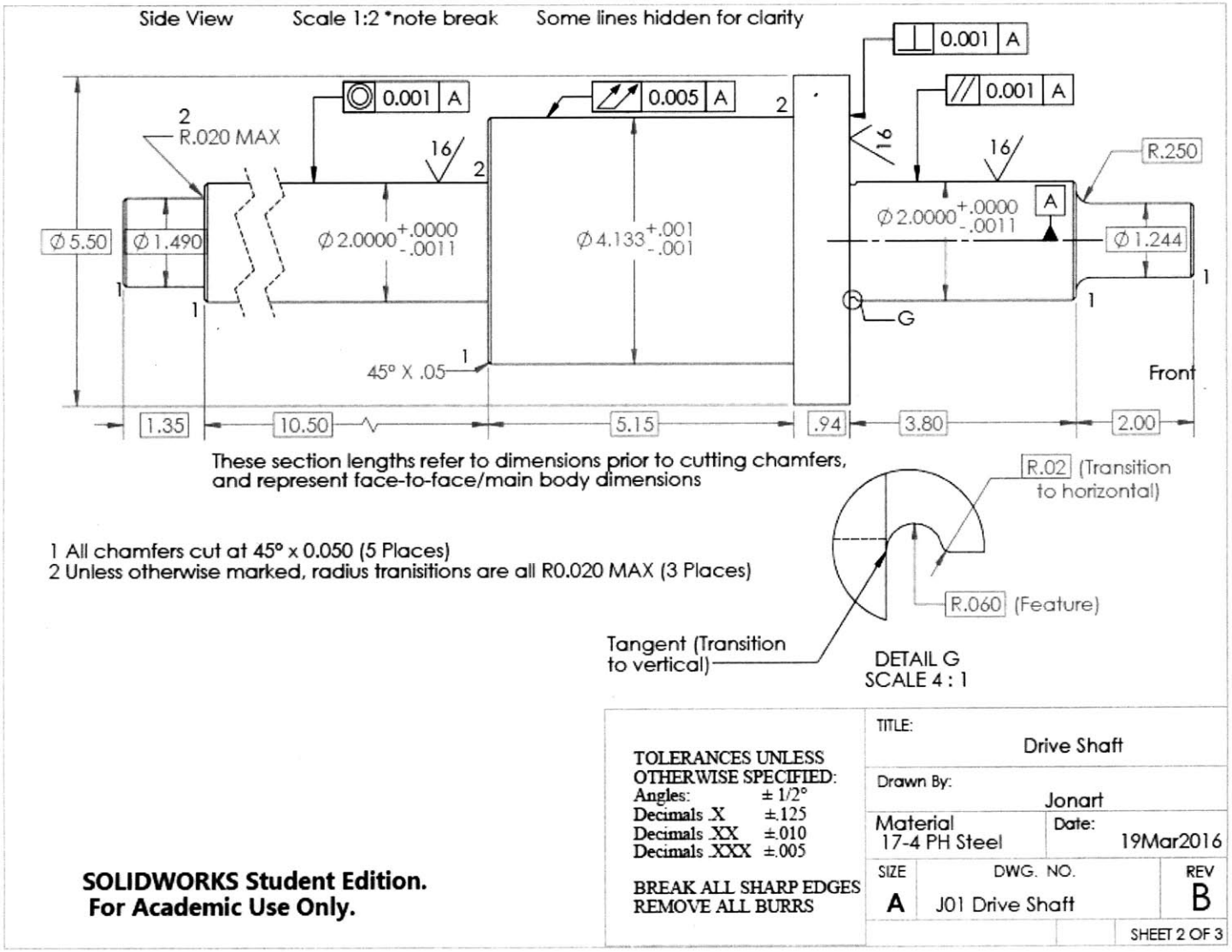
Side View
Scale 1:2 *note break
Some lines hidden for clarity
0.001 A
0.005 A
0.001 A
0.001 A
2
R.020 MAX
16
16
16
R.250
Ø5.50
Ø1.490
Ø2.0000 +.0000 -.0011
Ø4.133 +.001 -.001
Ø2.0000 +.0000 -.0011
A
Ø1.244
G
45° X .05
Front
1.35
10.50
5.15
.94
3.80
2.00
These section lengths refer to dimensions prior to cutting chamfers, and represent face-to-face/main body dimensions
1 All chamfers cut at 45° x 0.050 (5 Places)
2 Unless otherwise marked, radius tranisitions are all R0.020 MAX (3 Places)
R.02 (Transition to horizontal)
R.060 (Feature)
Tangent (Transition to vertical)
DETAIL G
SCALE 4 : 1
TOLERANCES UNLESS OTHERWISE SPECIFIED:
Angles: ± 1/2°
Decimals .X ±.125
Decimals .XX ±.010
Decimals .XXX ±.005
BREAK ALL SHARP EDGES
REMOVE ALL BURRS
TITLE:
Drive Shaft
Drawn By:
Jonart
Material
17-4 PH Steel
Date:
19Mar2016
SIZE
A
DWG. NO.
J01 Drive Shaft
REV
B
SHEET 2 OF 3
SOLIDWORKS Student Edition.
For Academic Use Only.

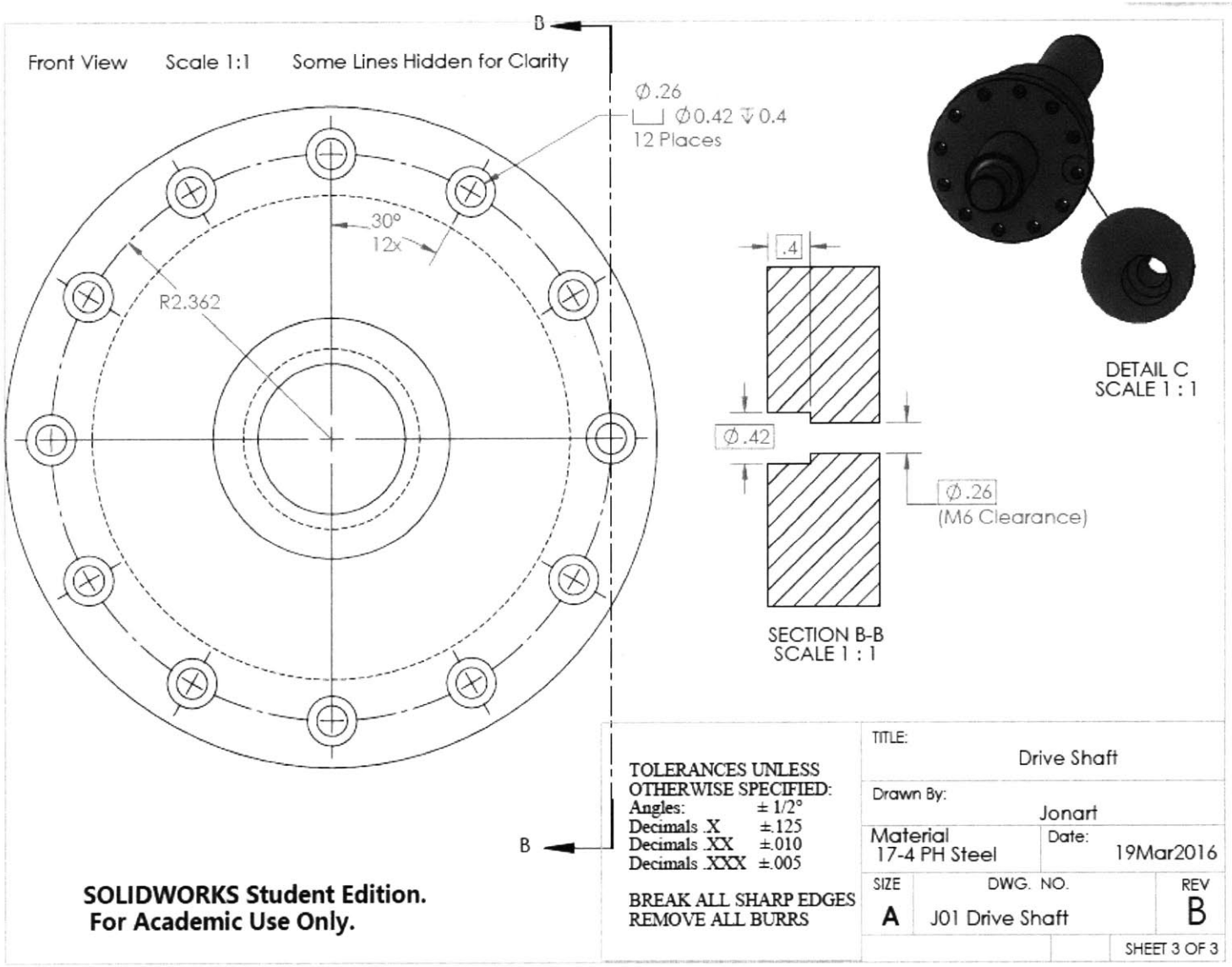
B
Front View Scale 1:1 Some Lines Hidden for Clarity
Ø.26
⌴ Ø0.42 ↧0.4
12 Places
30°
12x
R2.362
.4
Ø.42
Ø.26
(M6 Clearance)
SECTION B-B
SCALE 1 : 1
DETAIL C
SCALE 1 : 1
B
SOLIDWORKS Student Edition.
For Academic Use Only.
TOLERANCES UNLESS OTHERWISE SPECIFIED:
Angles: ± 1/2°
Decimals .X ±.125
Decimals .XX ±.010
Decimals .XXX ±.005
BREAK ALL SHARP EDGES
REMOVE ALL BURRS
TITLE:
Drive Shaft
Drawn By:
Jonart
Material
17-4 PH Steel
Date:
19Mar2016
SIZE
A
DWG. NO.
J01 Drive Shaft
REV
B
SHEET 3 OF 3

Housing A - Master Housing

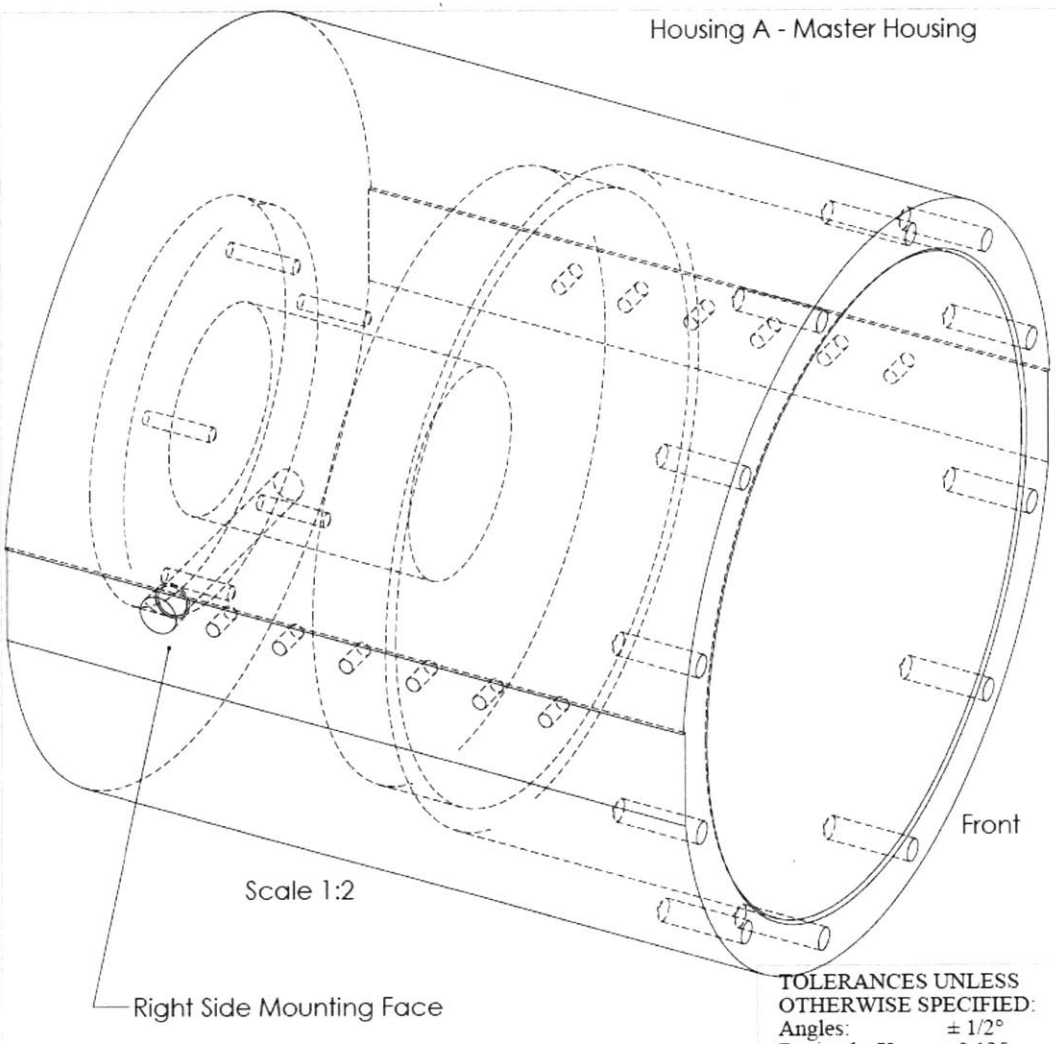

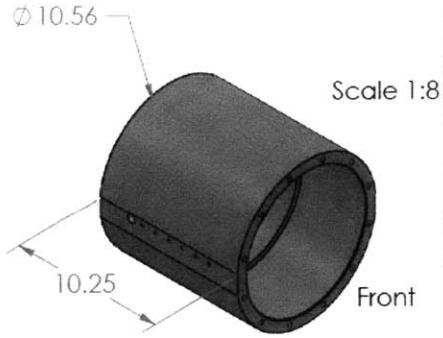

SOLIDWORKS Student Edition.
For Academic Use Only.

TOLERANCES UNLESS OTHERWISE SPECIFIED:
Angles: ± 1/2°
Decimals .X ± 0.125
Decimals .XX ± 0.010
Decimals .XXX ± 0.005

BREAK ALL SHARP EDGES
REMOVE ALL BURRS

TITLE:	Master Housing
Drawn By:	Jonart
Material: 6061 Aluminum	Date: 03Apr2016
SIZE: A	DWG. NO.: J02 Housing A-Master
REV: E	SHEET 1 OF 6

Front View: Primary Dimensions

Scale 1:4

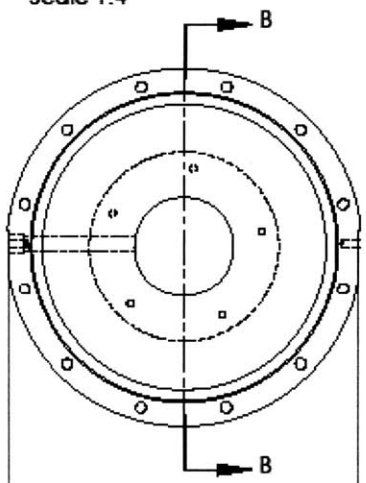

10.400 Flat-to-Flat
Nominal distance
See details on sheet 4

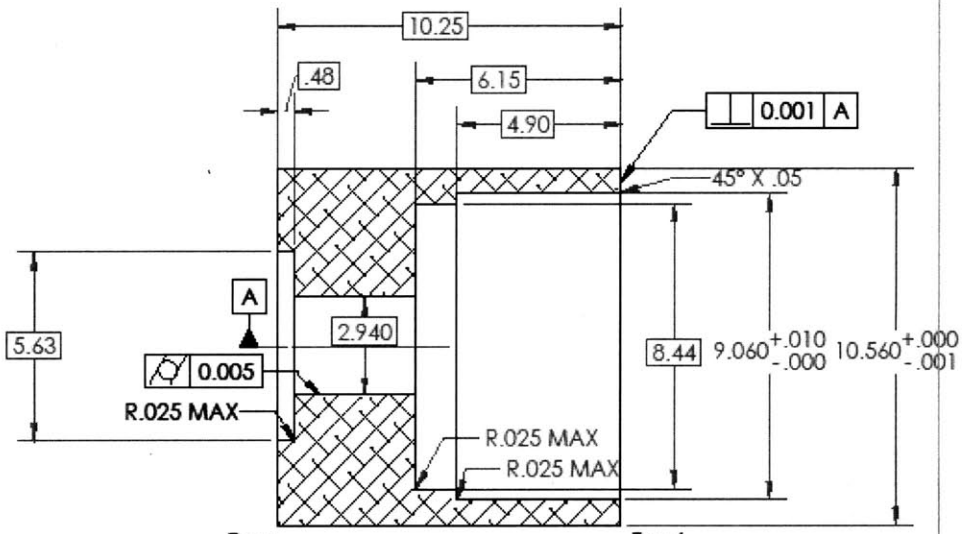

SECTION B-B
SCALE 1 : 4

This part must mate up with Housing B (Pinch Housing) such that the cylinders at each Datum A are concentric within 0.001"
Mating surfaces are the bolting rings perpendicular to Datum A.

SOLIDWORKS Student Edition.
For Academic Use Only.

TOLERANCES UNLESS OTHERWISE SPECIFIED:	TITLE: Master Housing
Angles: ± 1/2°	Drawn By: Jonart
Decimals .X ± 0.125	
Decimals .XX ± 0.010	Date: 03Apr2016
Decimals .XXX ± 0.005	
BREAK ALL SHARP EDGES REMOVE ALL BURRS	SIZE A · DWG. NO. J02 Housing A-Master · REV E
	SHEET 2 OF 6

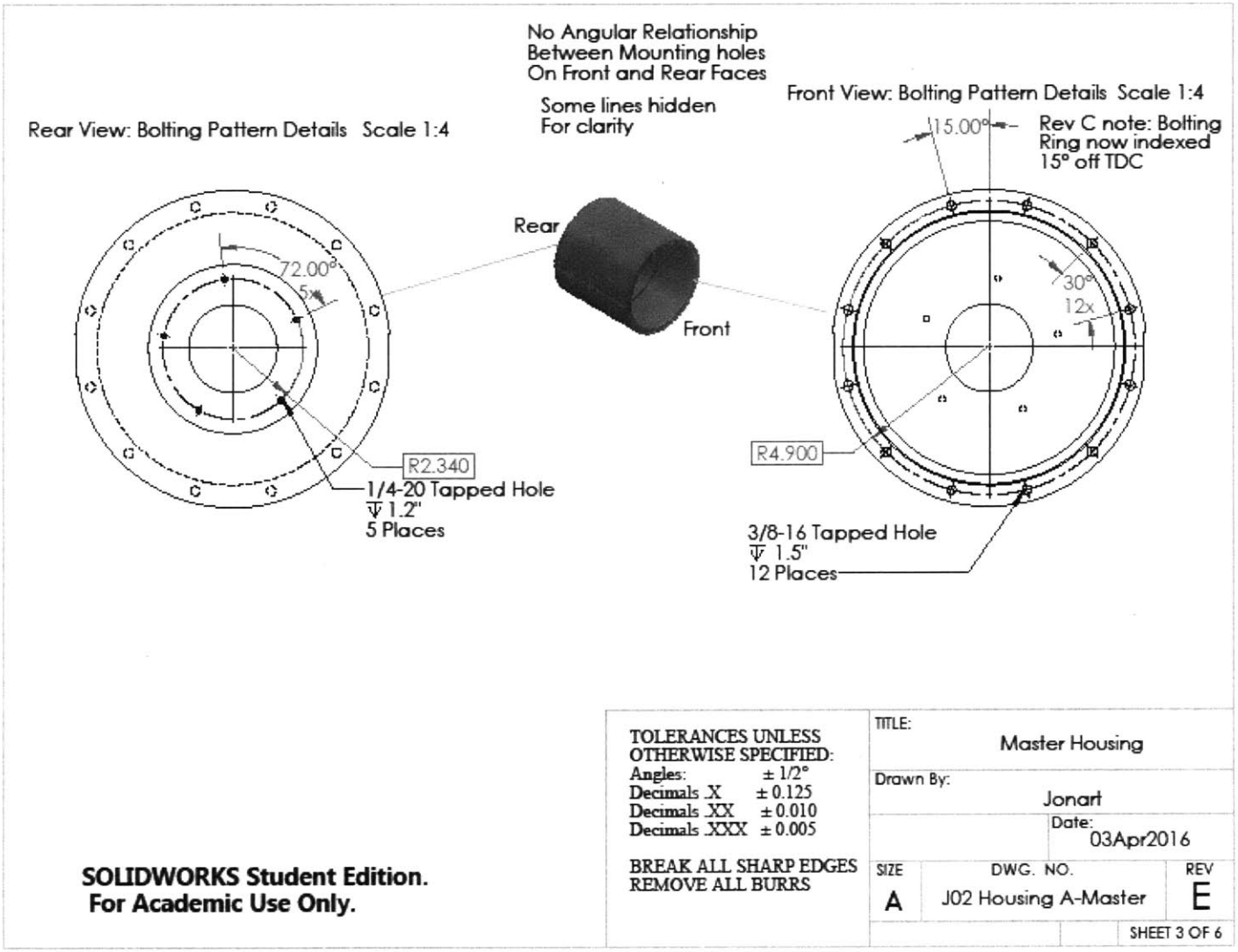
No Angular Relationship
Between Mounting holes
On Front and Rear Faces
Some lines hidden
For clarity
Rear View: Bolting Pattern Details Scale 1:4
Front View: Bolting Pattern Details Scale 1:4
15.00°
Rev C note: Bolting
Ring now indexed
15° off TDC
Rear
Front
72.00°
5x
30°
12x
R2.340
1/4-20 Tapped Hole
⌖ 1.2"
5 Places
R4.900
3/8-16 Tapped Hole
⌖ 1.5"
12 Places
TOLERANCES UNLESS
OTHERWISE SPECIFIED:
Angles: ± 1/2°
Decimals .X ± 0.125
Decimals .XX ± 0.010
Decimals .XXX ± 0.005
BREAK ALL SHARP EDGES
REMOVE ALL BURRS
TITLE:
Master Housing
Drawn By:
Jonart
Date:
03Apr2016
SIZE
A
DWG. NO.
J02 Housing A-Master
REV
E
SHEET 3 OF 6
SOLIDWORKS Student Edition.
For Academic Use Only.

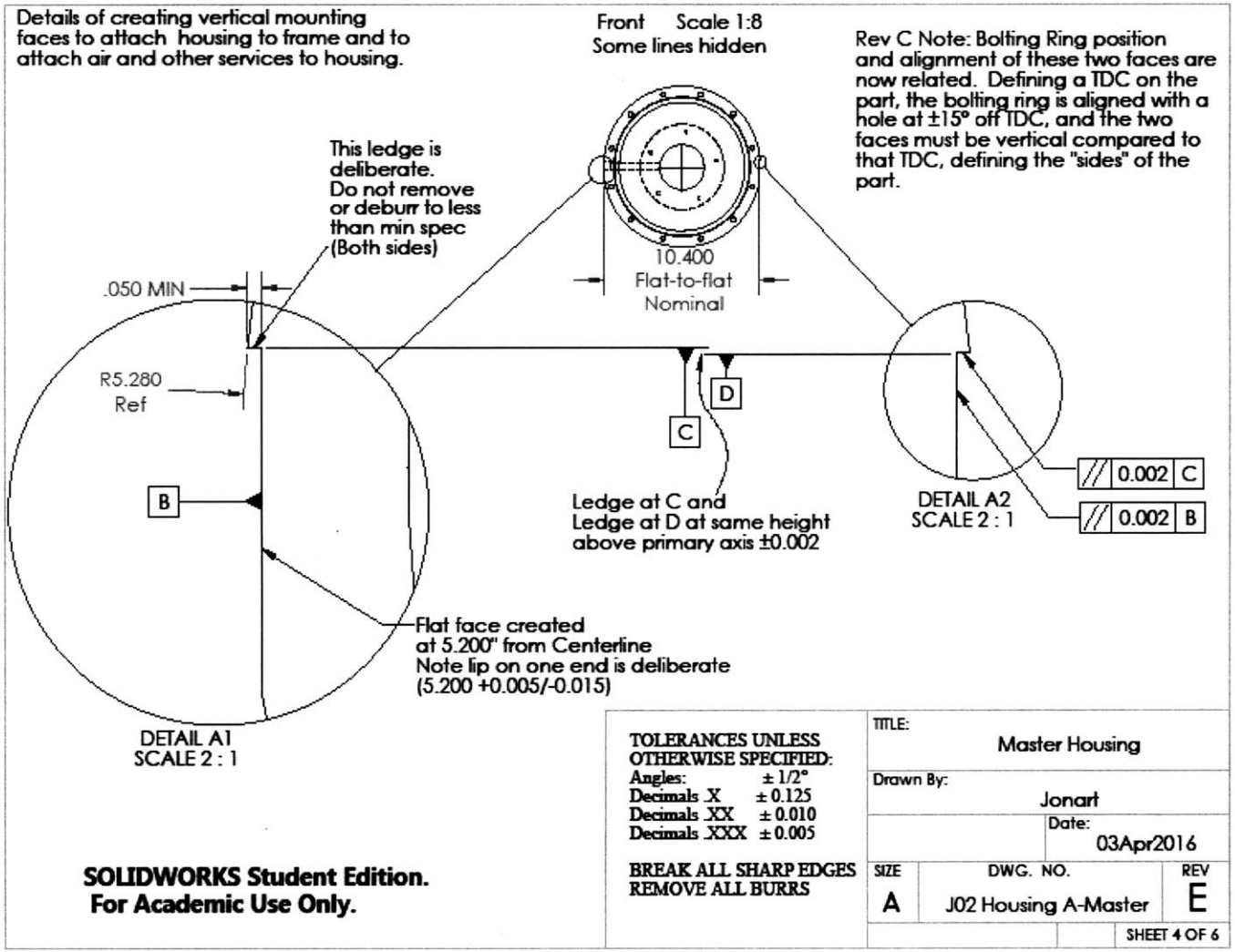
Details of creating vertical mounting faces to attach housing to frame and to attach air and other services to housing.
Front Scale 1:8
Some lines hidden
Rev C Note: Bolting Ring position and alignment of these two faces are now related. Defining a TDC on the part, the bolting ring is aligned with a hole at ±15° off TDC, and the two faces must be vertical compared to that TDC, defining the "sides" of the part.
This ledge is deliberate. Do not remove or deburr to less than min spec (Both sides)
.050 MIN
10.400
Flat-to-flat
Nominal
R5.280
Ref
B
C
D
Ledge at C and
Ledge at D at same height
above primary axis ±0.002
// 0.002 C
// 0.002 B
DETAIL A2
SCALE 2 : 1
Flat face created
at 5.200" from Centerline
Note lip on one end is deliberate
(5.200 +0.005/-0.015)
DETAIL A1
SCALE 2 : 1
SOLIDWORKS Student Edition.
For Academic Use Only.
TOLERANCES UNLESS OTHERWISE SPECIFIED:
Angles: ± 1/2°
Decimals .X ± 0.125
Decimals .XX ± 0.010
Decimals .XXX ± 0.005
BREAK ALL SHARP EDGES
REMOVE ALL BURRS
TITLE:
Master Housing
Drawn By:
Jonart
Date:
03Apr2016
SIZE
A
DWG. NO.
J02 Housing A-Master
REV
E
SHEET 4 OF 6

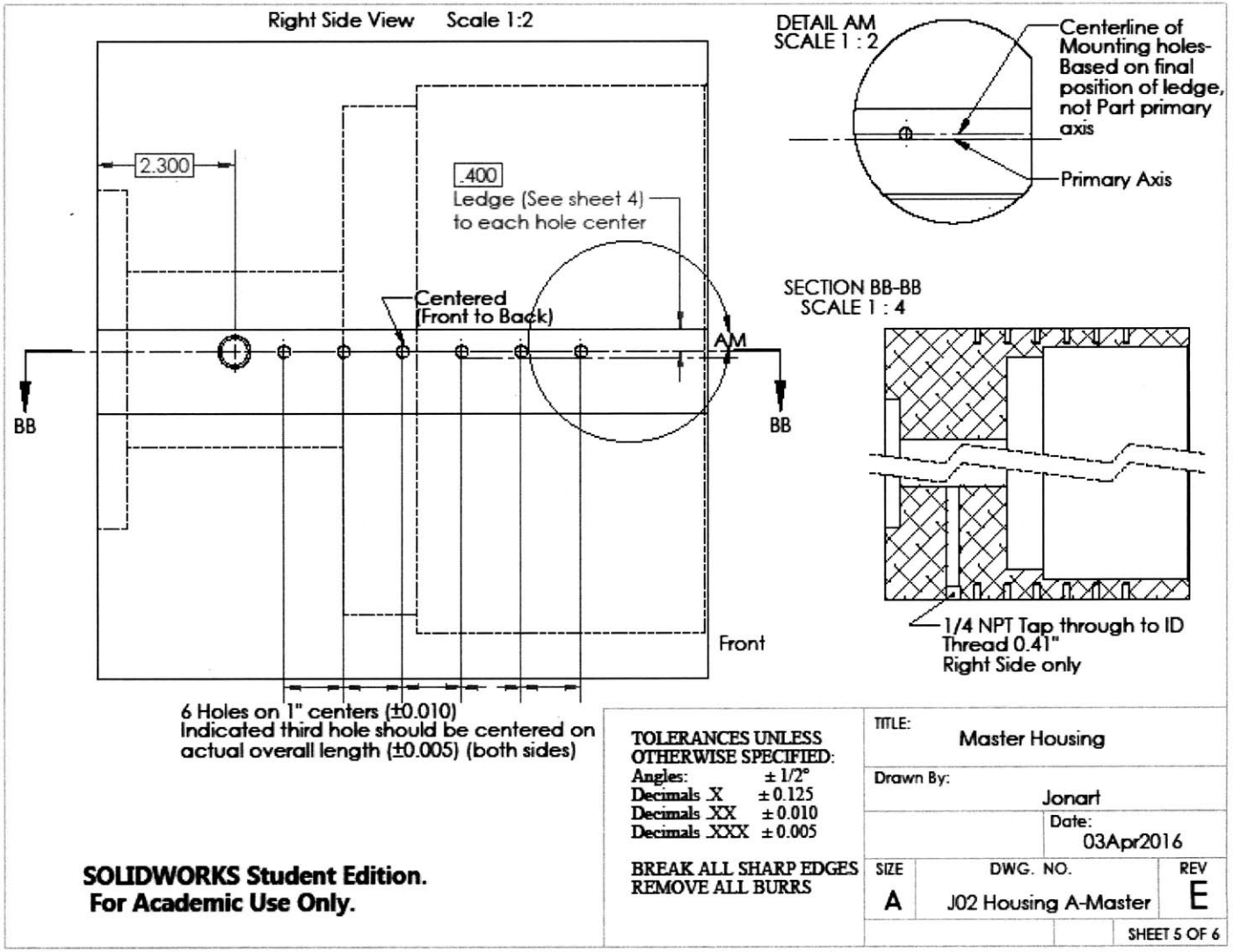
Right Side View Scale 1:2
2.300
.400
Ledge (See sheet 4)
to each hole center
Centered
(Front to Back)
AM
BB
BB
Front
6 Holes on 1" centers (±0.010)
Indicated third hole should be centered on
actual overall length (±0.005) (both sides)
DETAIL AM
SCALE 1 : 2
Centerline of
Mounting holes-
Based on final
position of ledge,
not Part primary
axis
Primary Axis
SECTION BB-BB
SCALE 1 : 4
1/4 NPT Tap through to ID
Thread 0.41"
Right Side only
TOLERANCES UNLESS
OTHERWISE SPECIFIED:
Angles: ± 1/2°
Decimals .X ± 0.125
Decimals .XX ± 0.010
Decimals .XXX ± 0.005
BREAK ALL SHARP EDGES
REMOVE ALL BURRS
TITLE:
Master Housing
Drawn By:
Jonart
Date:
03Apr2016
SIZE
A
DWG. NO.
J02 Housing A-Master
REV
E
SHEET 5 OF 6
SOLIDWORKS Student Edition.
For Academic Use Only.

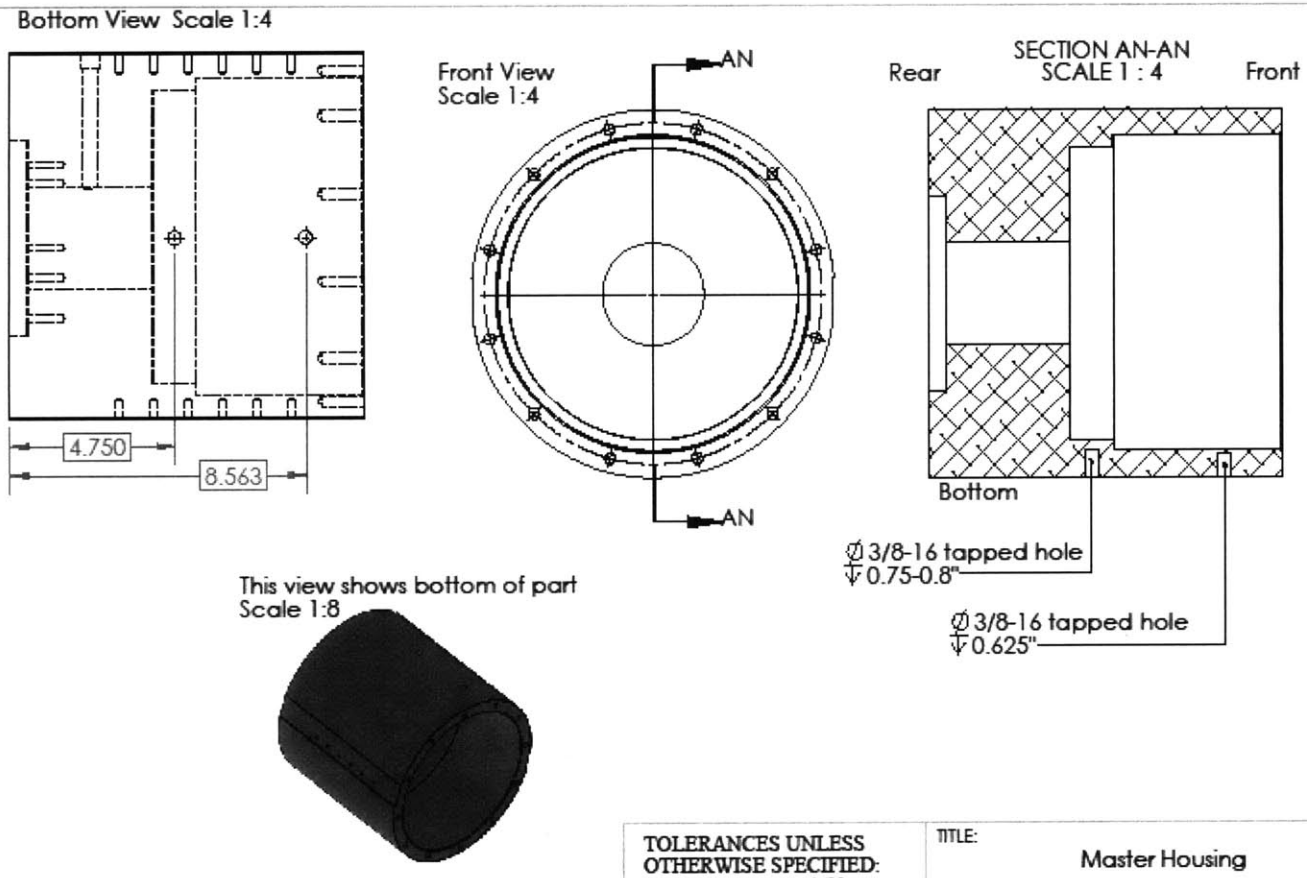
Bottom View Scale 1:4
4.750
8.563
Front View
Scale 1:4
AN
AN
SECTION AN-AN
SCALE 1 : 4
Rear
Front
Bottom
Ø 3/8-16 tapped hole
↧ 0.75-0.8"
Ø 3/8-16 tapped hole
↧ 0.625"
This view shows bottom of part
Scale 1:8
SOLIDWORKS Student Edition.
For Academic Use Only.
TOLERANCES UNLESS OTHERWISE SPECIFIED:
Angles: ± 1/2°
Decimals .X ±.125
Decimals .XX ±.010
Decimals .XXX ±.005
BREAK ALL SHARP EDGES
REMOVE ALL BURRS
TITLE:
Master Housing
Drawn By:
Jonart
Material
6061 Aluminum
Date:
03Apr2016
SIZE
A
DWG. NO.
J02 Housing A - Master
REV
E
SHEET 6 OF 6

Master View, Scale 1:2

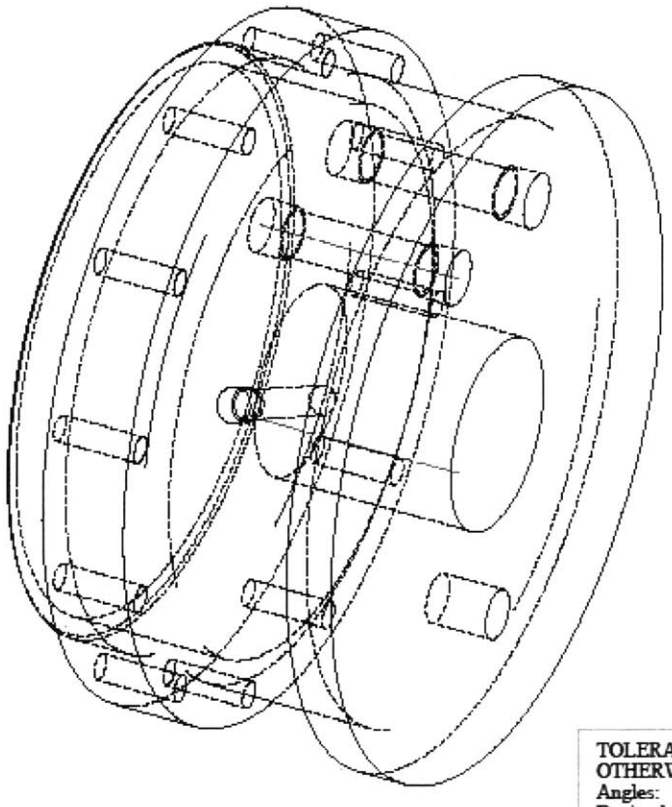

Scale 1:4

SOLIDWORKS Student Edition.
For Academic Use Only.

TOLERANCES UNLESS OTHERWISE SPECIFIED:	
Angles:	± 1/2°
Decimals .X	±.125
Decimals .XX	±.010
Decimals .XXX	±.005
BREAK ALL SHARP EDGES REMOVE ALL BURRS	

TITLE: Housing B: Pinch Housing		
Drawn By: Jonart		
Material 6061 Aluminum	Date: 05APR2016	
SIZE A	DWG. NO. J03 Housing B - Pinch	REV E
		SHEET 1 OF 4

Front View: Primary Dimensions Scale 1:4 Some Lines Hidden

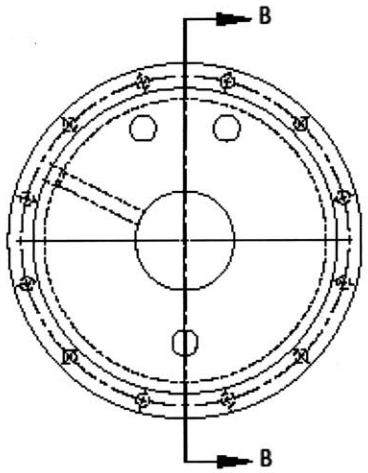

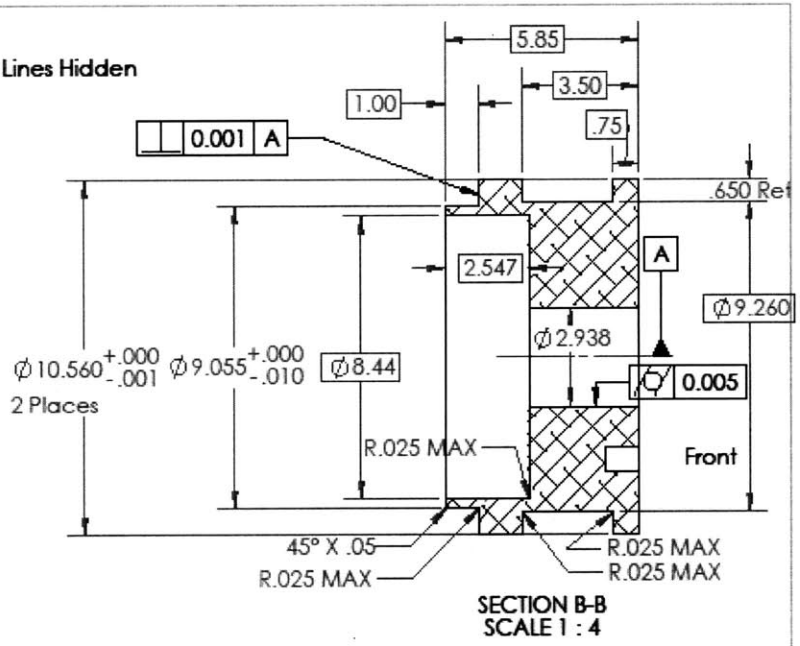

SECTION B-B
SCALE 1 : 4

This part must slide into and mate up with Housing A (Master Housing)
Such that the cylinders at Datum A are concentric within 0.001"
Mating surfaces are the bolting rings perpendicular to Datum A.

SOLIDWORKS Student Edition.
For Academic Use Only.

TOLERANCES UNLESS OTHERWISE SPECIFIED:	
Angles:	± 1/2°
Decimals .X	±.125
Decimals .XX	±.010
Decimals .XXX	±.005

BREAK ALL SHARP EDGES
REMOVE ALL BURRS

TITLE: Housing B: Pinch Housing		
Drawn By: Jonart		
Material: 6061 Aluminum	Date: 05APR2016	
SIZE: A	DWG. NO.: J03 Housing B - Pinch	REV: E
		SHEET 2 OF 4

Rear View: Bolting Pattern Details

Scale 1:4 Some Lines Hidden

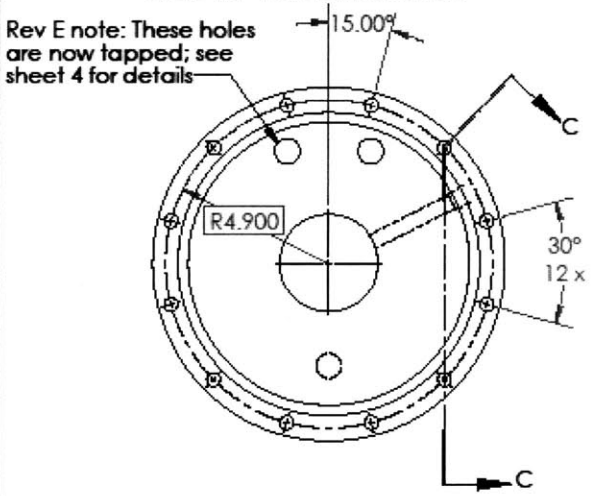

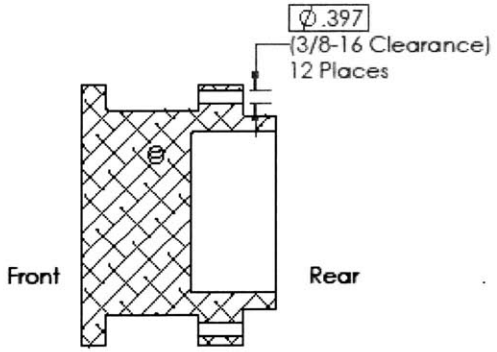

SECTION C-C
SCALE 1 : 4

These 12 bolt holes align with the tapped receiving Holes in the Master Housing, Housing A.

Rev C Note:
Bolt pattern is now indexed to 15° off TDC. 3/4-10 tapped hole on front face must be at 180° from TDC.

SOLIDWORKS Student Edition.
For Academic Use Only.

TOLERANCES UNLESS OTHERWISE SPECIFIED:	
Angles:	± 1/2°
Decimals .X	±.125
Decimals .XX	±.010
Decimals .XXX	±.005
BREAK ALL SHARP EDGES REMOVE ALL BURRS	

TITLE: Housing B: Pinch Housing		
Drawn By: Jonart		
Material 6061 Aluminum	Date: 05APR2016	
SIZE A	DWG. NO. J03 Housing B - Pinch	REV E
		SHEET 3 OF 4

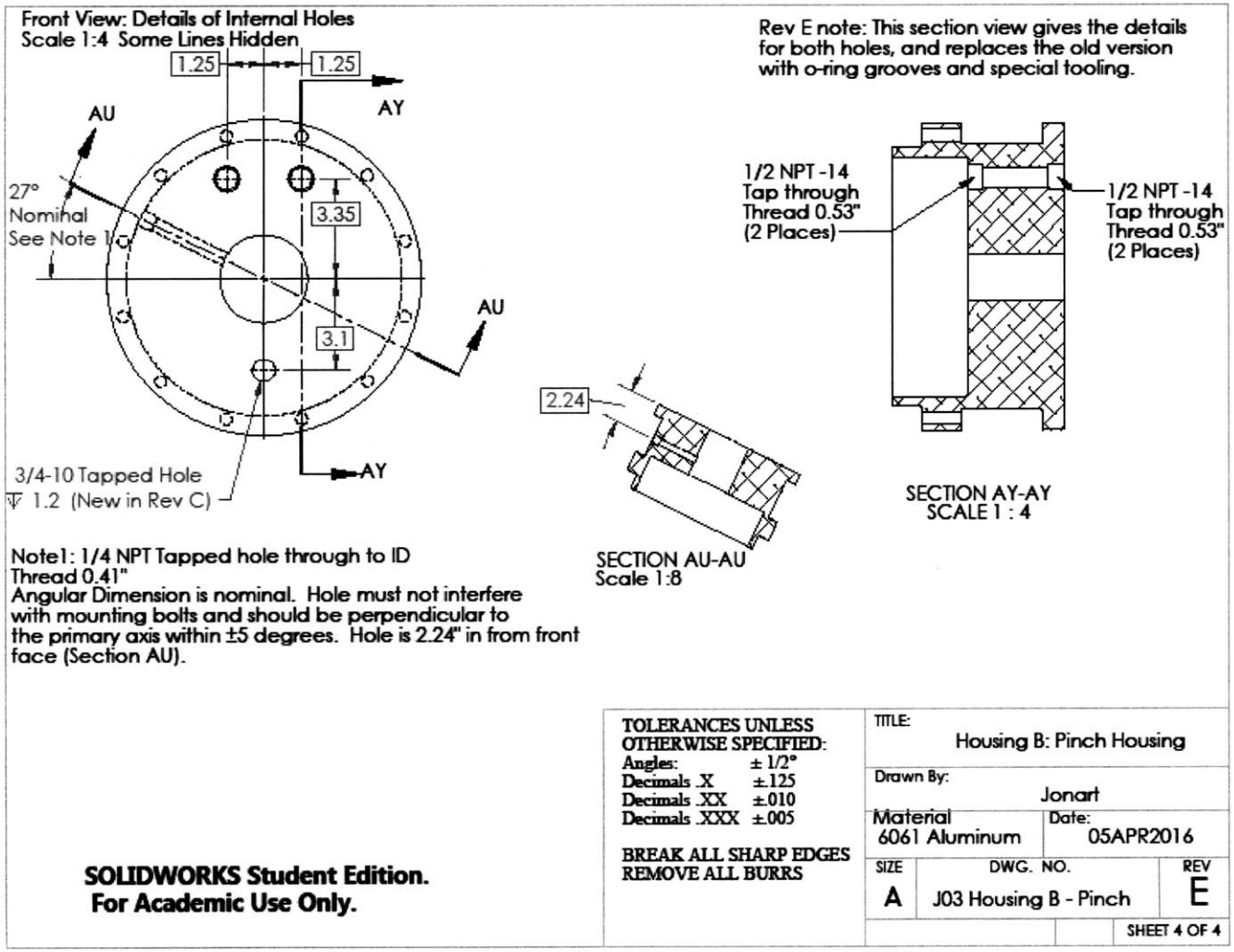
Front View: Details of Internal Holes
Scale 1:4 Some Lines Hidden
1.25
1.25
AU
AY
27°
Nominal
See Note 1
3.35
3.1
AU
AY
3/4-10 Tapped Hole
⌀ 1.2 (New in Rev C)
Rev E note: This section view gives the details for both holes, and replaces the old version with o-ring grooves and special tooling.
1/2 NPT -14
Tap through
Thread 0.53"
(2 Places)
1/2 NPT -14
Tap through
Thread 0.53"
(2 Places)
SECTION AY-AY
SCALE 1 : 4
2.24
SECTION AU-AU
Scale 1:8
Note1: 1/4 NPT Tapped hole through to ID
Thread 0.41"
Angular Dimension is nominal. Hole must not interfere with mounting bolts and should be perpendicular to the primary axis within ±5 degrees. Hole is 2.24" in from front face (Section AU).
TOLERANCES UNLESS OTHERWISE SPECIFIED:
Angles: ± 1/2°
Decimals .X ±.125
Decimals .XX ±.010
Decimals .XXX ±.005
BREAK ALL SHARP EDGES
REMOVE ALL BURRS
TITLE:
Housing B: Pinch Housing
Drawn By:
Jonart
Material
6061 Aluminum
Date:
05APR2016
SIZE
A
DWG. NO.
J03 Housing B - Pinch
REV
E
SHEET 4 OF 4
SOLIDWORKS Student Edition.
For Academic Use Only.

Magnetic Sleeve
Master View

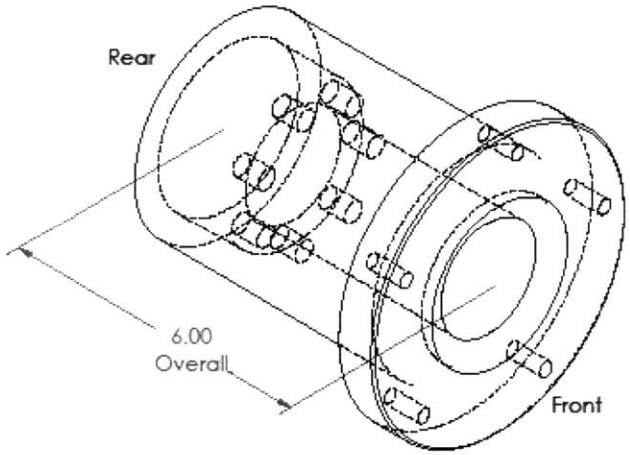

SOLIDWORKS Student Edition.
For Academic Use Only.

TOLERANCES UNLESS OTHERWISE SPECIFIED:	
Angles:	± 1/2°
Decimals .X	±.125
Decimals .XX	±.010
Decimals .XXX	±.005
BREAK ALL SHARP EDGES REMOVE ALL BURRS	

TITLE: Magnet Sleeve		
Drawn By: Jonart		
Material 6061 Aluminum	Date: 17Mar2016	
SIZE A	DWG. NO. J04 Magnet Collar	REV B
		SHEET 1 OF 3

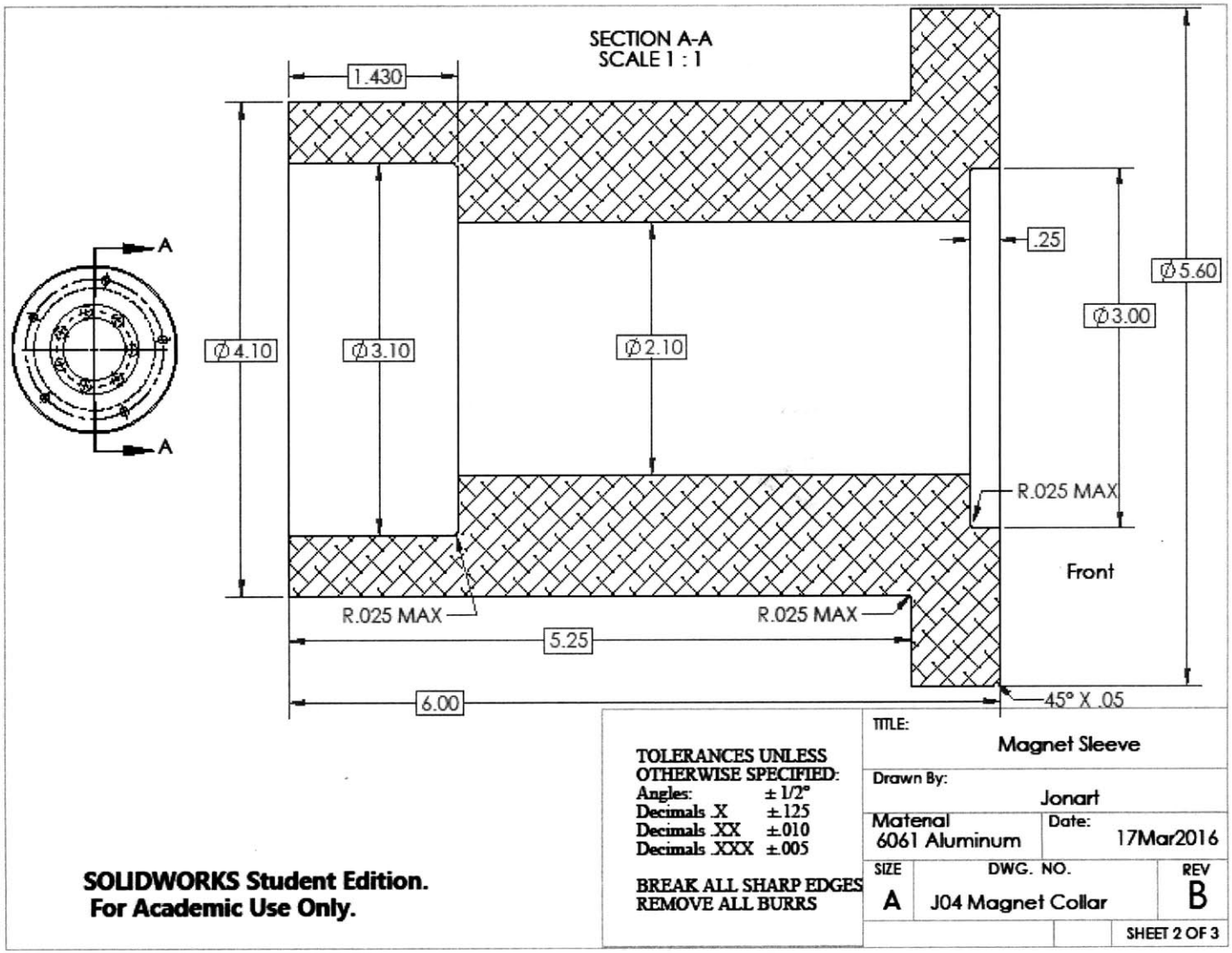
SECTION A-A
SCALE 1 : 1
1.430
Ø4.10
Ø3.10
Ø2.10
.25
Ø5.60
Ø3.00
R.025 MAX
Front
R.025 MAX
R.025 MAX
5.25
6.00
45° X .05
A
A
TOLERANCES UNLESS OTHERWISE SPECIFIED:
Angles: ± 1/2°
Decimals .X ±.125
Decimals .XX ±.010
Decimals .XXX ±.005
BREAK ALL SHARP EDGES
REMOVE ALL BURRS
TITLE:
Magnet Sleeve
Drawn By:
Jonart
Material
6061 Aluminum
Date:
17Mar2016
SIZE
A
DWG. NO.
J04 Magnet Collar
REV
B
SHEET 2 OF 3
SOLIDWORKS Student Edition.
For Academic Use Only.

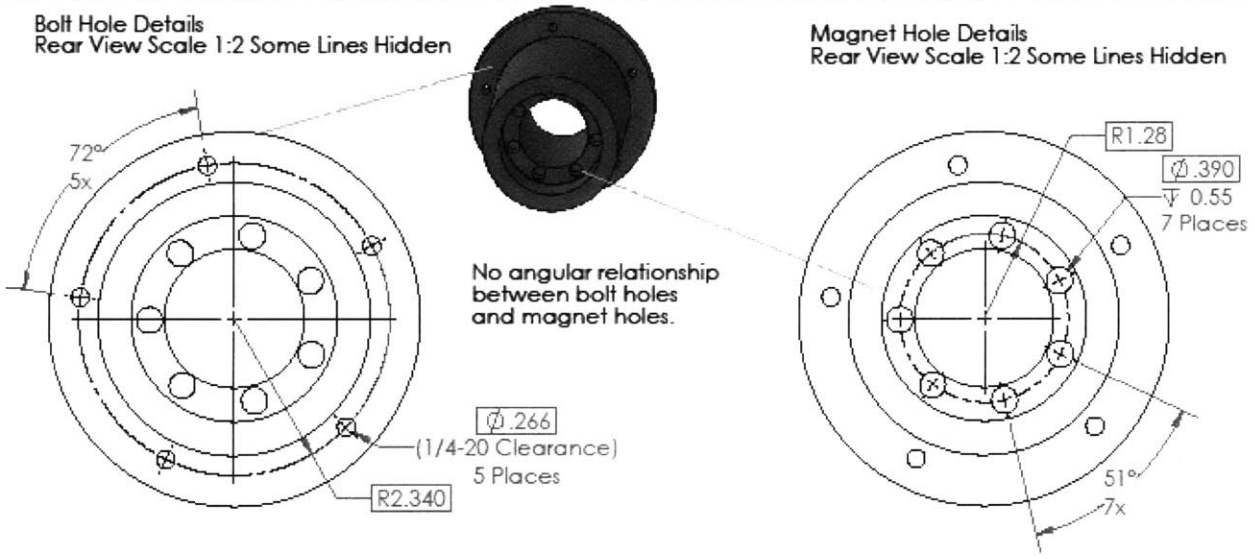

Bolt Holes to Mate up with Rear Bolting Face of Housing A (Master Housing) with 5 1/4-20 bolts

SOLIDWORKS Student Edition.
For Academic Use Only.

TOLERANCES UNLESS OTHERWISE SPECIFIED:	
Angles:	± 1/2°
Decimals .X	±.125
Decimals .XX	±.010
Decimals .XXX	±.005
BREAK ALL SHARP EDGES REMOVE ALL BURRS	

TITLE: Magnet Sleeve		
Drawn By: Jonart		
Material 6061 Aluminum	Date: 17Mar2016	
SIZE A	DWG. NO. J04 Magnet Collar	REV B
		SHEET 3 OF 3

Appendix E: Full code for updated model

```
# Time Calcs
# 4/14/16
library(VGAM)
library(ggplot2)
library(tidyr)
source('Code/Normal Updating.R')
source('Code/TimesToFailFNC.R')

ips_data <- rnorm(1000,0.01,0.001) #m
tpi_data <- rnorm(1000,2500,2500*0.05) #days

## simulation parameters
monte_size <- 1000000

### distibution parameters ###

## Time to Water Ingress (days)
twi_weib_shape <- 1
twi_weib_scale <- 1875

## Time to pit initiation (days)
tpi_COV <- 0.05
tpi_lnorm_mean <- 1500 #days
tpi_lnorm_sd <- tpi_COV*tpi_lnorm_mean    #days

##initial pit size
ips_COV <- 0.05
ips_norm_mean <- 1.98E-6 #meters
ips_norm_sd <- ips_COV*ips_norm_mean #meters

##pitting current constant
pcc_pareto_shape <- 3
pcc_pareto_scale <- 4


## Prior ##
tPrior <-
TimesToFail(monte_size,twi_weib_shape,twi_weib_scale,tpi_lnorm_mean,tpi_lnorm_sd,ips_norm_mean,ips_norm
_sd,pcc_pareto_shape,pcc_pareto_scale)

## Bayesian Updating of Means ##
newVals <-BayesianUpdateNormal2Normal(ips_data,ips_norm_mean,ips_norm_sd^2,plot=FALSE)
ips_norm_mean_post <- newVals[1]
ips_norm_sd_post <- sqrt(newVals[2])

newVals <-BayesianUpdateLogNormal2LogNormal(tpi_data,tpi_lnorm_mean,tpi_lnorm_sd^2,plot=FALSE)
tpi_lnorm_mean_post <- newVals[1]
tpi_lnorm_sd_post <- sqrt(newVals[2])
```

```
## Posterior ##
tPosterior <-
TimesToFail(monte_size,twi_weib_shape,twi_weib_scale,tpi_lnorm_mean_post,tpi_lnorm_sd_post,ips_norm_mean
,ips_norm_sd,pcc_pareto_shape,pcc_pareto_scale)

## Merging, Formatting, Graphing ##

tPosterior$Bayes <- 'Posterior'
tPrior$Bayes <- 'Prior'
tUpdate <- rbind(tPrior,tPosterior)
tUpdate$Bayes <- factor(tUpdate$Bayes)

ggplot(tUpdate,aes(x=Time/365))+
  geom_density()+
  facet_grid(Bayes~TimeType)+ #,scales = "free_y"
  xlim(0,100)+
  #ylim(0,1)+
  xlab('Years')+
  ylab('Probability')+
  ggtitle('Likelihood of Compromising the Shaft')

ggplot(tUpdate,aes(x=Time/365,color=Bayes,linetype=Bayes))+
  geom_density()+
  facet_wrap(~TimeType,ncol=1)+ #,scales = "free_y"
  xlim(0,100)+
  #ylim(0,1)+
  xlab('Years')+
  ylab('Probability')+
  ggtitle('Likelihood of Compromising the Shaft')
ggsave('Figures/PDF_ByType_Bayesian.pdf',width=6,height=8)

ggplot(tUpdate,aes(x=Time/365,color=TimeType,linetype=TimeType))+
  stat_ecdf()+
  facet_wrap(~Bayes,ncol=1)+ #,scales = "free_y"
  xlim(0,100)+
  #ylim(0,1)+
  xlab('Years')+
  ylab('CDF')+
  ggtitle('Likelihood of Compromising the Shaft')
ggsave('Figures/CDF_Bayesian.pdf',width=6,height=8)

ggplot(tUpdate,aes(x=Time/365,color=TimeType,linetype=Bayes))+
  stat_ecdf()+
  #facet_wrap(~TimeType,ncol=1)+ #,scales = "free_y"
  xlim(0,100)+
  #ylim(0,1)+
  xlab('Years')+
  ylab('CDF')+
  ggtitle('Likelihood of Compromising the Shaft with Bayesian Updating Example')
```